International journal
for science, technics and
innovations for the industry

MACHINES TECHNOLOGIES MATERIALS

YEAR XV Issue 6 / 2021 ISSN PRINT 1313-0226
ISSN WEB 1314-507X

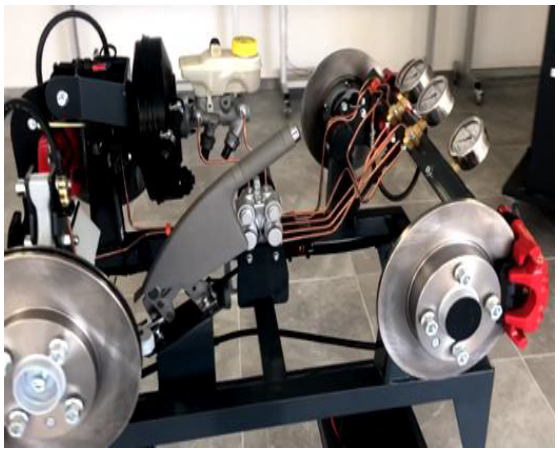

Published by
Scientific technical
Union of Mechanical Engineering

MACHINES. TECHNOLOGIES. MATERIALS

INTERNATIONAL SCIENTIFIC JOURNAL

ISSN PRINT 1313-0226, ISSN WEB 1314-507X, YEAR XV, ISSUE 6 / 2021

INTERNATIONAL EDITORAL BORARD

EDITOR IN CHIEF:

Georgi Popov	Technical University of Sofia	BG

MEMBERS:

Abdrakhman Naizabekov	Rudny industrial institute	KZ
Ahmet H. Ertas	Bursa Technical University	TR
Albert Albers	Karlsruhe Institut of Technology	DE
Andrzej Golabczak	Lodz University of Technology	PL
Andrzej Huczko	Warsaw University	PL
Dimitar Karaivanov	University of Chemical Technology and Metallurgy, Sofia	BG
Emilia Abadjieva	Akita University	JP
Erdem Camurlu	Akdeniz University, Antalya	TR
Eugen Sheregii	University of Rzeszow	PL
Franz Haas	Graz University of Technology	AT
Galina Nicolcheva	Technical University of Sofia	BG
Gennadii Bagliuk	Institute for Problems of Materials Science NAS of Ukraine, Kiev	UA
Georgii Raab	Ufa State Aviation Technical University	RU
Gregory Gurevich	Shamoon College of Engeeniring, Ashdod	IL
Hiroyuki Moriyama	Tokai University, Hiratsuka	JP
Idilia Batchkova	University of Chemical Technology and Metallurgy, Sofia	BG
Ivan Kralov	Technical University of Sofia	BG
Ivan Kuric	University of Zilina	SK
Julieta Kaleicheva	Technical University of Sofia	BG
Katia Vutova	Institute of Electronics, Bulgarian Academy of Sciences	BG
Maria Nikolova	Angel Kanchev University of Ruse	BG
Natasa Naprstkova	Jan Evangelista Purkyne University in Usti nad Labem	CZ
Oana Dodun	Gheorghe Asachi Technical University of Iasi	RO
Ognyan Andreev	Technical University of Sofia	BG
Predrag Dasic	High Technical Mechanical School of Trstenik	RS
Rasa Kandrotaite	Kaunas University of Technology	LT
Raul Turmanidze	Georgian Technical University, Tbilisi	GE
Roumen Petrov	Ghent University	BE
Sergey Dobatkin	National University of Science and Technology "MISIS", Moscow	RU
Souren Mitra	Jadavpur University, Kolkata	IN
Svetlana Gubenko	National Metallurgical Academy of Ukraine, Dnipro	UA
Vedran Mrzljak	University of Rijeka	HR
Wu Kaiming	Wuhan University of Science and Technology	CN

TECHNICAL EDITORS:

M. Sc. Eng. Radoslav Daskalov, M. Sc. Eng. Oleg Mihailov

Scientific and technical union of mechanical engineering
108 R. S. Rakovski str., Sofia, Bulgaria
www.stumejournals.com, office@stumejournals.com

C O N T E N T S

MACHINES

Coupled two-carrier planetary gearboxes for two-speed drives
Sanjin Troha, Dimitar Karaivanov, Željko Vrcan, Kristina Marković, Antonio Šoljić 212

Impact of the Number of Passengers in the Vehicle Braking Performances Equipped with Modern Mechatronics Braking System
Shpetim Lajqi, Agron Syla, Naser Lajqi, Gazmend Krasniqi 219

A new commercial dishwasher design using mineral additives in its drying system
Zafer Kahraman, Soner Gürcü, Murat Hacı, Hakan Serhad Soyhan 223

TECHNOLOGIES

Development and computer modeling of a new forging technology in step-wedge strikers
Andrey Volokitin, Andrey Tolkushkin, Evgeniy Panin, Irina Volokitina 226

Design and mechanical properties of high-voltage transmission line composite insulators
Monika Fidanchevska, Bojan Mitev, Kristina Micova, Marko Naseski, Atanas Kochov 230

One of the methods for improving the electrodes cleaning system of the electrostatic precipitator with the purpose of increasing the intensity of checking dust
Kazak Iryna 234

Ecological aspects of metallurgy and mechanical engineering at the beginning of the 21st century
Yavor Lukarski, Hristo Argirov 237

MATERIALS

Microcrystallites, granularity and agglomerates of detonation nanodiamonds

Evgeny Petrov, Vetrova Anastasia, Pribavkin Andrey Borisovich, Udalova Anastasia 241

Analysis of the influence of environmental factors on the properties of cellulosic electrical insulating materials
Ardeleanu Mircea-Emilian, Scornea Aurelia, Stănescu Dan-Gabriel, Sîrbu Ioana-Gabriela, Buligioiu Alexandru 244

The impact of high voltage electric discharge treatment on the properties of Cu – Al powder mixture
Syzonenko Olha, Torpakov Andrii, Lypian Yevhen, Prystash Mykola 248

Coupled two-carrier planetary gearboxes for two-speed drives

Sanjin Troha[1], Dimitar Karaivanov[2], Željko Vrcan[1], Kristina Marković[1], Antonio Šoljić[1]
[1]University of Rijeka, Faculty of Engineering, Vukovarska 58, 51000 Rijeka, Croatia
[2]University of Chemical Technology and Metallurgy, 8 Kl. Ohridski Blvd, 1756 Sofia, Bulgaria
E-Mail: sanjin.troha@riteh.hr; dipekabg@yahoo.com; zeljko.vrcan@riteh.hr; kristina.markovic@riteh.hr; antonio.soljic@riteh.hr

Abstract: *The following paper reviews all the possible cases of coupled two-carrier planetary gears with four external shafts. An emphasis is made on the work of these gears with one degree of freedom, one input and one output shaft and brakes on the other two shafts. When switching over the gears, the speed ratio of the gear is changed, thus allowing the use in two-speed mechanical transmissions of technological lifting and other machines. Some relations are deduced for determining the speed ratios and the efficiency of all structural schemes.*
Recommendations for the selection of the most appropriate structural scheme according to the current necessities can be made. A 3D model of the S13V3 two-speed, two-carrier gearbox was created to demonstrate the process of determining the viability of a particular gearbox layout.
KEYWORDS: COUPLED PLANETARY GEARS, STRUCTURAL ANALYSIS, EFFICIENCY, 3D MODEL.

1. Introduction

In some cases of machinery there comes the need of using two-speed transmissions with a definite ratio between the two speeds. The ability to switch over while in motion and loaded is a certain advantage and in some cases an inevitable necessity. One proper solution is the use of a coupled two-carrier planetary gear with four external shafts and two brakes (Fig. 1).

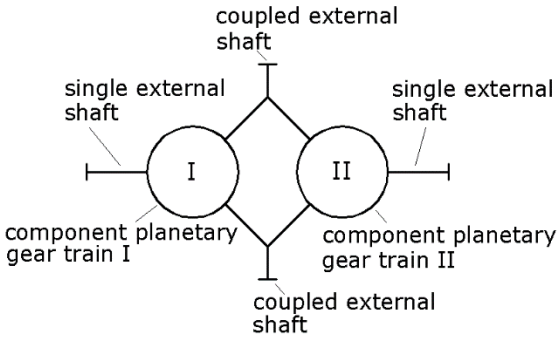

Fig. 1. *Schematic layout of a two-carrier planetary gear with four external shafts, two coupled and two single external shafts*

In [1-7] there is a review on the various possible ways of brake mounting and power flowing in the above-mentioned gear when it consists of two simple gears of the most common type (Fig. 2) [5-8] (consisting of a sun-gear 1, a ring-gear 3 and one-rimmed satellites 2, situated on the carrier *S*).
Practice shows that in the structural analysis of coupled planetary gears it is appropriate to use the structural symbol of Wolf, indicating the simple gear with a circle and the three external shafts with three different in width lines, corresponding to the torque magnitude of the corresponding shaft [1-7, 9, 10, 11].

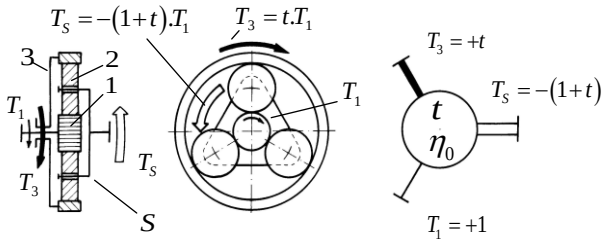

Prerequisite: $\eta_0 = \eta_{13(S)} = \eta_{31(S)} = 1$

Torque ratio: $t = \frac{T_3}{T_1} = \frac{T_{D\max}}{T_{D\min}} = \left|\frac{z_3}{z_1}\right| > +1$

Torques: $T_1 : T_3 : T_S = T_{D\min} : T_{D\max} : T_\Sigma =$

$$= T_1 : t.T_1 : -(1+t).T_1 = +1 : +t : -(1+t)$$

$$T_1 \equiv T_{D\min} < T_3 \equiv T_{D\max} < |T_S| \equiv |T_\Sigma|$$

Fig. 2. *The most often used single-carrier planetary gear train and its torques*

The main force and kinematic characteristic of the simple planetary gear is the torque ratio *t*, through which the speed ratios in the gear can be expressed for all 6 cases of work with one degree of freedom [1-7, 9, 10, 11]:

$$t = \frac{T_3}{T_1} = \frac{T_{D\max}}{T_{D\min}}, \quad (1)$$

where: $T_1 \equiv T_{D\min}$ is the torque of the sun gear (the lowest torque), and $T_3 \equiv T_{D\max}$ is the torque of the ring gear (the higher differential torque).
The aim of the following paper is to analyze the possibilities given by all structural schemes of two-carrier planetary gears with four external shafts, consisting of simple planetary gears of the most common type (Fig. 2).

2. Structural Analysis

Table 1 shows all the possible ways of connecting the coupling gears [1]. The arrows indicate the isomorphism, thanks to which there are only 12 structural schemes for review (11, 12, 13, 14, 15, 16, 33, 34, 35, 36, 55 and 56).
The conducted analysis shows that the most clarity is achieved when reviewing 6 basic variants (according to the situation of the brakes), each of which with two sub-variants according to which brake is activated (Fig. 3).
When situating the two brakes on the two single shafts (V6 – Fig. 3) only one of the coupling gears will be working and the speed ratio of the coupled gear will depend only on the torque ratio of the working gear.
When situating the two brakes on the two coupled shafts (V1 – Fig. 3) the two coupling gears are connected in series and the speed ratio of the coupled gear will be equal to the product of the corresponding speed ratios of the coupling gears. It will depend on the torque ratios t_I, t_{II}, the structural scheme and on which of the brakes is closed.

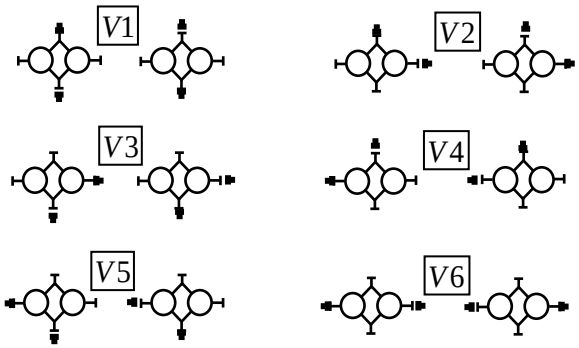

Fig. 3. *Variants of work of the gears in review*

When situating the two brakes on one single and one coupled shaft there are four possible variants in one structural scheme. Having in mind that in the reviewed structural schemes there are different possible ways of power flowing (branching or circulation) with a fixed single shaft, the variants become eighth. When the brake of the coupled shaft is closed the speed ratio will depend only on the torque ratio of one of the coupling gears.

When the brake of the coupled shaft is open the speed ratio will depend on the torque ratios t_I, t_{II} of the coupling gears and the structural scheme in question. Essentially, the gear will be working as a two-carrier one with three external shafts, a case reviewed in detail in [4].

The cases from V1 – Fig. 3 can also be referred to the coupled two-carrier gears with three external shafts. However, they must work with a fixed coupled shaft.

Table 1. *Structural schemes of coupled two-carrier planetary gears with four external shafts*

	...1	...2	...3	...4	...5	...6
1...	11	12 ≡ 21	13 ≡ 31	14 ≡ 41	15 ≡ 51	16 ≡ 61
2...	21 ≡ 12	22	23 ≡ 32	24 ≡ 42	25 ≡ 52	26 ≡ 62
3...	31 ≡ 13	32 ≡ 23	33	34 ≡ 43	35 ≡ 53	36 ≡ 63
4...	41 ≡ 14	42 ≡ 24	43 ≡ 34	44	45 ≡ 54	46 ≡ 64
5...	51 ≡ 15	52 ≡ 25	53 ≡ 35	54 ≡ 45	55	56 ≡ 65
6...	61 ≡ 16	62 ≡ 26	63 ≡ 36	64 ≡ 46	65 ≡ 56	66

3. Kinematic Analysis

The coupled two-carrier planetary gears with four external shafts are appropriate for two-speed drives.

The two-speed drive with one main speed and one micro-speed is common for mechanisms of lifting machines with higher positioning accuracy or operating with dangerous loads. It is also observed in technological and other machines.

In this case, given a certain angular velocity ω_A, three angular velocities of the output shaft when closing different brakes should be obtained. For example, a main speed ω_B and a micro-speed $\omega_{B\mu}$. Of particular interest is the possibility of reversing the motion - working displacement at low velocity (and high torque) and rapid return to initial position.

The torque ratios of the two coupling gears t_I and t_{II} can vary within the construction limited interval [4],

$$2 \le t_{I\min} \le t_I \le t_{I\max} \le 12,$$

$$2 \le t_{II\min} \le t_{II} \le t_{II\max} \le 12.$$

Therefore, if the necessary speed ratios of the two speeds $i_{AB} = \dfrac{\omega_A}{\omega_B}$ and $i_{AB\mu} = \dfrac{\omega_A}{\omega_{B\mu}}$ can be accomplished by a simple planetary gear, it is good to use structural schemes with brakes on the single shafts (V6 – Fig. 3).

With high-speed ratios i_{AB} and $i_{AB\mu}$ it is possible that the above-mentioned gear is a second stage, which gives the desired ratio between the two speed ratios. For example, in scheme 45 in Table 1 this ratio could be $2 \le \dfrac{\omega_B}{\omega_{B\mu}} \le 13$.

For all the different structural schemes in Table 1 relations are deduced for determining the speed ratios for the 12 cases of work with one degree of freedom.

Fig. 4 exemplifies the way of determining the speed ratios for variant V2 in scheme 16 when activating the various brakes (V21 and V22). In this case there is an internal power division, while Fig. 5 shows an example with internal power circulation.

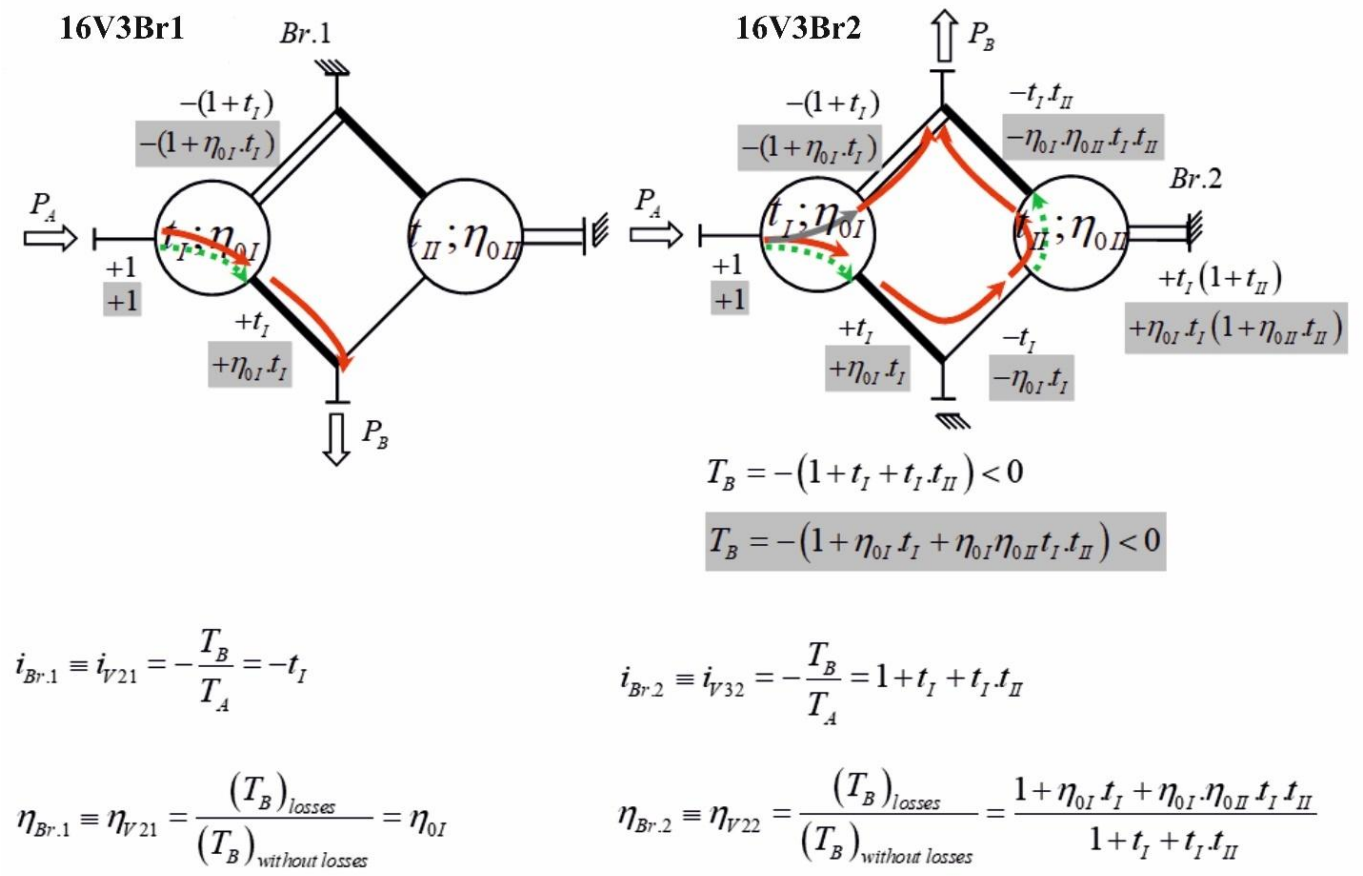

Fig. 4. *Determining the speed ratios and efficiency for variant V3 in structural scheme 16 in Table 1*
- transmitted power; - rolling power

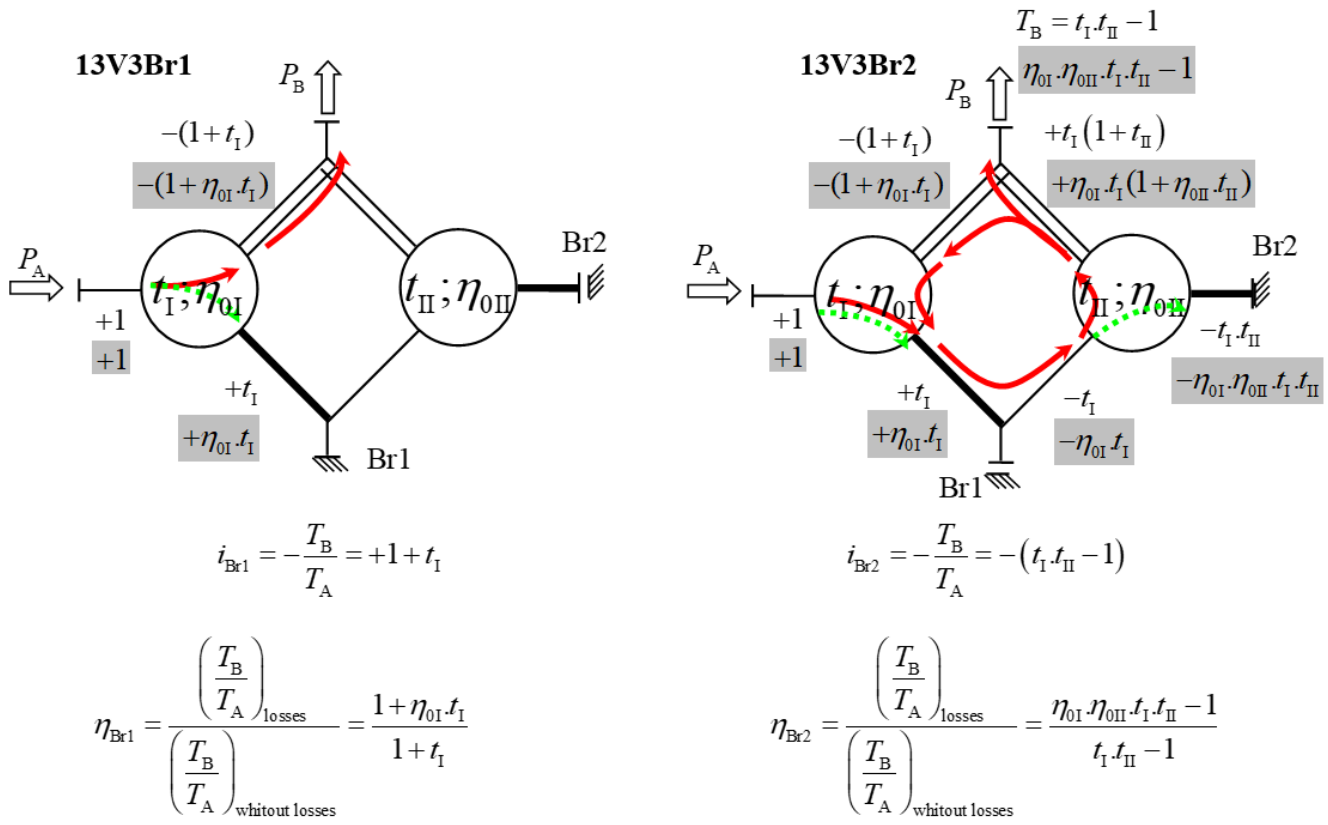

Fig. 5. *Determining the speed ratios and efficiency for variant V3 in structural scheme 13 in Table 1*
- transmitted power; - rolling power

4. Efficiency

In this case it is most appropriate to determine the efficiency η from the input T_A and output T_B torques following the expression [1, 3, 4, 6, 7]

$$\eta = \frac{\left(\frac{T_B}{T_A}\right)_{losses}}{\left(\frac{T_B}{T_A}\right)_{without\ losses}}, \quad (2)$$

where the torques with losses are determined with reading the direction of rolling power flow in the coupling gears. Relations are deduced for all the structural schemes in Table 1 for determining the efficiencies for the 12 cases of work with one degree of freedom as a function of the torque ratios t_I and t_{II} and the basic (when working with a fixed carrier) efficiencies η_{0I} and η_{0II} of the coupling gears. The latter could be assumed as constants [4], but they had better be determined with reading the impact of the number of teeth (i.e., of t_I and t_{II}) on the mesh losses by the methods described in [5].

Fig. 4 and Fig. 5 exemplify the way of determining the efficiency of the given variants. The torques of the shafts (the values on a dark background) are determined with reading the losses and direction of the rolling power in the coupling simple gears. In the case in review $(T_A)_{without\ losses} = (T_A)_{losses} = +1$, which simplifies formula (2).

It has been established that in all cases the expression in the numerator of (2) is obtained when in the denominator the torque ratios of the coupling gears (t_I or t_{II}) are multiplied by the corresponding basic efficiencies (η_{0I} or η_{0II}) when in the simple gear the rolling power is transmitted from the sun 1 to the ring 3. When the rolling power is transmitted from the ring to the sun the torque ratio of this simple gear is divided by the basic efficiency. In the examples in Fig. 4 and Fig. 5 only the first case is shown.

5. Geometrical modelling of the S13V3 planetary gearbox

To validate the feasibility of a gearbox layout, a kinematic or geometrical model should be used. Taking S13V3 as an example, we can summarize the following from the Wolf structural symbols:

1. The sun gear of the first gearset is the input element.
2. The planet carriers of the gearsets are coupled together to a common output shaft.
3. The ring gear of the first gearset is coupled to the sun gear of the second gearset.
4. Brake Br2 acts on the ring gear of the second gearset.
5. Brake Br1 acts on the ring gear of the first gearset, and consequently also on the sun wheel of the second gearset as it is coupled to the ring gear of the first gearset.

As soon as these basic concepts have been determined, a kinematic model of the gearbox can be created (Fig. 6), and appropriate attention may be given to specific parts of the design (e.g., the need for hollow shafts or specific brake placement).

With the kinematic model settled, a geometrical model may be created (Fig. 7).

This model will have appropriately sized gears fit for the purpose for which the gearbox is being designed, as well as a preliminary layout of bearings. Finally, an actual layout will be created, and brake actuation will be dealt with at this stage. Hydraulically actuated clutch-type brakes are used in modern planetary gearboxes.

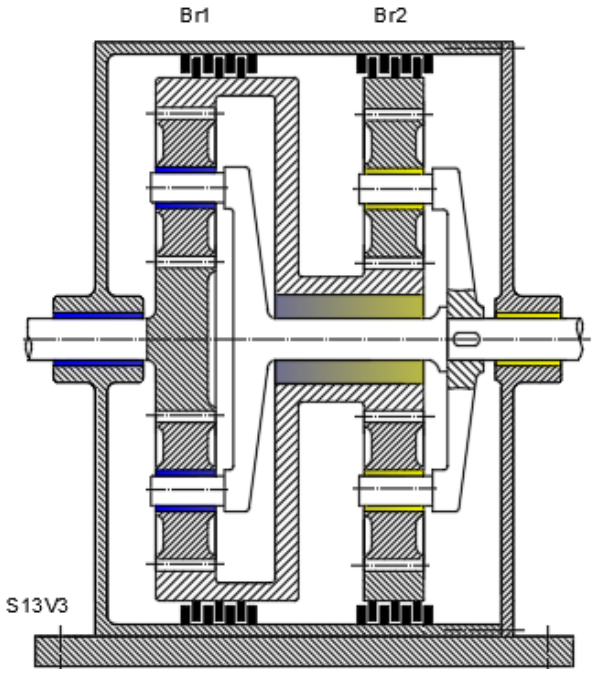

Fig. 6. *Kinematic model of S13V3 planetary gearbox*

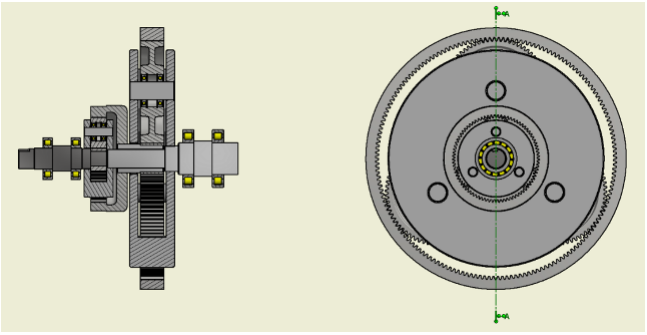

Fig. 7. *Geometrical model of S13V3 planetary gearbox*

However, band brakes and electric or electromechanical actuation may be used for ease of servicing or operation. In this case, electrically actuated band brakes are used to change the transmission ratio of the gearbox (Fig. 8).

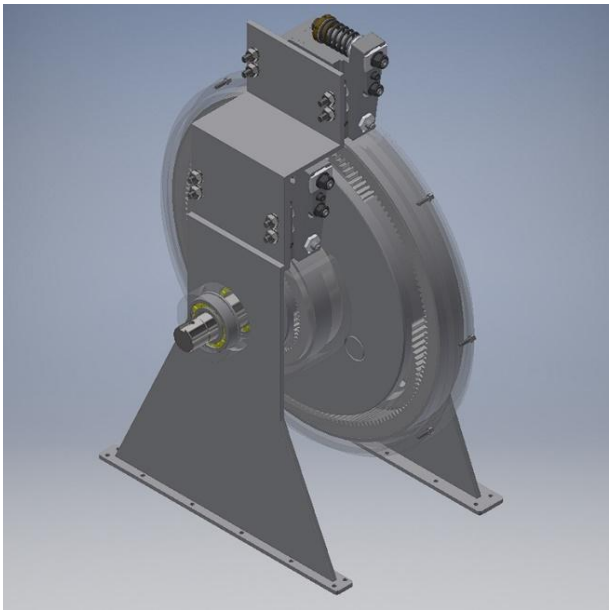

Fig. 8. *Complete model of S13V3 planetary gearbox*

6. Analysis and Discussion of the Results

The conducted structural analysis and the deduced formulae give the following conclusions (generalizations):
According to the structural scheme and the way of situating the brakes (the variant) different ratios of the output angular velocities are obtained with one and the same input velocity (i.e., of the two speed ratios).
In some cases when switching over the brakes the rotational direction of the output shaft is retained (12V1, 12V3, 13V1, 13V5, etc.), whereas in other cases it is reversed (12V2, 13V2, 13V3, 13V4, 14V2, etc.) In both cases it is possible that the gear continues its work as a reducer (respectively as a multiplier) or it might change its way of working – from reducer to multiplier (respectively from multiplier to reducer) [8, 12-15].

6.1 Retaining the rotational direction

In some of the cases of retaining the rotational direction the two speed ratios are close in value (15V3), sometimes close to 1 (15V4), even when the gear works as a reducer with one brake and as a multiplier with the other one (16V5, 36V5).
In other cases of retaining the rotational direction there is a significant difference between the two speed ratios (13V1, 13V6, 34V6, 36V2 and particularly 16V3) when the gear works as a reducer. In schemes 12V6, 13V5, 14V6, 15V5, 35V5 it works as a reducer with one brake and as a multiplier with the other one. Thus, a higher difference between the two speed ratios could be obtained (especially in 35V5). In scheme 56V6 when $i_{Br.1} = t_I$, $i_{Br.2} = \frac{1}{t_{II}}$, which allows the obtaining of $i_{Br.1} = \frac{1}{i_{Br.2}}$ when necessary.

6.2 Reversing the rotational direction

A great variety of options exists in the variants where the rotational direction is reversed. In 36V1 both speed ratios are close to 1, in 12V2 $i_{Br.1} = -t_I$ and $i_{Br.2} = 1 + \frac{1+t_I}{t_{II}}$, in 13V2 $i_{Br.1} = -t_I$ and $i_{Br.2} = \frac{t_I.t_{II} - 1}{1+t_{II}}$, whereas in 14V2 a great difference is obtained between the two speed ratios - $i_{Br.1} = -t_I$ and $i_{Br.2} = 1 + t_{II} + t_I.t_{II}$. The case is similar in 16V1. These schemes are appropriate for a technological machine with one displacement with high resistance (and low speed) and reversion to initial position with a higher speed (for increasing the productivity).
In other variants the gear works as a reducer with one brake and as a multiplier with the other one (15V6, 34V5, 35V1, 35V6) as in some cases there is a significant difference between the speed ratios.
In the structural schemes of the main diagonal in Table 1 for variants V2 and V3, according to the values of the torque ratios t_I and t_{II} of the coupling gears the rotational direction could be either retained or reversed. In the borderline case, when $t_I = t_{II}$, no motion is transmitted. The input shaft rotates, while the output one is motionless. In these cases, $i = \frac{\omega_A}{\omega_B} = \infty$ is obtained analytically, but the efficiency equals zero.
The formulae deduced for the speed ratios as a function of the torque ratios of the coupling gears serve as a basis for the establishment of a kinematic analysis program for the structural schemes in Table 1.

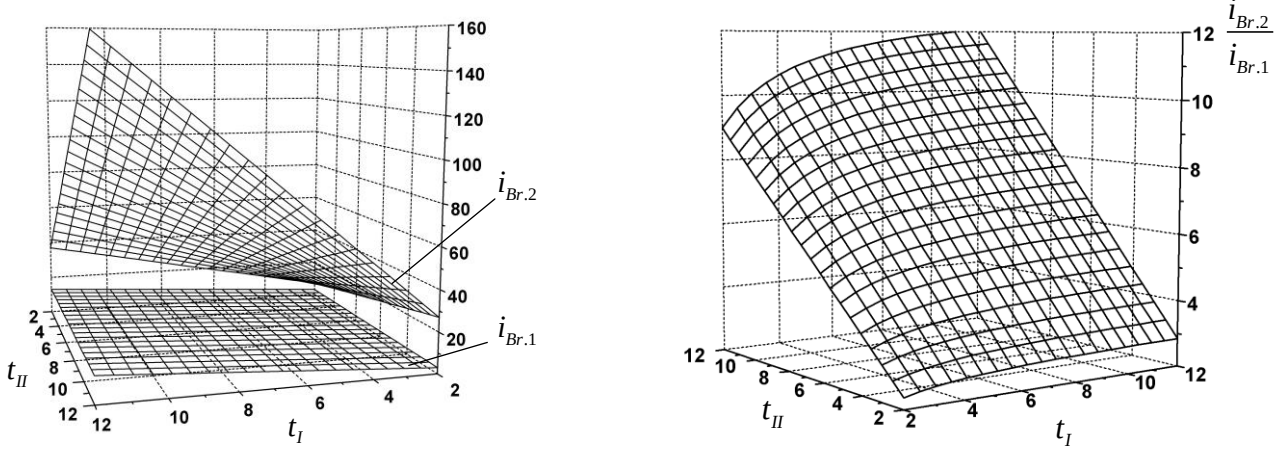

Fig. 9. *The speed ratios i_{Br1} and i_{Br2} (left) and their correlation (right) for variant V3 in structural scheme 16 (with activating different brakes) as a function of the torque ratios and of the coupling gears*

It can be used for picking out the structural schemes which can provide the desired ratio between the speed ratios in the case of a two-speed drive. The graphical representation of valid transmission ratios $i_{Br.1}$ and $i_{Br.2}$ as a function of the torque ratios of the coupling gears t_I and t_{II} (Fig. 9), facilitates the quick orientation of the designer about the capabilities of the various structural schemes and their variants.
The diagrams in (Fig. 9) may be used for computer-based generation of induced diagrams, an example of which may be seen in (Fig. 10).
This diagram provides an insight into the valid transmission ratio combinations of the gearbox, white the equations enable the basic torque ratios to be determined for the respective numbers of gear teeth.

Based on the formulae deduced for the efficiency as a function of the torque ratios and the basic efficiencies of the coupling gears, a program is established for determining the most appropriate structural scheme and its parameters from the standpoint of minimal losses.

6.3 Power circulation

Of all the schemes in review 15, 16, 35 and 36 are with internal power division (branching out) and the others are with internal power circulation (as in the case of gears with three external shafts [4]).
It has been established that in the schemes of the main diagonal of Table 1 (the symmetrical structural schemes) the direction of power circulation in one and the same variant is changed according to the magnitude of the torque ratios of the coupling gears. In the rest of

the structural schemes with power circulation the direction of the circulating power is not changed.

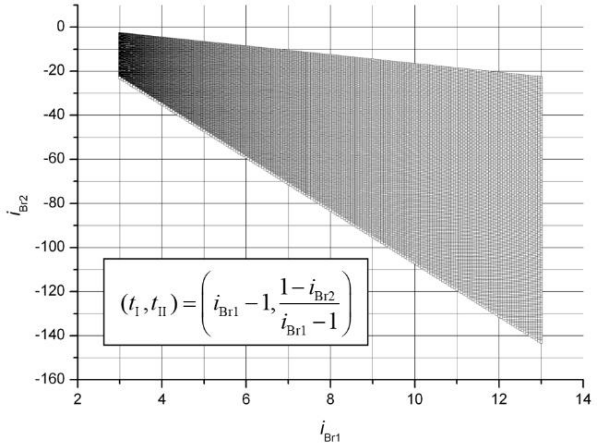

Fig. 10. *Diagram of valid transmission ratio combinations for S13V3 planetary gearbox*

7. Conclusion

All possible structural schemes of coupled two-carrier planetary gears with four external shafts and two brakes, working with one degree of freedom have been reviewed.

The analysis shows that it is sufficient to review just 12 structural schemes with the 6 possible variants for locating the brakes.

Relations have been deduced for determining the speed ratios and efficiencies for all the variants of the schemes in review.

An analysis has been conducted and recommendations have been given for when a certain scheme is appropriate to be used.

The analytical results are shown in Table 2, which allows the quick orientation in the kinematic capabilities of the structural schemes in review.

Program products have been established for kinematic and force analysis of the structural schemes, facilitating the designer in the choice of the most appropriate structural scheme and its parameters.

A 3D model of the S13V3 was developed for $i_{Br1} = 5$ and $i_{Br2} = -30$.

Table 2. *Kinematic capabilities of the different variants of the structural schemes in review*

11	**12**	**13**	**14**	**15**	**16**
V1 – **ret.**	V1 – **ret.**	V1 – **ret.** **!**	V1 – **ret.** **!**	V1 – **rev.**	V1 – **rev.** **!**
V2 – **ret.** $t_I > t_{II}$ – **rev.** $t_I < t_{II}$	V2 – **rev.**	V2 – **rev.**	V2 – **rev.** **!**	V2 – **ret.**	V2 – **ret.**
V3 – **rev.** $t_I > t_{II}$ – **ret.** $t_I < t_{II}$	V3 – **ret.**	V3 – **rev.** **!**	V3 – **ret.**	V3 – **ret.**	V3 – **ret.** **!!**
V4 ≡ V2	V4 ≡ V3	V4 – **rev.**	V4 – **ret.**	V4 – **ret.** $i_{V41} \approx i_{V42} \approx 1$	V4 – **ret.** $i_{V41} \approx i_{V42} \approx 1$
V5 ≡ V3	V5 ≡ V2	V5 – **ret.** r.-m.	V5 – **rev.**	V5 – **ret.** r.-m.	V5 – **ret.** r.-m. $i_{V51} \approx i_{V52} \approx 1$
V6 – **ret.**	V6 – **ret.** r.-m.	V6 – **ret.** **!**	V6 – **ret.** r.-m. $i_{V61} = 1 + t_{II}$ $i_{V62} \approx 1$	V6 – **rev.** r.-m.	V6 – **rev.** $i_{V61} \approx 1$ $i_{V62} = t_{II}$
33	**34**	**35**	**36**	**55**	**56**
V1 – **ret.**	V1 – **ret.** r.-m.	V1 – **rev.** r.-m.**!**	V1 – **rev.** $i_{V11} \approx i_{V12} \approx 1$	V1 – **ret.** $\frac{i_{V11}}{i_{V12}} = \frac{t_I}{t_{II}}$	V1 – **rev.** **!**
V2 – **ret.** $t_I > t_{II}$ – **rev.** $t_I < t_{II}$	V2 – **rev.** r.-m. **!**	V2 – **ret.** r.-m. **!**	V2 – **ret.** **!**	V2 – **ret.** $t_I > t_{II}$ – **rev.** $t_I < t_{II}$	V2 – **ret.**
V3 – **rev.** $t_I > t_{II}$ – **ret.** $t_I < t_{II}$	V3 – **ret.** $i_{V31} \approx 1$ $i_{V32} = t_{II} + 1$	V3 – **ret.** $i_{V31} \approx i_{V32} \approx 1$	V3 – **ret.** $i_{V31} \approx 1$ $i_{V32} = 1 + \frac{t_I}{t_{II}}$	V3 – **rev.** $t_I > t_{II}$ – **ret.** $t_I < t_{II}$	V3 – **rev.** r.-m.
V4 ≡ V2	V4 – **ret.** $i_{V41} \approx i_{V42} \approx 1$	V4 – **ret.** $i_{V41} \approx i_{V42} \approx 1$	V4 – **ret.**	V4 ≡ V2	V4 ≡ V3
V5 ≡ V3	V5 – **rev.** r.-m. **!**	V5 – **ret.** r.-m. **!**	V5 – **ret.** r.-m.	V5 ≡ V3	V5 ≡ V2
V6 – **ret.**	V6 – **ret.** r.-m. **!**	V6 – **rev.** r.-m. **!**	V6 – **rev.** **!**	V6 – **ret.**	V6 – **ret.** r.-m. Suitable for $i_{Br.2} = \frac{1}{i_{Br.1}}$

Note: The following abbreviations are used in the table:
ret. – the rotational direction is retained when working with different brakes;
rev. – the rotational direction is reversed when working with different brakes;
r.-m. – the gear works either as a reducer or as a multiplier according to which brake is activated;
! – the variant is capable of obtaining a significant difference between the two output angular velocities.

It was proven that the layout variant is kinematically feasible, and that there is a noticeable difference in the size of the simple component gearsets. The gearset will have a complex arrangement, as hollow shafts will be required for its operation, and electrically operated band brakes will be used to change the transmission ratio.

8. References

[1] Arnaudow, K., D. Karaivanov. Systematik, Eigenschaften und Möglichkeiten von zusammenge-setzten Mehrsteg-Planetengetrieben. Antriebstechnik, Nr. 5, 2005, 58-65.
[2] Arnaudov, K., D. Karaivanov. Planetary gear trains. Boca Raton. CRC Press, 2019.
[3] Arnaudov, K., D. Karaivanov. Planetary gear trains. Chapter 22. In: Dudley's handbook of practical gear design and manufacture. IV Edition. Edited by Stephen P. Radzevich, Boca Raton, CRC Press, 2021.
[4] Karaivanov, D., K. Arnaudov. Kinematic and power analysis of multi-carrier planetary change-gears through the torque method, pp. 291-325. In: Advances in gear design and manufacture. Edited by Stephen P. Radzevich. Boca Raton, CRC Press, 2019.
[5] Troha, S., Ž. Vrcan, D. Karaivanov, M. Isametova. The selection of optimal reversible two-speed planetary gear trains for machine tool gearboxes. Facta Universitatis, Series: Mechanical Engineering. 18-1, 2020, 121-134.
[6] Troha, S., J. Stefanović-Marinović, Ž. Vrcan, M. Milovančević. Selection of the optimal two-speed planetary gear train for fishing boat propulsion. FME Transactions 48-2, 2020, 397-403.
[7] Troha, S., N. Lovrin, M. Milovančević. Selection of two-carrier shiftihg planetary gear train controlled by clutches and brakes. Transactions of FAMENA. XXXVI-3, 2012, 1-12
[8] Kudryavtsev, V. N., Iu. N. Kirdyashev (ed.). Planetary gears. Handbook. Leningrad, Mashinostroenie, 1977 (in Russian).
[9] Arnaudov, K., D. Karaivanov. Engineering analysis of two-carrier planetary gearing through the lever analogy. In: Proceedings of the International Conference on Mechanical Transmissions, April 5-9, 2001, Chongqing, China, *China Machine Press*, 44-49.
[10] Karaivanov, D. Theoretical and experimental studies of the influence of the structure of the coupled two-carrier planetary gear trains on its basic parameters [dissertation], Univ. of Chem. Technology and Metallurgy, Sofia, 2000 (in Bulgarian).
[11] Karaivanov, D, S. Troha. On the structural Analysis of Coupled Planetary Gears. Mashinostroene & elektrotehnika, Special edition – science edition 9, 2005, 76-83.
[12] Looman, J. Zahnradgetriebe. Berlin, Springer Verlag, 1996.
[13] Müller, H. W., Epicyclic drive trains. Detroit, Wayne State University Press, 1982.
[14] Lechner, G., H. Naunheimer. Automotive transmissions. Berlin, Springer-Verlag, 1999.
[15] Leistner, F., G. Lörsch, O. Wilhelm. Umlaufrädergetriebe. 3. Auflage. Berlin, VEB Verlag Technik, 1987.

Impact of the Number of Passengers in the Vehicle Braking Performances Equipped with Modern Mechatronics Braking System

Shpetim Lajqi, Agron Syla, Naser Lajqi, Gazmend Krasniqi*
University of Prishtina "Hasan Prishtina", Faculty of Mechanical Engineering, Kosovo
*Corresponding author: gazmendkrasniqi89@gmail.com

Abstract: *Modern vehicle braking systems mainly are based on deceleration of vehicle and tire slip control. Trends in improving vehicle braking performance give rise to a large variety of braking systems and control strategies. An anti-lock braking system is an electronic braking process control system, which greatly increases the ability of the driver and vehicle to avoid road accidents even during difficult braking conditions or circumstances. The load (number of passengers in the vehicle) which is transmitted to the road surface through the vehicle tires is an issue which directly affects the braking efficiency of the vehicle during stopping. The braking efficiency also depends on the material of the road surface, climatic condition, road condition, vehicle speeds and tire condition.*

The purpose of this paper is investigation the impact of the number of passengers in the vehicle during the braking process, respectively to determine the performance of the braking of vehicles equipped with modern mechatronic braking systems such as: Antilock Braking System, Electronic Braking System, Emergency Brake System and Electronic Brake-force Distribution System.

The braking performance of the vehicle was determined experimentally through the XL Meter device which was fixed on the windshield of the VW Polo vehicle. The tests were performed on asphalt roads for different speeds of 40, 60 and 80 km/h. The determination of the center of gravity of the vehicle and the reaction forces in the front and rear axles was performed through the devices in the Motor Vehicle Laboratory of the Faculty of Mechanical Engineering and the developed mathematical model for calculating static and dynamic reactions forces for the respective axes. The obtained results will help the traffic experts in the analysis of road accidents.

Keywords*: DISK BRAKE, ROAD, TIRES, REACTION FORCES, FRICTION COEFFICIENT, DECELERATION, BRAKING DISTANCE.*

1. Introduction

Vehicle safety devices are mainly categorized into two main categories: passive and active safety devices [1-3].

Passive safety devices are intended to minimize damage and reduce the risk of injury during the time of impact. Vehicle passive devices are: seat belts, airbags, and the construction of the vehicle and automatically deploy when the vehicles gets into a crash.

Active safety devices works to prevent a vehicle accident and stay active until drive vehicle by continually work to avoid from getting vehicle into an accident. Most active safety devices are: braking system, steering system and other vehicles systems electronically controlled by a computer.

Because of developments of electronics and mechatronics, active safety systems have been greatly improved. They include traction control, electronic stability control, and braking systems.

In order to increase braking efficiency, maintain the stability of the vehicle during the braking process and the maneuverability of the vehicle, Anti-lock Braking Systems (ABS) have been developed since the 80s.

Trends in improving vehicle braking performance give rise to a large variety of braking systems and control strategies. An anti-lock braking system is an electronic braking process control system, which greatly increases the ability of the driver and vehicle to avoid road accidents even during difficult braking conditions or circumstances [4].

ABS consists of the conventional braking system integrated with the Electronic Control Unit (ECU), the Electronic Brake Control Module (EBCM) and the Wheel Speed Sensors for receiving information about the speed of the wheel (rotation), Figure 1.



Fig. 1 *ABS braking system – Brake rigs*

2. Impact of load on the vehicle braking effectiveness - Case study

The calculation of disc and drum brakes is quite specific. During the calculation, the magnitude of the braking torque which can be realized by the brake must be calculated [5].

2.1. Calculation of the braking system

Calculating the forces and braking torque of the disc brakes is relatively simple. Figure 2 shows the scheme of the disc brake and the forces that acting during the braking process. In the given scheme we can see that the force for activating the brake (F_a) is equal to the reaction force of the disk (N).

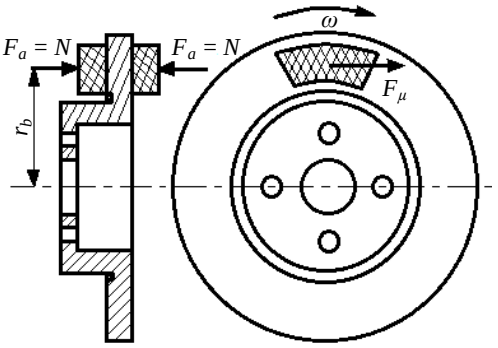

Fig. 2 *Forces acting on the disc brake*

The value of the friction force (F_μ) that acting on both sides of the disc is defined by the expression:

$$F_\mu = 2 \cdot \mu \cdot N = 2 \cdot \mu \cdot F_a \quad (1)$$

The braking torque (T_b) for this case is determined by the expression:

$$T_b = F_\mu \cdot r_b \quad (2)$$

where are:

r_b [m] – radius from the center of disc to the point of action of the frictional force
F_μ [N] – friction force
F_a [N] – braking activating force

This research is focus on the influence of load on the tires and not on the calculation of forces and torques which act on the system.

2.2. Contact between tire and road surface

The contact between the tire and the road surface plays a key role in vehicle dynamics. The interaction between the tire and the road surface can be described by the three forces and three moments as shown in Figure 3.

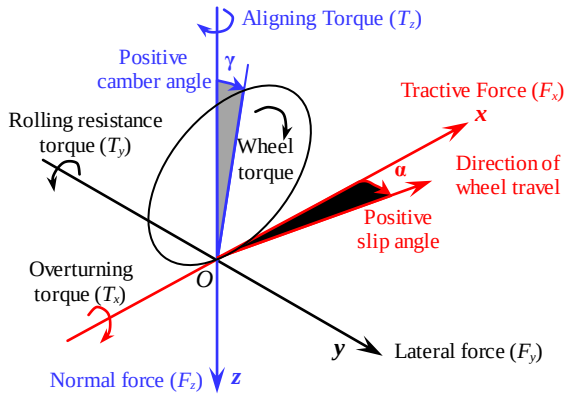

***Fig. 3** Tire contact with road surface*

Tractive force (F_x) can be expressed as a function of the friction coefficient (μ_x):

$$F_x = \mu_x\,(\lambda, \alpha, \gamma, F_z) \tag{3}$$

2.3. Calculation of friction coefficient

To determine the friction coefficient is required to know values of normal force (F_z), longitudinal slip (λ), lateral slip angle (α), and wheel slope angle (γ), Figure 3.

Since in our case we are not dealing with lateral slipping to simplify the calculation and to make the impact of the changes easier the angles α and γ are assumed zero ($\alpha = 0$, $\gamma = 0$), so friction remains a function of normal load and longitudinal slip.

On the other hand, the longitudinal slip (λ) is:

$$\lambda = \frac{v - r\cdot\omega}{\max(v,\ r\omega)} = \frac{v - \omega\cdot r}{v} \tag{4}$$

when is:

r [m] - is the dynamic radius of the wheel and its value depends on several factors such as: load, number of wheel rotations, and air pressure in the tires.

Since during the measurements are obtained the deceleration values, it will be calculate the coefficient of friction from the expression for calculating the deceleration, as written in the follow:

$$a = \mu_x \cdot g \Rightarrow \mu_x = \frac{a}{g} \tag{5}$$

2.4. Calculation of forces acting on the vehicle during the braking process

The process of braking the vehicle is influenced by many different factors, from the psycho-motor skills of the driver to the smallest element of the system. In terms of forces that affect the braking process there are a number of different forces such as: normal, longitudinal, inertia, air forces and other forces that appear within the system.

In this paper it's foreseen to compare the impact of loads during braking of the vehicle in its longitudinal direction, therefore is calculate only normal and longitudinal forces.

2.5. Calculation of axles reaction forces

To determine axle's reaction forces it is necessary to determine the Center of Gravity of the vehicle (CG), which can be found experimentally by measuring the vehicle curb weight and weight of rear wheel when the vehicle is horizontal plane [6]. The determination of the CG was done by several measurements performed in the Laboratory of the Faculty of Mechanical Engineering, University of Prishtina "HASAN PRISHTINA".

Figure 4 shows the measured dimensions of the vehicle examined in the Faculty Laboratory.

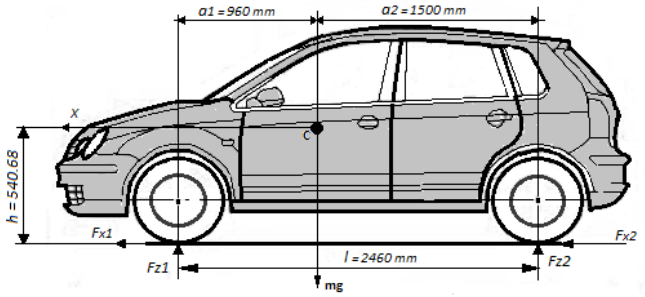

***Fig. 4** Geometric dimensions of VW POLO vehicle*

After the measurement of the mass of the vehicle through digital weight scales in the wheel of the first and rear axles, can be define:

$$a_1 = \frac{2\cdot l}{\text{m}\cdot g}\cdot F_{z2} = \frac{2\cdot l}{2\cdot(F_{z1}+F_{z2})}\cdot F_{z2} = \frac{l\cdot m_2}{m_1+m_2} \tag{6}$$

$$a_1 = \frac{2460\cdot 245}{380+245} = 960\ mm = 0.96\ m \tag{7}$$

$$a_2 = l - a_1 = 2460 - 960 = 1500\ mm = 1.5\ m \tag{8}$$

where are:

F_{z1}, N – Front axle reaction in horizontal plane
F_{z2}, N – Rear axle reaction in horizontal plane
m, kg – Curb mass of vehicle
m_1, m_2– Mass of the half front and rear axles
a_1, m – Distance between CG behind the front axle
a_2, m – Distance between CG in front the rear axle
l, m – Car wheel base

The height of the center of gravity of the vehicle (h) can be determined by assuming the vehicle is set at a certain angle (assume an angle of 30^0), then we have:

$$h = \left(a_2 - 2\cdot\frac{F_{z1(\theta)}}{\text{m}\cdot g}\cdot l\right)\cdot ctg\theta + r_d \tag{9}$$

$$h = \left(a_2 - \frac{m_1}{m_1+m_2}\cdot l\right)\cdot ctg\alpha + r_d \tag{10}$$

$$h = \left(1.5 - \frac{343.75}{380+245}\cdot 2.46\right)\cdot ctg30^0 + 0.293 \tag{11}$$

$$h = 540.68\,mm = 0.5468\,m \tag{12}$$

where are:

h, m - Height of center of gravity from ground level
R, m - Wheel radius (R = 293 mm = 0.293 m for tire 165/70 R14)

Vehicle axle's reaction forces acting on the vehicle during deceleration (a) in a straight horizontal road are affected by components of the static and dynamic forces [5] and can be defined as follows:

$$F_{z1} = (F_{z1})_{sta} + (F_{z1})_{dyn} \tag{13}$$

$$F_{z2} = (F_{z2})_{sta} + (F_{z2})_{dyn} \tag{14}$$

$$(F_{z1})_{sta} = \frac{1}{2}\cdot m\cdot g\cdot\frac{a_2}{l} \tag{15}$$

$$(F_{z1})_{dyn} = \frac{1}{2}\cdot m\cdot g\cdot\frac{h}{l}\cdot\frac{a}{g} \tag{16}$$

$$(F_{z2})_{sta} = \frac{1}{2}\cdot m\cdot g\cdot\frac{a_1}{l} \tag{17}$$

$$(F_{z2})_{dyn} = -\frac{1}{2}\cdot m\cdot g\cdot\frac{h}{l}\cdot\frac{a}{g} \tag{18}$$

As the vehicle deceleration increases, the normal forces on the front wheels increase while on the rear ones decrease, as we only

need the normal forces on the front wheel then only the results of the normal force on the front wheel will be given (F_{z1}).

2.6. Calculation of braking forces

The braking forces acting on the wheels of the vehicle are a function of the normal reaction forces and the coefficient of friction of the wheels and is given by the expression:

$$F_{x1} = F_{z1} \cdot \mu_x \quad (19)$$

where is:

μ_x - Coefficient of friction between tires and road surface

3. Methodology for Evaluation of the Vehicle Braking Performances

The place where the tests were performed is located around of the city of Pristina. For evaluation of braking performance is used professional XL Meter ™ Gamma Pro device which measure acceleration/deceleration in two direction (longitudinal and transverse site).

The ECE R13 regulation is mandatory for measuring braking efficiency. According to this "The efficiency of the braking system is determined by the braking distance or the average deceleration during braking".

The braking distance (S_f) is calculated from the double integration of the acceleration data in the braking interval. The Successful evaluation gives the following results:

- Distance in the time of braking (S_f[m]),
- Initial vehicle speed at the time of braking (V_0 [km/h]),
- Time from the start till the end of braking (T_{br} [s]), and
- Averaged maximal vehicle deceleration (*MFDD* [m/s^2]).

The vehicle deceleration (*MFDD* = a_2) is estimated as the average deceleration of the vehicle motion distance in the range from speed V_b to speed V_e as written in the follow:

$$MFDD = \frac{V_b^2 - V_e^2}{25.92 \cdot (S_e - S_b)} \quad (20)$$

In Figure 5 are presented equipment and type of road surface (old and new asphalt) for measuring vehicle braking performance.





Fig. 5 *Equipment and testing polygon for measuring vehicle braking performance [7]*

4. Measuring results from test drive

Type of the vehicle used to test braking performance has been VW Polo, 2002 model year, with ABS braking system. Test drives have been performed in the testing polygon with different loads and road surfaces (old asphalt and new asphalt), Figure 5.

The evaluation of the braking performance has been carried out with a professional devices called "XL Meter" where in each testing cases on the board of vehicle was one and four passengers [8-9].

In Table 1 are presented vehicle technical data in order to known performance of braking system for VW Polo.

Table 1 *Technical vehicle data for VW Polo*

Characteristics		Data
Year of production:		*2002*
ABS (ON/OFF) :		*ON*
Tire dimension:		*165/70 R14*
Weather temperature:		*22 [°C]*
Road surface:		*Dry asphalt with significant roughness*
Seat numbers:		*5*
Vehicle geometry	length:	*3897 [mm]*
	width:	*1650 [mm]*
	height:	*1465 [mm]*
Engine	Fuel:	*Petrol*
	Volume:	*1198 [cm^3]*
	Power:	*54 [HP]*
	Torque:	*106 [Nm]*
Capacity of reservoir:		*45 [l]*
Total weight:		*1530 [kg]*

The investigation on the vehicle braking performance was done with the vehicle VW Polo, manufactured in 2002 and equipped with ABS system. Testing was performed on roads with old and new asphalt through the XL Meter device. The obtained results are presented through diagrams and tables.

Figure 6 shows the braking efficiency parameters for the initial braking speed V_0 ~ 60 [km/h] when there were driver + 3 passengers and when there was only the driver.

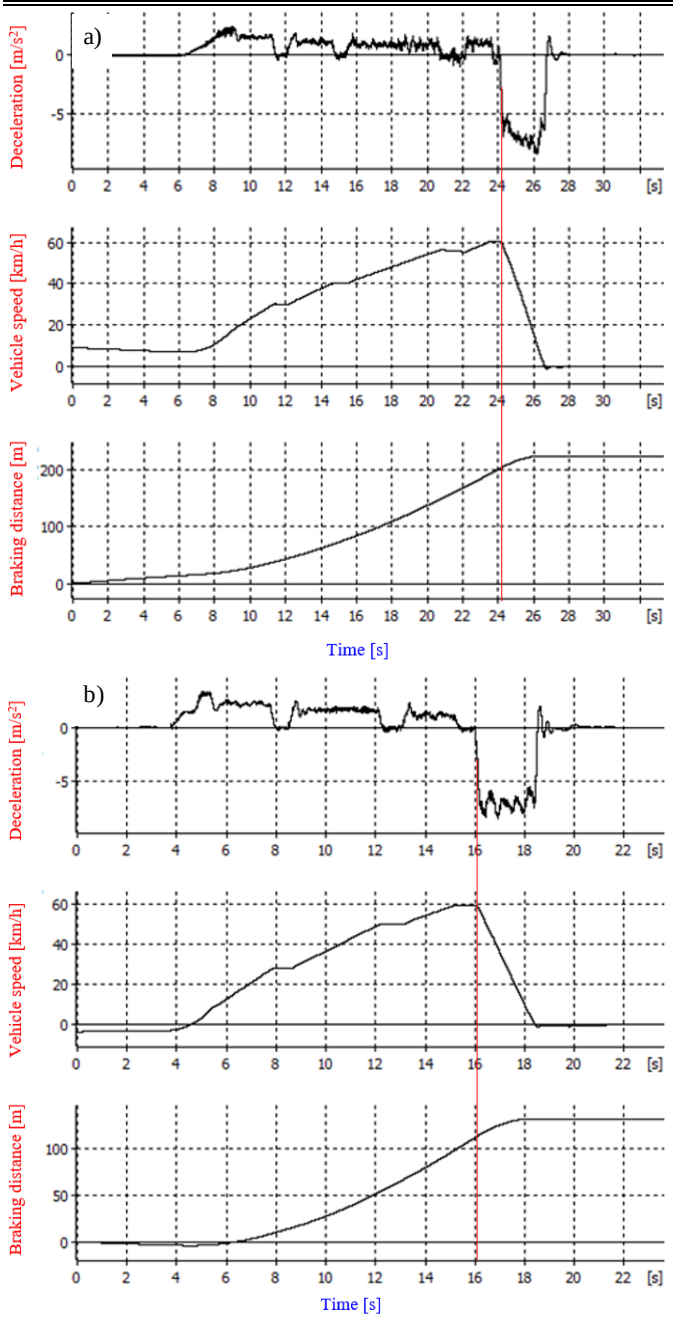

Fig. 6 *Braking parameters for the initial braking speed V_0 ~ 60 [km/h] for the case when in the vehicle board were: a) driver + 3 passengers and b) driver*

In Table 2 are presented the main braking parameters for VW POLO obtained by measuring during the vehicle braking process on the road with old asphalt for two cases when in the vehicle board were: driver + 3 passengers and only the driver. Test was done when during braking process driver has pressed clutch and initial braking speed was 60 and 80 [km/h].

Table 2 *Obtained braking parameters for the initial braking speed of 60 & 80 [km/h] when in the vehicle board were: driver+3 passengers and only driver*

Characteristics	Driver + 3 passengers		Driver		Differences | [%] |	
V_0 [km/h]	61.28	80.49	60.57	81.65	~60.00	~ 80.00
S_f [m]	22.98	37.62	20.87	39.65	10.11	5.12
T_{br} [s]	2.62	3.37	2.48	3.50	5.65	3.71
MFDD [m/s²]	7.12	6.92	7.13	6.59	0.14	5.01
Z (MFDD) [%]	72.50	70.60	72.70	68.90	0.28	2.47
$\mu_x = MFDD/g$	0.72	0.70	0.73	0.67	1.37	4.48
F_{z1} [N]	6231.11	6191.11	6058.15	5971.43	2.86	3.68
$F_{x1} = F_{z1} \cdot \mu_x$ [N]	4486.40	4333.78	4422.45	4011.39	1.45	8.04

In Table 3 are presented the main braking parameters for VW POLO obtained by measuring during the vehicle braking process on the road with old and new asphalt for case when in vehicle board was only driver. Test was done when during braking process driver has pressed clutch and initial braking speed was 40 and 60 [km/h].

Table 3 *Obtained braking parameters for initial braking speed of 40 & 60 [km/h] when in the vehicle was only driver on road with old and new asphalts*

Characteristics	Old asphalt		New asphalt		Differences | [%] |	
V_0 [km/h]	40.17	60.57	39.99	59.14	~40.00	~60.00
S_f [m]	9.99	20.87	9.22	17.75	8.35	17.58
T_{br} [s]	1.76	2.48	1.64	2.09	7.32	18.66
MFDD [m/s²]	6.68	7.13	7.07	8.36	5.51	14.71
Z (MFDD) [%]	68.1	72.70	72.10	85.20	5.55	14.67
$\mu_x = MFDD/g$	0.68	0.73	0.72	0.85	5.56	15.29
F_{z1} [N]	5989.22	6058.15	6058.63	6284.21	1.45	3.60
$F_{x1} = F_{z1} \cdot \mu_x$ [N]	4072.67	4422.45	4362.21	5341.57	6.64	17.20

5. Conclusions

Based on the performed tests and the calculations done, it can be seen that in cases of loading the vehicle with different loads, the forces acting on the vehicle tires, as well as the coefficient of friction, will change by affects the overall performance of the braking system.

From the performed tests it is noticed that the braking efficiency for the case when in the vehicle is only driver is about 10% higher than in the case when except driver are 3 passengers in the vehicle. It has been proven that the braking distance is shorter in the case when driver during braking press clutch pedal.

For different road surfaces, the coefficient of friction between tire and road surface has different values and plays a major role in braking efficiency. Different loads and vehicle speeds takes different values of coefficient of friction. The measurement confirmed that the braking distance is 17.58% less for new asphalt compared with old asphalt at initial braking speed 60 [km/h].

6. References

[1] Shpetim Lajqi, Stansilav Pehan. *Designs and Optimizations of Active and Semi-Active Non-linear Suspension Systems for a Terrain Vehicle*. Strojniški vestnik - Journal of Mechanical Engineering, pp. 732-743, 58(12), 2012.

[2] Sh. Lajqi, J. Gugler, N. Lajqi, A. Shala, R. Lika. *Possible Experimental Method to Determine the Suspension Parameters in a Simplified Model of a Passenger Car*. International Journal of Automotive Technology, pp. 615-621, 13(4), 2012,

[3] Shpetim Lajqi. *Mechatronic of Vehicle*. Dispense for students. University of Prishtina, Faculty of Mechanical Engineering, Prishtina, 2020.

[4] Agron Syla. *Examination of Advanced braking systems of the vehicles and their effectiveness on the braking*. *Master Thesis*. University of Prishtina "HASAN PRISHTINA", Faculty of Mechanical Engineering, Prishtina, 2020.

[5] Heset Cakolli. Methods for calculation of motor vehicles. Dispense for students. University of Prishtina, Faculty of Mechanical Engineering, Prishtina, 2015.

[6] Naser Lajqi. *Exploitation and Maintenance of Vehicle*. Dispense for students. University of Prishtina, Faculty of Mechanical Engineering, Prishtina, 2010.

[7] XL Meter ™ Gamma Pro / http://www.nehodar.cz/docs/xlmdatasheet.pdf (access 15.01.2021).

[8] Ramadan Mazrekaj, Naser Lajqi, Egzon Tofaj. *Influence of Tires Age on Vehicle's Braking Performance: a Case Study*. International Review of Mechanical Engineering, Volume 14, No 10 (2020), pp. 646-657, DOI: https://doi.org/10.15866/ireme.v14i10.20235.

[9] Ramadan Mazrekaj, Shpetim Lajqi, Fevzi Mema, Naser Lajqi. *The Influence of the Vehicle Shock Absorber Wearing on the Performance of the Braking System – A Case Study*. International Journal on Engineering Applications, Volume 9, No 3 (2021), pp. 137-147, DOI: https://doi.org/10.15866/irea.v9i3.20493

A new commercial dishwasher design using mineral additives in its drying system

Zafer Kahraman[1], Soner Gürcü[1], Murat Hacı[1], Hakan Serhad Soyhan[2,3]
[1]Öztiryakiler Madeni Eşya San. Ve Tic. A.Ş, R&D Technology Center
34500 Büyükçekmece, İstanbul, Turkey
[2]Sakarya University, Faculty of Engineering, Department of Mechanical Engineering
54050 Serdivan, Sakarya, Turkey
[3]Team-San Ltd. Sti., Esentepe Campus, Sakarya University, 54050, Sakarya, Turkey
zkahraman@oztiryakiler.com.tr

Abstract: *Commercial dishwashers in different performance classes are used in all industrial kitchens. In contrast to existing commercial dishwashers, there is an increasing demand for products that use drying technology to meet customer wishes and needs. Various household dishwashers having zeolite mineral during drying prevents water droplets and detergent stains (including surfaces of plastic containers) on the surfaces of dishes and rinsing of sensitive products (crystal glass glasses, etc.). By pointing out that they prevent excess steam from spreading when opened, they highlight these products as environmentally friendly and value-adding compared to conventional household products. In this work, we developed a new commercial dishwasher prototype using a mineral in the drying process. Technical simulations and experiments are used during the development of our innovative prototype with a drying system using a mineral that stores moisture and converts it into thermal energy. This is the first prototype in commercial dishwashers with its innovative drying system.*

Keywords*: COMMERCIAL DISHWASHERS, MINERAL ADDITIVE DRYING TECHNOLOGY*

1. Introduction

Commercial dishwashers of different capacities are used in all commercial catering establishments (restaurants, factories, universities, dormitories, etc.). Our company manufactures commercial dishwashers in various models and capacities.

Commercial dishwashers are quite different from household dishwashers according to their working principle and international standards. Commercial dishwashers wash in a very short time compared to household dishwashers. While household dishwashers can wash in 2-3 hours, commercial dishwashers can wash in 60-180 seconds according to the program.

Conveyor-type commercial dishwashers only dry with a snail fan and no minerals are used during the drying process. However, there are mineral additive drying systems in various household dishwashers. Adsorbent minerals can be used as drying minerals.

Adsorbent minerals (zeolite, activated alumina, silica gel, etc.) are widely used as solid desiccants in different fields (chemistry, medical, ventilation, food, etc.) due to their high moisture absorption properties [1-5].

There is no scientific publication on the commercial dishwasher that saves energy and cleaning chemicals with its mineral-added drying system. The limited studies on mineral additive drying applications only in household dishwashers are summarized below.

Italian Santori and his research group evaluated their absorbent properties thermodynamically by using various commercial desiccant minerals (13X zeolite, SAPO-34 zeolite and silica gel, etc.) in a household dishwasher. The specific heat values of the drying minerals (13X zeolite, SAPO-34 zeolite and silica gel, etc.) were investigated with increasing temperature and the specific heat values of all minerals increased linearly with increasing temperature (Fig. 1) [6].

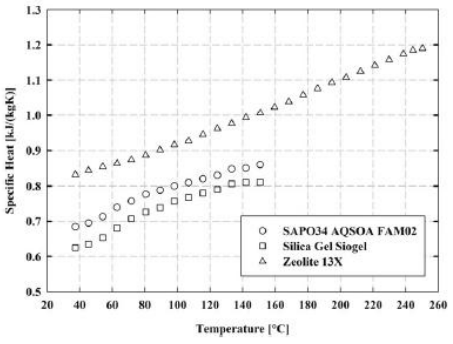

Fig. 1 *Specific heats of the investigated adsorbent materials [6].*

They reported that they contributed to energy saving at various rates by using these dryers in the standard washing process. They stated that electrical energy consumption (0.636 kWh) decreased by 41% in the standard washing process compared to standard type household dishwashers labeled with A energy class [6].

A. Hauer and F. Fischer from Germany evaluated the energy consumption of the household dishwasher they developed compared to standard household dishwashers with the adsorption process using Zeolite (X13 commercial model). They reported that the developed mineral-added (zeolite) household dishwasher saves up to 24% of energy compared to standard household dishwashers [7].

The schematic description of the adsorption and desorption processes is shown in Fig. 2 [7].

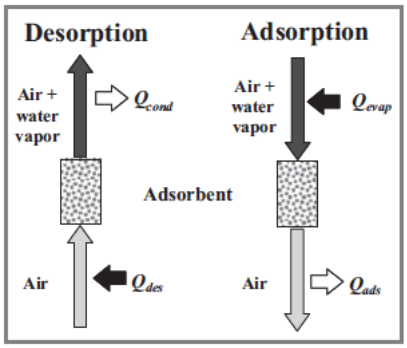

Fig. 2 *Open sorption system (heat and mass fluxes) [7].*

The schematic view of the household dishwasher with an adsorption drying system and the temperatures measured using zeolite are shown above. They reported that energy consumption was reduced by up to 24% by reducing the energy consumption values from 1.05 kWh to 0.8 kWh compared to the standard product in household dishwashers with zeolite mineral additive drying system. In addition, they reported that an environmentally friendly product was obtained by contributing to the reduction of CO2 emission rates with the mineral additive drying system [7].

The effects of Zeolite 13X, Silica Gel 125, SWS-1L and SBA-15 E120 on the drying process in household dishwashers were investigated by M. Erdogan from Aachen University in Germany and her research group [8].

D. Lefebvre from Canada and his research group investigated thermal energy storage processes in heating applications for energy storage technologies. The adsorption process is an exothermic reaction [9].

There are different studies using various minerals in the drying process. Within the scope of this study, the drying performance was evaluated for the first time in the field of the first commercial dishwasher by using adsorbent minerals for the drying process.

2. Methodology

The commercial dishwasher prototype, which provides innovative mineral additive drying, was developed based on our company's most widely used under-counter model in the industrial field.

A mineral additive drying system has been placed on the back of the commercial dishwasher prototype, specific to the design. With the air suction channel on the upper part of the washing chamber, the suction of the steam is provided towards the mineral container. The absorbed steam is sent to the mineral container with the help of the fan. With the exothermic reaction in the mineral container, mineral moisture is absorbed and the hot air formed is sent to the dishes from the bottom with the fan. Thus, effective drying of the dishes in the washing chamber is ensured.

The innovative commercial dishwasher prototype captures the steam coming from the upper part of the washing chamber and converts it into heat energy. The heated air is sent from the lower part to the dishes waiting in the washing chamber, and the drying process is carried out.

Drawing of innovative commercial dishwasher prototype with mineral additive drying system is given in Fig. 3.

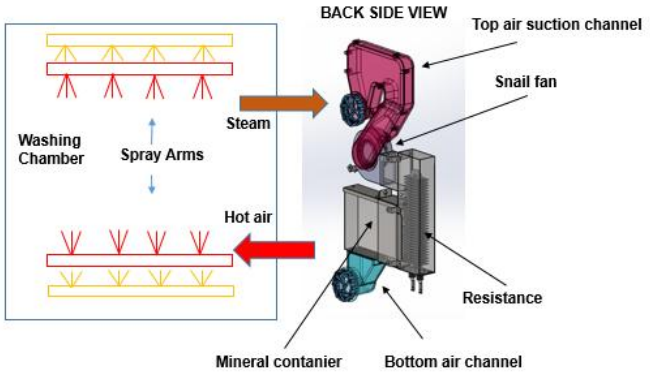

Fig. 3 *Drawing of innovative commercial dishwasher prototype with mineral additive drying system.*

The drawing of the commercial dishwasher prototype (backside) providing drying with mineral additives is given in Fig. 4

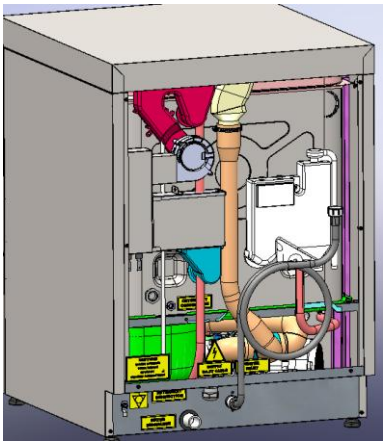

Fig. 4 *Schematic representation of the commercial dishwasher prototype (back side).*

A view of the innovative commercial dishwasher prototype (from the front side) is given in Fig. 5.



Fig. 5 *View of the innovative commercial dishwasher prototype from front side.*

The appearance of the commercial dishwasher prototype (interior and backside) is given in Fig. 6.



Fig. 6 *View of the innovative commercial dishwasher prototype from different sides (interior and back side).*

3. Experimental procedure

After the design verification phase of the innovative prototype was completed, prototype manufacturing and assembly were carried out. After this stage, testing and evaluation were carried out. Drying performance with different minerals (zeolite and activated alumina) on the drying system of the innovative commercial dishwasher prototype was evaluated.

The photos of the minerals (zeolite and activated alumina) used in the drying process in the innovative commercial dishwasher prototype are given in Fig. 7.



Fig. 7 *Minerals (zeolite and activated alumina) used in the drying process in the innovative commercial dishwasher prototype.*

The images of the various parts that make up the drying system of the commercial dishwasher prototype, which saves energy and cleaning chemicals with its innovative drying system, are given in Fig. 8.

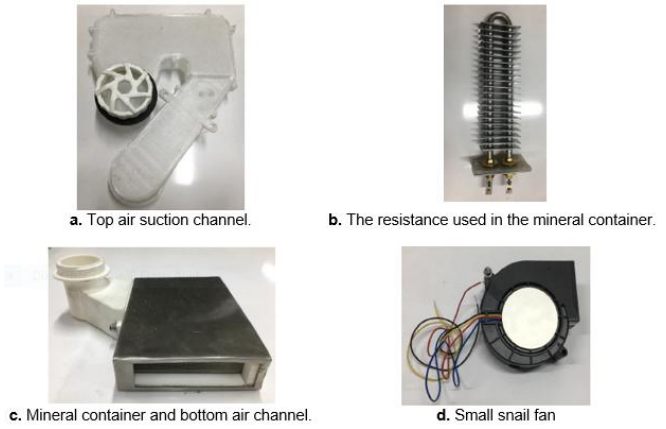

Fig. 8 *The images of the various parts that make up the drying system of the commercial dishwasher prototype.*

Temperature values were measured by using zeolite in the drying process (from the upper suction point and the lower blowing point) in the innovative commercial dishwasher prototype (Fig. 9).

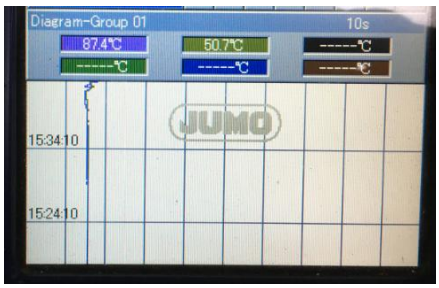

Fig. 9 *Temperature values measured by using zeolite in the drying process (from the upper suction point and the lower blowing point) in the innovative commercial dishwasher prototype.*

4. Conclusions

Following the R&D studies on the innovative drying system commercial dishwasher prototype, the following outputs were achieved;

With studies based on R&D systematics in the industrial kitchen sector, 100% adsorbent minerals (zeolite, activated alumina) are used in the drying system compared to our standard commercial dishwasher (OBY 500 model – no drying system) in the innovative drying system commercial dishwasher.

In the innovative prototype, the temperature of the air drawn into the drying system by the fan after the washing process is 50.7°C at the upper entrance, while the hot air is blown into the washing chamber from the lower part as 87.4°C with the zeolite drying system, contributing to drying. In the use of activated alumina, the blowing temperature remained only around 60°C. After the tests for drying performance, it was determined that zeolite adsorbent provides more drying compared to activated alumina.

In the sector of commercial dishwashers, for the first time in our country, 20,51% energy consumption (4.372 kW/h) has been reduced in the innovative drying system commercial dishwasher compared to our standard commercial dishwasher (OBY 500 model – 5.5 kW/h).

With the original design and prototype manufacturing, an innovative drying system commercial dishwasher using minerals (zeolite and activated alumina) was obtained for the first time in our country compared to existing commercial dishwashers. In addition, it has been achieved to obtain an innovative product with high added value in the industrial kitchen area by providing features that contribute to energy savings.

Acknowledgement

This study was prepared within the scope of TÜBİTAK-TEYDEB 1501 coded Industrial Research Technology Development and Innovation Projects Support Program titled "Commercial Dishwasher Design and Prototype Manufacturing with the Innovative Drying System to be Developed" and numbered 3191398. We would like to thank TÜBİTAK-TEYDEB Machine-Manufacturing Technologies Group (MAKİTEG) for their contribution to the project.

5. References

1. L. Cao, Z. Li, S. Xiang, Z. Huang, R. Ruan, Y. Liu, Bioresource Tech., **284**, 448-455, (2019)
2. L. Zhang, B. Xue, T. Chen, G. Li, Energy Conv. and Management, **244**, 114457, (2021)
3. X. Mou, Z. Chen, Ult. Sonoche., **70**, 1-11, (2021)
4. H. Abou-Ziyan, D. Abd El-Raheim, O. Mahmoud, M. Fatouh, Applied Energy, **190**, 29-42, (2017)
5. Y. Yang, P. Zhang, L. Wang, Appl. Thermal Eng., **141**, 762-774, (2018)
6. G. Santori, A. Frazzica, A. Freni, M. Galieni, L. Bonaccorsi, F. Polonara, G. Restuccia, Energy, **50**, 170-176, (2013)
7. A. Hauer, F. Fischer, Chem. Ing. Tech., **83**, 61-66, (2010)
8. M. Erdoğan, S. Graf, U. Bau, F. Lanzerath, A. Bardow, Appl. Thermal Eng., **125**, 1075-1082, (2017)
9. D. Lefebvre, F.H. Tezel, Ren. and Sust. Energy R., **67**, 116-125, (2017)

Development and computer modeling of a new forging technology in step-wedge strikers

Andrey Volokitin[1], Andrey Tolkushkin[2], Evgeniy Panin[3], Irina Volokitina[1]
[1]Rudny industrial Institute, 50 let Oktyabrya str. 38, Rudny, 115000, Kazakhstan; e-mail: dyusha.vav@mail.ru
[2]Ural Federal University named after the First President of Russia B. N. Yeltsin, Ekaterinburg, Russia; e-mail: a.o.tolkushkin@urfu.ru
[3]Karaganda Industrial University, Republic av. 30, Temirtau, 101400, Kazakhstan; e-mail: cooper802@mail.ru

Abstract: *A computer simulation of the broaching of the workpiece in step-wedge-shaped strikers of the first and second configurations was carried out by the finite element method. The comparison was made according to the following parameters of the stress-strain state: equivalent strain, average hydrostatic pressure, damage criterion, as well as the deformation force. A comparative analysis of the stress-strain state showed that the second configuration of step-wedge-shaped strikers is the most optimal option for implementing the process of broaching rectangular or square blanks. When using them, a more uniform distribution of the stress state is realized, the deformation processing is sufficiently realized in comparison with the broaching in step-wedge-shaped strikers of the first configuration.*
KEYWORDS: *FORGING, BROACHING, SHEAR DEFORMATION, COMPUTER MODELING, STRESS-STRAIN STATE*

1. Introduction

Achieving real, sustainable and increasing rates of economic growth is one of the long-term priorities of the development strategy of both Russia and Kazakhstan. A significant contribution to the implementation of this priority is made by the metallurgical, mechanical engineering and other metalworking branches of the national economy, which should produce competitive metal products for the markets of the CIS countries and non-CIS countries in the current conditions of a market economy. Obtaining competitive products is conditioned by improving the quality and reducing the cost of its production.

One of the progressive types of metalworking, which allows to significantly reduce the consumption of metal in the production of machine parts, devices, as well as to improve their quality, is metal forming, including forging. However, until recently, the forging processes of ingots and blanks were based on the use of traditional forging tools and inefficient deformation modes. These processes are characterized by low yield coefficients of suitable forgings, their low quality and large forging coefficients, and as a result require significant energy and labor costs.

In this regard, the production of blanks and forgings by new forging methods with a significant reduction in energy and labor costs, improving the quality of forgings is economically profitable. One of the ways to achieve this goal is to use deformation methods and tools that implement shear and alternating deformations in the entire volume of the metal. At the moment, there are many tools for forging that allow both shear and alternating deformations to be realized during the deformation process [1-5]. They have both their advantages and disadvantages. But at the moment there is still no perfect or at least universal tool for forging that implements shear and/or alternating deformations during the deformation process.

For example, the tools that allow metal to be deformed by shear include step strikers [6] and strikers having a wedge-shaped profile in the cross section [7]. These designs of strikers allow to realize intensive shear deformations over the entire volume of the deformed metal in the process of broaching blanks to obtain forgings such as plates and plates made of ferrous metals and alloys. At the same time, the intensification of shear deformations during forging in step strikers occurs to a greater extent in the longitudinal direction, and when using wedge strikers, on the contrary, in the transverse direction.

It was proposed to combine two designs of strikers: stepped and wedge (Fig. 1a) [8]. And on the basis of the already combined design of the strikers, another design of strikers for forging was proposed, characterized in that the lower striker is not a wedge, but a wedge-shaped depression (Fig. 1b) [9].

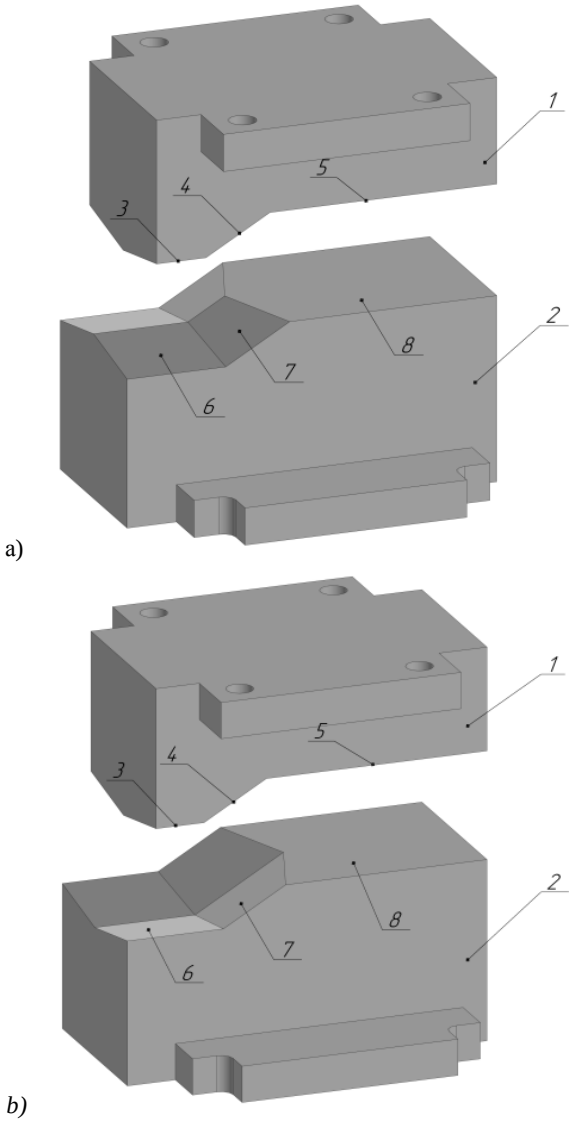

1 – upper striker; 2 - lower striker; 3 – smaller stage with a wedge of the upper striker, 4 - inclined section with a wedge of the upper striker; 5 – large flat stage of the upper striker; 6 – smaller stage with a wedge (a) and a wedge-shaped depression (b) of the lower striker; 7 – inclined section with a wedge (a) and a wedge-shaped depression (b) of the lower striker; 8 - large flat stage of the lower striker

Figure 1 - Step-wedge strikers

2. Simulation methodology

In order to determine the most optimal configuration of step-wedge-shaped strikers, a computer simulation of the broaching

process of blanks in these forging tools was carried out in the Deform-3D software package.

For these studies, two solid-state models of step-wedge-shaped strikers of the first and second configurations with a wedge angle of 160° were constructed. AISI-1035 steel was chosen as the model material for the workpiece. The cross-section of the workpiece was 30x30 mm. The deformation was carried out at a temperature of 1050° with a degree of deformation equal to 10%. After modeling the broaching process, a comparative analysis was carried out on the following parameters: equivalent strain, average hydrostatic pressure, damage criterion, as well as the deformation force. The compared stress-strain state parameters were considered in the longitudinal section of the workpiece, since the broaching operation implies a sequence of compressions when the workpiece moves along its axis.

3. Results and discussion

Fig. 2 shows the results of the distribution of equivalent strain over the entire length of the workpiece. The equivalent strain shows the intensity of the metal processing. Fig. 2 shows that the strikers of both types provide intensive metal processing in the contact layers of the workpiece, where the strain level reaches a value of 1.3-1.5. The central part of the workpiece receives a slightly smaller increase in strain to the level of 1.0-1.1. At the same time, it was revealed that the strikers with a double convexity (Fig. 2a) due to the construction design, they provide greater penetration of strain deep into the workpiece due to a greater degree of compression by inclined sections. However, this effect cannot be called positive. Due to the bi-directional flow of metal in the center of the width of the workpiece (in the area of the junction of the inclined faces), metal clamps will occur, which will negatively affect the condition of the surface, as well as at the level of the damage criterion, which is an indicator of the plasticity resource. Its distribution is shown in Figure 3.

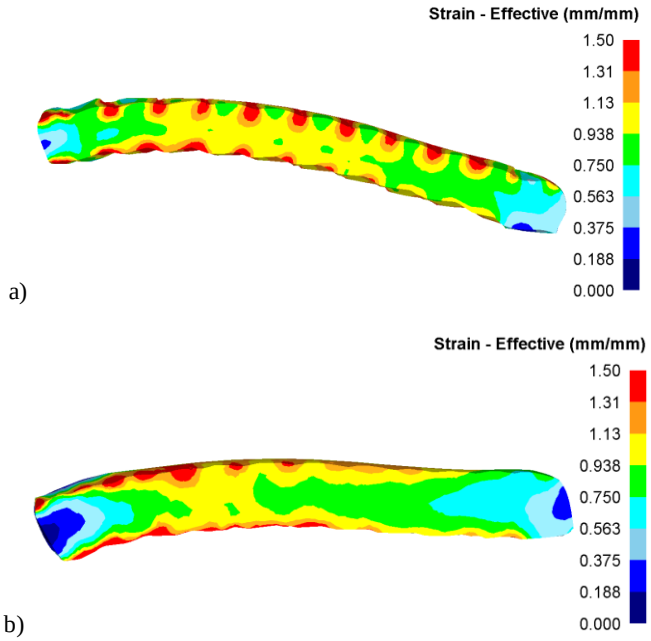

a – strikers with double convexity, b - convex-concave strikers
Figure 2 - Equivalent strain

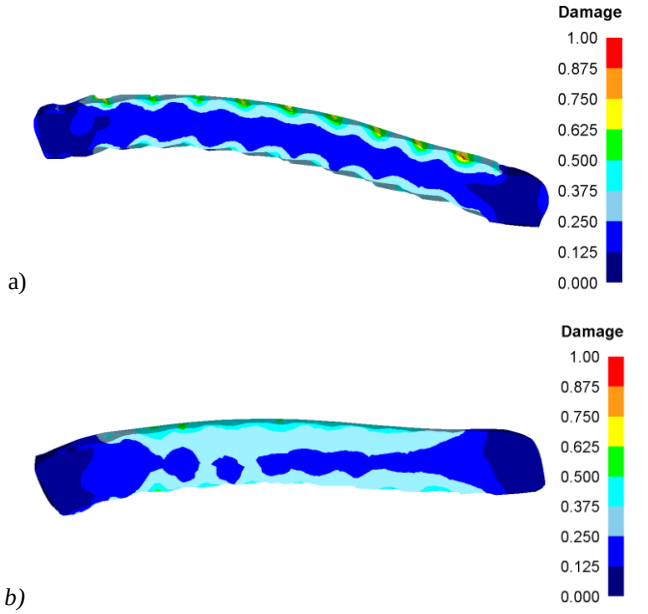

a – strikers with double convexity, b - convex-concave strikers
Figure 3 – Damage criterion

This indicator is calculated by default as the Cockcroft-Latham criterion, and depends on the intensity of the main tensile stresses. Figure 3 shows that in convex-concave strikers, due to the direction of the metal flow along the height in one direction, the level of damage penetrates almost the entire depth of the workpiece, while its level does not exceed 0.5. In strikers with a double convexity, the distribution pattern is diametrically opposite. The depth of penetration of damage is much less here, the main increase in this indicator is in the contact layers of the workpiece. However, due to the occurrence of clamps, the damage level reaches 0.85. This indicates that the option of convex-concave strikers is more preferable from the point of view of the occurrence of surface defects.

To study the average hydrostatic pressure, an intermediate step of deformation was considered, when the workpiece is compressed by all three sections of the strikers at once. This choice is due to the fact that the stress state indicators, in contrast to the equivalent strain, are not cumulative indicators, i.e. they do not accumulate during the deformation process and they are reset when the load is removed. Also, for a correct comparative analysis, it is necessary to set identical dimensional scales regardless of the stresses that occur, which will help to assess the level of stress distribution over the cross-section. The distribution of the average hydrostatic pressure is shown in Figure 4.



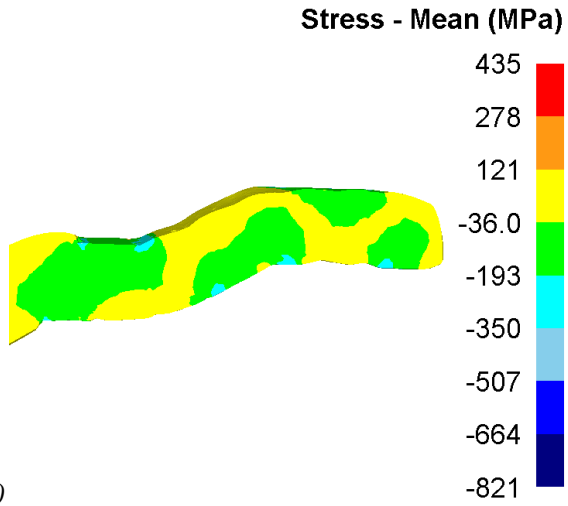

b)

a – strikers with double convexity, b - convex-concave strikers

Figure 4 – Average hydrostatic pressure

Comparing the data in Figure 4, it can be noted that differences in the values of the average hydrostatic pressure and its distribution over the cross-section are observed only in the first two zones of the strikers, where, in fact, there are structural differences. When metal gets into the last zone, which is identical in both structures, there is no special difference in the values of this parameter. Analyzing the obtained values, it can be concluded that the use of strikers with a double convexity due to additional compression by the angle of the joint of the faces on both sides leads to an intensification of compressive stresses. The maximum values are created in the contact layers, reaching -350 MPa, while almost the entire section of the workpiece is also covered by compressive stresses at the level of -180÷-150 MPa. In the strikers of a convex-concave structure, the development of compressive stresses is less intense. Here, the maximum values in the contact layers reach -210 MPa, and in the section of the workpiece they are at the level of -50÷-30 MPa.

After analyzing the obtained distribution pattern of the main parameters of the stress-strain state, it can be concluded the following: the two-way influence of the protruding wedge on the first and second sections in the strikers of the first configuration leads to an intensification of the development of equivalent strain along the entire section of the workpiece, as well as to a higher level of compressive stresses. However, such a scheme of metal flow also leads to an increase in the damage criterion, which, when using strikers with a double convexity, approaches its critical value equal to 1. Convex-concave strikers realize a slightly lower level of metal processing, but in this case the level of damage is much lower. There are also significant differences in the condition of the workpiece surface after broaching. The presence of clamps after the strikers of the first configuration is a negative effect.

Earlier in the work [10] it was shown that the use of step-wedge-shaped strikers is more energy efficient, since the values of the pulling forces in these strikers in comparison with conventional step strikers were on average 30-35% less. Figure 5 shows the graphs of the force during broaching in the strikers of the first and second configurations, built according to the values of the maximum forces in each pass.

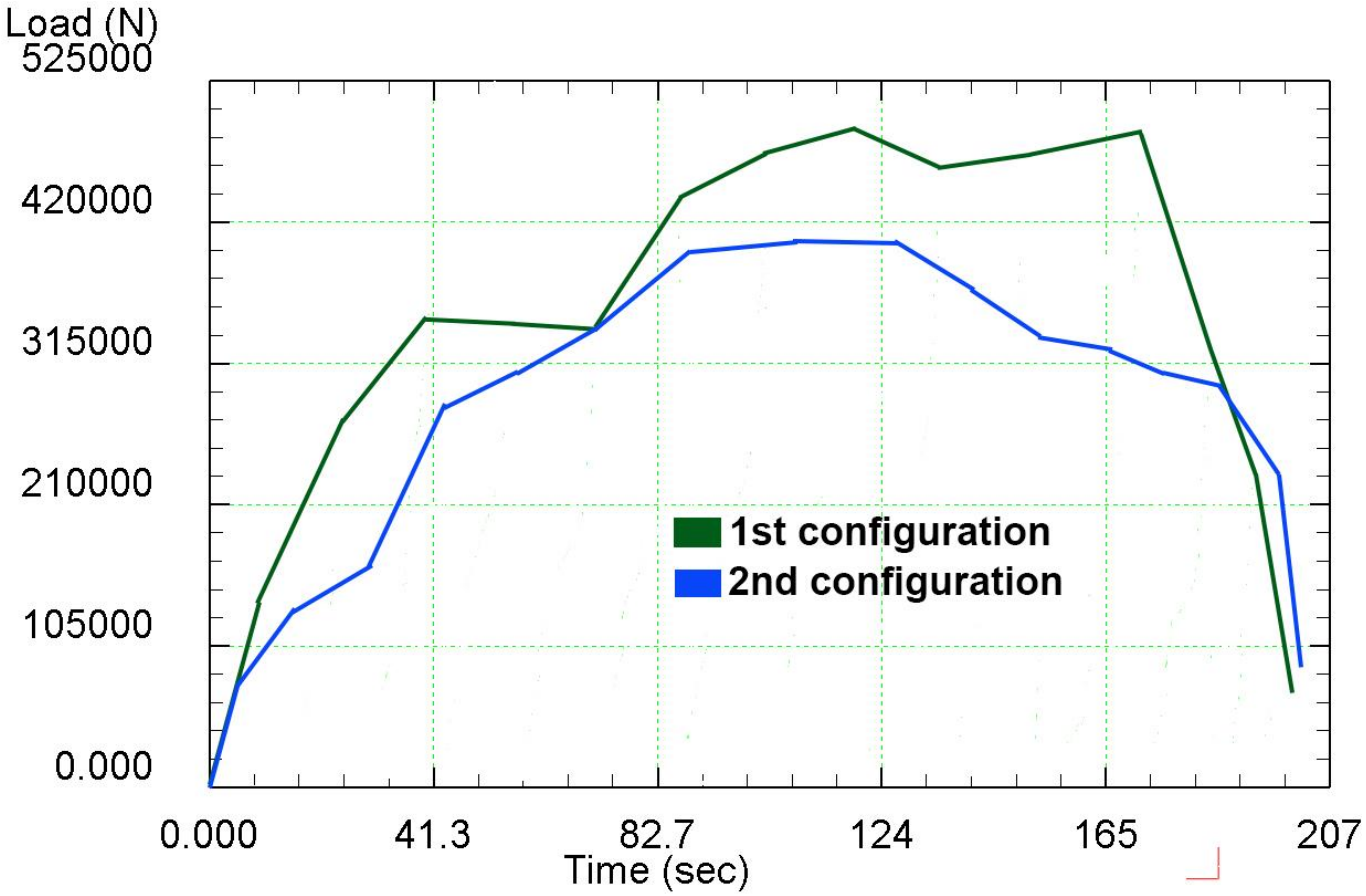

Figure 5 – The values of the forces during broaching in step-wedge-shaped strikers

It can be seen from the graphs that when broaching the workpiece in the strikers of the first configuration due to the intensification of compression, the deformation force has more higher value than when broaching in the strikers of the second configuration, this is especially noticeable when comparing the central areas of the graphs that correspond to the presence of metal in all three zones of the strikers. In the last passes, when the workpiece is no longer located on the first two sections, the force values become comparable.

4. Выводы

A computer simulation of the drawing of the workpiece in step-wedge-shaped strikers of the first and second configurations was carried out by the finite element method. The comparison was made according to the following parameters of the stress-strain state: equivalent strain, average hydrostatic pressure, damage criterion, as well as the deformation force. A comparative analysis of the stress-strain state showed that the second configuration of step-wedge-shaped strikers is the most optimal option for implementing the process of broaching rectangular or square blanks. When using them, a more uniform picture of the distribution of the stress state is realized, the deformation processing is sufficiently realized in comparison with the broaching in step-wedge-shaped strikers of the first configuration. The two-way influence of the protruding wedge on the first and second sections in the strikers of the first configuration leads to an intensification of the development of equivalent strain along the entire section of the workpiece, as well as to a higher level of compressive stresses. However, such a scheme of metal flow also leads to an increase in the damage criterion, which, when using strikers with a double convexity, approaches its critical value. When using convex-concave strikers, the level of damage is significantly lower. There are also significant differences in the condition of the workpiece surface after broaching. The presence of clamps after the strikers of the first configuration is a negative effect. Thus, the expediency of using step-wedge strikers of the second configuration is proved.

Acknowledgments

This research was funded by the Science Committee of the Ministry of education and science of the Republic of Kazakhstan (Grant № AP09057965).

References

1. Шлякман, Б.М., Л.П. Белова, Совершенствование кузнечного инструмента и процесса ковки широких плит, Кузнечно-штамповочное производство, 1990, №6, С. 9-10.

2. Алиев, И.С., Я.Г. Жбанков, И.А. Грачев, Исследование процесса ковки плит плоскими бойками со скосами, Обработка материалов давлением, 2014, №2, С. 69-74.

3. Найзабеков, А.Б., С.Н. Лежнев, С.Ю. Голумбовская, Исследование процесса деформирования заготовок в бойках с упругими элементами, Заготовительное производство в машиностроении, 2006, №7, С. 21-26.

4. Найзабеков, А.Б., С.Н. Лежнев, К.А. Ногаев, Исследование процесса деформирования заготовок в инструменте, реализующем поперечный сдвиг, Изв. вузов. Черная металлургия, 2007, №2, С. 37-41.

5. Андреященко, В.А., Ю.Б. Ичева, Особенности деформационного поведения конструкционной стали при ковке, Вестник Пермского национального исследовательского политехнического университета. Механика, 2018, № 4, С. 7-19.

6. Воронцов, В.К., А.В. Котелкин, А.Б. Найзабеков, Способ изготовления поковок и инструмент для его осуществления, Патент СССР №1409394,1984.

7. Марков, О.Е. Исследование технологического процесса ковки крупных поковок клиновыми бойками, Изв. вуз. Черная металлургия, 2012, №12, С.24-27.

8. Найзабеков, А.Б., С.Н. Лежнев, Е.А. Панин, А.О. Толкушкин, Инструмент для изготовления поковок, Инновационный патент РК №30420, 2015.

9. Найзабеков, А.Б., С.Н. Лежнев, Е.А. Панин, А.А. Богатов, А.О. Толкушкин, Инструмент для изготовления поковок, Патент РК №33694, 2019.

10. Naizabekov, A.B., S.N. Lezhnev, O.N. Krivtsova, A.O. Tolkushkin, Simulation of the new technology of forging of blanks such as slabs and plates made of ferrous metals and alloys, Journal of Achievements in Materials and Manufacturing Engineering, 2014, Vol. 62/2, p. 75-80.

Design and mechanical properties of high-voltage transmission line composite insulators

Monika Fidanchevska, Bojan Mitev, Kristina Micova, Marko Naseski, Atanas Kochov
Ss. Cyril and Methodius University in Skopje, Faculty of Mechanical Engineering, Skopje, Republic of North Macedonia

E-mail: fidancevskam97@gmail.com, bojanmitev77@gmail.com, kristina.micova@yahoo.com, marko.naseski2016@gmail.com, atanas.kochov@gmail.com

Abstract: *Design of high-voltage insulators with a capacity of 12 kV and 24 kV according to standard specifications and determination of the mechanical properties in virtual environment, as well as verification and validation of the results in laboratory conditions was the aim of this paper. The composition of the insulators was 50 vol. % epoxy resin and 50 vol. % SiO_2. Based on the physical and mechanical parameters of high-voltage insulators, 3D models were generated to correlate with them. Virtual simulations of the optimized models were performed by using SolidWorks software based on Finite Element Method. In order to re-examine the results, laboratory tests on physical specimens for determination of tensile, compression and three-point bending strength were conducted. The simulations were positively verified and gave promising results. The research conclusions show that the simulations in virtual environment provide easier and faster design and development of high-voltage insulators, which is of great importance for power transmission network industry.*

KEYWORDS: HIGH-VOLTAGE INSULATORS, VIRTUAL SIMULATIONS, COMPOSITE MATERIAL, POWER TRANSMISSION NETWORK

1. Introduction

There has been huge development in recent years in the field of electrical insulators manufactured from composite materials. Their application is highly dependent on their mechanical, electrical and thermal properties. Major transmission lines consider utilization of non-ceramic insulators and these have become more economically competitive with ceramic types. Composite insulators are beneficial because of their properties, such as: light weight, lower costs of transportation and construction, high strength to weight ratio, better contamination performance and also better transmission line aesthetics [1]. They are gradually replacing ceramic insulators for high voltage transmission and distribution. Various environmental factors (precipitation, pollution, winds, temperature variations) have huge impact on degradation of insulators. Flashover of insulators can cause interruptions in power supply. Therefore insulation performance is of great importance. Parts of composite insulator are: core material, end fitting and rubber insulating housing. The core distributes the tensile load, the end-fitting transmits the tension to the cable and the rubber housing provides electrical insulation [2]. Wide range of polymers are used for outdoor insulation applications, such as: silicon rubber, acryclic resin, nylon, epoxy resin, lignin etc. In order to reduce their drawbacks, suitable micro/ nano inorganic fillers like: zinc oxide, silica, titania, barium titanate have been added to the polymer matrix. Properties of composites can be modified due to the dispersion of the filler in the polymer matrix [3]. Epoxy resins have been of great importance for production of electrical insulators and in order to achieve better performance and commercialization they have been impregnated with inorganic microfillers such as silica. This inorganic microfiller provides not only excellent level of electrical insulation and mechanical strength, but also relatively low cost [4,5].

The utilization of CAD/CAM/CAE software plays important role in the rate and accuracy of decision making in tasks involved for insulators development for new applications. As maintained by the concept of concurrent engineering (CE), integrated system (CAD/CAM/CAE) could reduce the cycle of insulators design and production and proceed the manufacturing of insulators in a less time-consuming period [6].

2. Experimental

2.1 Technical specifications and 3D models of 12 kV and 24 kV high-voltage insulators

The dimensions of 12 and 24 kV insulators made in SolidWorks program are presented in (Fig.1) and suitable 3D models are presented in (Fig.2), respectively. The insulators were designed according to the prescribed standards for the size and dimensions. The design was created by following the basic form of insulators, with small changes in size, thickness and dimension of the ribs. However, height and diameter were maintained according to the standards. This design was obtained, because the insulator should be resistant to mechanical loads and natural influences (rain, atmospheric precipitations and other influences). Additionally, good aerodynamics, which is an important factor needs to be maintained.

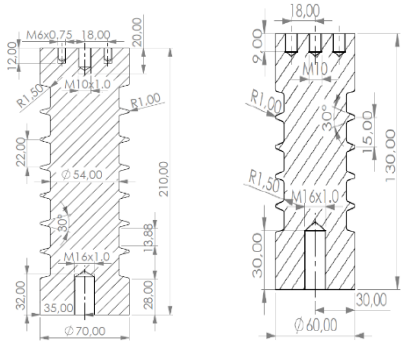

Fig. 1. *Design of 12 kV (left) and 24 kV (right) high-voltage insulator*

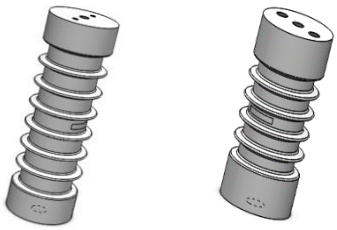

Fig. 2. *3D models of 12 kV (left) and 24 kV (right) high-voltage insulator*

2.2 Materials

Insulators were fabricated from composite material, consisting of 50 vol.% epoxy resin and 50 vol.% silica (SiO_2). As a matrix, two-pack epoxy resin system (epoxy resin and hardener) was obtained from TCM Triune Chemicals and Materials Co.(TCM HE2857/HH2857). Micronized silica with granulation less than 71μm was supplied by company Renova, Tetovo, Republic of North Macedonia.

2.3 Methods- static analysis and laboratory tests verification

The previously created 3D models, shown in (Fig.2), were analyzed via SolidWorks simulation, a static analysis. Simulations were performed according to the standard characteristics of each component and its ratio in the composite. The applied values for elastic modulus and tensile strength were 32820 N/mm^2 and 69 N/mm^2, respectively. In order to compare the 12 kV and 24 kV insulators, 100 kN force was used for each of the simulations. Additionally, the maximum force according to laboratory tests was used in simulation, in order to compare the values between simulations and laboratory tests. For obtaining more reliable results, the external forces and fixtures of the models in the simulations were made to match those of the real tests. Three operations were included in order simulation to be performed: applying external forces, determining the restriction of movement of the body and meshing the body, that are evident in (Fig. 3). Meshing is the process of subdividing the model into small pieces.

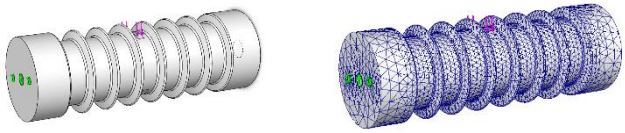

Fig. 3. *External forces and fixtures (left) and meshing (right) in simulation*

Finite element analysis looks at the model as networks of interconnected elements, therefore meshing is crucial in design analysis.

Mechanical testing of both types of insulators (12 and 24kV), shown in (Fig.4), was done in the accredited laboratory for testing of mechanical properties LT-04 at the Faculty of Mechanical Engineering in Skopje on a Shimadzu 25T AGX tensile testing machine.



Fig. 4. *Insulators 12 and 24kV (left), top surface (middle), bottom surface (right)*

3. Results and discussion

3.1 Compression test-static analysis

Compression simulations were performed by applying external, compressive force on the top surface. The 3D model of 12 kV insulator under compression force of 100 kN used during the simulation is evident in (Fig. 5). The bottom face was geometrically fixed. After simulation, maximum compression stress [N/mm^2], maximum displacement [mm] and maximum strain were attained and the results from the virtual compressive simulations are shown in Table 1.

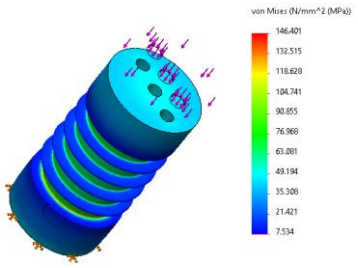

Fig. 5. *3D model of 12 kV insulator under compression simulation of 100 kN, maximum stress*

3.2 Compression test- laboratory test verification

Specimen was placed on flat surface and compressive force was acting on it. The force was transmitted through flat plate on the front surface of the insulator. In (Fig. 6) is evident specimen while being tested and the created breakage on its surface. Results for maximum stress, maximum displacement and maximum strain are apparent in Table 1.

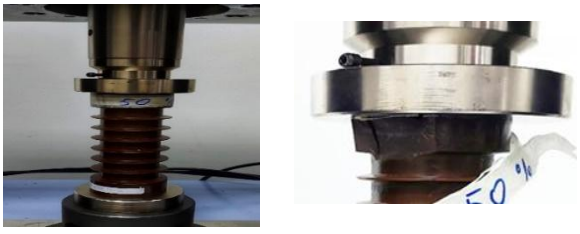

Fig. 6. *Compression test of insulator (left) and insulator after the test (right)*

Table 1: *Compression test- virtual static simulation and laboratory test*

Compression test	Simulation		Laboratory test
12 kV			
Force [kN]	100	207 075	207 075
Maximum stress [N/mm^2]	146.401	303.161	73.27
Maximum displacement [mm]	0.171	0.354	3.37
Maximum strain	0.003	0.006	
	24 kV		
Force [kN]	100	250 266.7	250 266.7
Maximum stress [N/mm^2]	112.046	280.402	65.06
Maximum displacement [mm]	0.218	0.546	4.48
Maximum strain	0.002	0.005	

Table 2: Tensile test- *virtual static simulation and laboratory test*

Tensile test	Simulation		Laboratory test
12 kV			
Force [kN]	100	18467.03	18467.03
Maximum stress [N/mm^2]	236.921	180.670	7.19
Maximum displacement [mm]	0.166	0.064	3.68
Maximum strain	0.005	0.004	
	24 kV		
Force [kN]	100	18219.23	18219.23
Maximum stress [N/mm^2]	272.099	106.404	5.08
Maximum displacement [mm]	0.222	0.063	4.35
Maximum strain	0.006	0.002	

3.3 Tensile test- static analysis

The external force was applied on the top face in the opposite direction comparing to compression test. 3D model after the simulation under force of 100 kN is evident in (Fig.7). The acquired results are presented in Table 2.

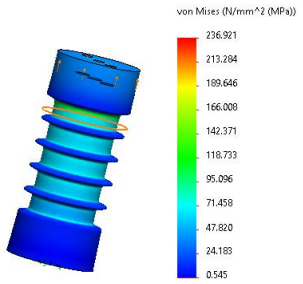

Fig. 7. *3D model of 12 kV insulator under tensile simulation of 100 kN, maximum stress*

3.4 Tensile test- laboratory test verification

In order the tensile test of insulators to be performed, screws were inserted into the specimens both ends. The tensile force was transmitted through the screws from the instrument. Given the composition of the material, as well as its brittleness, the destruction occurred in the joint of the built-in nut of the ends of the insulator, (Fig. 8). The results of tensile test are shown in Table 2.



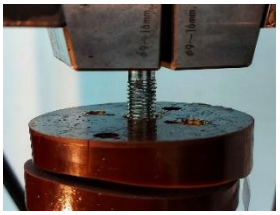

Fig. 8. *Tensile test of insulator and insulator after tensile test*

3.5 Three-point bending test – static analysis

Three-point bending test simulation was conducted by applying external force on the middle of the insulator. The insulator was supported by the screws of the bending test machine and the force acting on the middle of the insulator. After the three-point bending simulation under force of 100 kN, 3D model is apparent in (Fig. 9) and the obtained results are shown in Table 3.

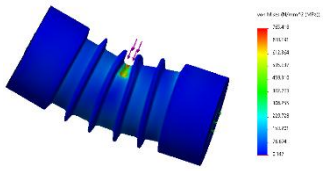

Fig. 9. *3D model of 12 kV insulator under three-point bending simulation of 100 kN, maximum stress*

3.6 Three-point bending test- laboratory test verification

The specimens were examined in the process of three-point bending, according to the standards prescribed for the test. The test was performed at a bending speed of 10mm/min. 12 kV insulator was ruptured close to the right support, at the three threaded inserts and built-in screws. On the other hand, 24 kV was broken in the middle of the length of the specimen, where force was acting, (Fig. 10). The obtained results are shown in Table 3.



Fig. 10. *Three-point bending test of insulator*

Table 3: *Three-point bending test- virtual static simulation and laboratory test*

Three-point bending	Simulation		Laboratory test
12 kV			
Force [kN]	100	24 760	24 760
Maximum stress [N/mm^2]	765.418	189.482	18.57
Maximum displacement [mm]	0.336	0.083	7.148
Maximum strain	0.016	0.004	
	24 kV		
Force [kN]	100	30 195	30 195
Maximum stress [N/mm^2]	546.861	172.547	24.42
Maximum displacement [mm]	0.588	0.178	7.148
Maximum strain	0.013	0.004	

4. Conclusion

Recent years have shown growing interest in the field of composite insulators for application in power transmission network. The crucial role is finding a suitable material that has improved properties comparing to conventional types. 3D modelling as well as virtual simulations are important for obtaining quite fast results with high accuracy.

This research saves time and money for manufacturers because potential errors would be identified in time and changes would be made before the product is ready to be presented on the market.

From this research it can be concluded that the insulators made from composite material consisting of 50 vol.% epoxy resin and 50 vol.% silica possess suitable properties for potential manufacturing. There is a difference between results in the simulations and laboratory conditions. In order to improve this, in real world conditions mixing of the materials need to be adjusted by inclusion of additives. In this way, air bubbles would be avoided and better dispersion of silica particles into the polymer matrix would be achieved.

High values of applied forces in laboratory conditions and possibility of insulators to withhold them provide information that they would be able to withhold them in manufacturing where more factors are included in the process.

5. References

1. H. M. Schneider, J. F. Hall, G. Karady and J. Renowden, Nonceramic insulators for transmission lines, IEEE Transactions on Power Delivery, **vol. 4**, no. 4, pp. 2214-2221, (1989)
2. J.-L.Bessede, Development of advanced materials for transmission and distribution (T&D) networks equipment, Electricity Transmission, Distribution and Storage systems, © Woodhead Publishing Limited, 133-142, (2013)
3. J. Zha, Z. Dang, W. Li, Y. Zhu and G. Chen, Effect of micro-Si3N4-nano-Al2O,sub>3 co-filled particles on thermal conductivity, dielectric and mechanical properties of silicone rubber composites, IEEE Transactions on Dielectrics and Electrical Insulation, **vol. 21**, no. 4, 1989-1996, (2014)
4. R.Sarathi, R.K. Sahu, P. Rajeshkumar, Understanding the thermal, mechanical and electrical properties of epoxy nanocomposites, Elsevier Materials Science and Engineering A, **Vol. 445-446**, 567-578, (2007)
5. G.Iyer, R. S. Gorur, R. Richert Dielectric properties of epoxy based nanocomposites for high voltage insulation, IEEE Transactions on Dielectrics and Electrical Insulation **Vol. 18**, No. 3, (2011)
6. G. Bhatt, Usage of integrated CAD/CAE/CAM system in foundaries, International Journal of Engineering Research & Technology, **Vol. 2** Issue 6, (2013

One of the methods for improving the electrodes cleaning system of the electrostatic precipitator with the purpose of increasing the intensity of checking dust

Kazak Iryna
National Technical University of Ukraine
"Igor Sikorsky Kyiv Polytechnic Institute", Kiev, Ukraine
asistentia@meta.ua

Abstract: *Electrostatic precipitators are designed for highly efficient cleaning of process gases and aspiration air from solid or liquid particles released during technological processes in various industries. To improve the design of the plate electrostatic precipitator and eliminate its lack of insufficient intensity of shaking of the electrostatic precipitator plates, a design of the system for cleaning electrodes of the electrostatic precipitator based on the prototype was chosen, which provides multilevel shaking (top, bottom, side of the plates) in the process of continuous operation of the plate electrostatic precipitator and increases the intensity of shaking dust from the plates of the electrostatic precipitator.*

Keywords*: ELECTROSTATIC PRECIPITATOR, ELECTRODE CLEANING SYSTEM, STRIKE INTENSITY, MULTI-LEVEL SHAKING, PLATE, ELECTRODE, DUST*

1. Introduction

Electrostatic precipitators are used in the energy, metallurgy, building materials industry, chemical and petrochemical industries, etc. Therefore, the dust cleaning stage should be considered an integral part of the effective operation of industrial enterprises, which ensures compliance with the permissible sanitary and hygienic standards for dusty emissions into the environment. The task of efficient cleaning of combustion products is performed, as a rule, by electrostatic precipitators of various designs, in which one of the most important is the system for cleaning the electrodes from dust.

2. Problem discussion

Cleaning systems refer to systems for the release of settled dust from the plates of electrostatic precipitators, carrying out beating, vibrating, shaking off or ultrasonic processes for cleaning the collecting electrodes. Electrode cleaning systems for electrostatic precipitators are designed to continuously or periodically free the electrodes from dust deposited on them, and operate in areas of high electrical voltage. Such systems are essential for the efficient operation of electrostatic precipitators.

Continuous cleaning systems are used to continuously clean the precipitation electrodes of an electrostatic precipitator. The regulation of the degree of cleaning of the electrodes is carried out by the constructive placement of the cleaning systems, their selection of a relatively selected electrostatic precipitator, and the determination of the forces by which they interact with the electrodes. More efficient cleaning is carried out due to the interaction of cleaning systems possible with a larger area of the collecting electrode. Thus, by increasing the area and forces of interaction of the cleaning systems with the collecting electrode, it is possible to increase the level of their cleaning.

The disadvantages of plate-type electrostatic precipitators are the relatively high cost of the apparatus and increased safety requirements during operation. Also in plate-type electrostatic precipitators there is a difficulty in removing the settled dust on the plates.

Of the listed disadvantages of plate-type electrostatic precipitators, this work will consider the problem of increasing the efficiency of the system for cleaning the electrodes from dust in order to increase the intensity of the stripping of the plates.

3. On the design features of electrostatic precipitators for choosing a method for improving the electrode cleaning system

Electrostatic precipitators are designed to capture dust with a particle size of up to 0.1 microns from air and gases of various chemical composition, humidity and temperature [1].

By design, the electrostatic precipitators are similar to the electric separators with corona electrodes. The precipitation electrodes of electrostatic precipitators are made in the form of grounded metal vertical pipes or plates, and the corona electrodes are in the form of metal rods installed inside the pipes or between the plates. Corona and collecting electrodes are installed in sealed chambers, through which a gas-dust mixture passes from bottom to top or from left to right between the electrodes.

According to the method of regeneration of collecting and corona electrodes, electrostatic precipitators are dry and wet. In wet electrostatic precipitators, the electrodes are rinsed with the required amount of liquid to remove dust. In dry electrostatic precipitators, vibration, magnetic-pulse, shock-hammer and shock-spring shaking systems are used to remove deposited dust [2].

In a plate electrostatic precipitator, collecting electrodes are made in the form of parallel smooth metal sheets or nets stretched on a frame, between which corona electrodes are suspended in the form of nichrome or fechral wires. To clean hot gases, collecting electrodes in the form of corrugated sheets or rods are used to avoid warping.

There are vertical plate electrostatic precipitators (with gas flow from bottom to top) and horizontal (with horizontal gas flow). To improve the cleaning of gases, multisection electrostatic precipitators are used with a series connection of sections [1].

The residence time of gases in the electrostatic precipitator greatly affects the quality of cleaning. Many years of experience have shown that the velocity of gases in electrostatic precipitators is low (within the range from 0.5 to 2 m / s), and the residence time in the filter is significant (from 2 to 9 s). Therefore, electrostatic precipitators are rather cumbersome. But their hydraulic resistance is low (from 50 to 200 Pa). The cleaning factor, especially with fine dust, is high (95-99%). They are good at capturing particles smaller than 10 microns. Energy consumption for cleaning is insignificant and amounts to 0.10-0.15 kWh per 1000 m^3 of gas to be cleaned. The main disadvantages of electrostatic precipitators: high cost and the need for highly qualified service personnel [2].

The process of collecting dust entering the electrostatic precipitator with flue gases can be roughly divided into four stages:

1) charging ash particles with ions formed in the ion discharge zone;

2) the movement of charged ash particles in the interelectrode space towards the collecting electrode under the action of electrical and aerodynamic forces;

3) deposition and retention of ash particles on the surface of the collecting electrodes;

4) removal of dust settled on the electrodes into the hopper.

It is the improvement of the cleaning system due to the choice of more intensive stripping of the electrodes in the plate-type electrostatic precipitator that will be given attention in this work.

Horizontal multi-field electrostatic precipitators are continuous devices. Dust is removed from the electrodes by shaking them without disconnecting the electrostatic precipitator from the power source and the flue gas flow. In this case, part of the dust will

inevitably enter the gas stream. This process is called re-entrainment and is the main reason for the reduced efficiency of dry electrostatic precipitators in comparison with wet ones, in which the deposition of particles occurs on a water or oil film and there is no re-entrainment. The amount of re-entrainment is in direct proportion to the interval between shaking of the collecting electrode and the intensity of dust blowing off.

In domestic electrostatic precipitators, each collecting electrode is shaken after 3 minutes, regardless of the dust content of gases, cleaning efficiency, gas velocity, etc.

Known serial electrostatic precipitators (analogue) of the UG, EGA type, in which the shaking of the collecting electrodes is carried out in the lower part from the side, and the discharge electrodes are shaken from the side in the middle part [2, 3].

There is also known an electrostatic precipitator, in which the shaking beam is located in the middle of the height of the collecting electrode.

The main disadvantage of analogs and the prototype is the fact that the shaking pulse is applied to the electrode in any one place. In this case, the shaking impulse decreases from the impact site to the periphery. In this case, shaking the electrodes with a height of 14 ÷ 25 m will be insufficient. Gentle shaking of the electrodes will lead to the deposition of dust on the electrodes and a decrease in the degree of gas purification.

The gas to be cleaned enters the active zone of the electrostatic precipitator, where the deposition of dust particles from the gas takes place. Most of the dust is deposited on the collecting electrodes, part of the dust is deposited on the corona electrodes. To capture dust with the design efficiency, it is necessary to ensure the required cleanliness of the deposition surface. For this purpose, shaking mechanisms are used. However, with an increase in the height of the electrode system, the existing design of electrostatic precipitators does not provide the required dust removal. The formed non-shake-off layers of dust reduce the electric power supply mode of the electrostatic precipitator, which leads to a decrease in the degree of gas purification by the electrostatic precipitator.

Therefore, as a result of a literature and patent search for options [1-4] for improving the system for cleaning electrodes from dust of a plate electrostatic precipitator, a prototype with a multilevel system of stripping (top, side and bottom) [4] was chosen to ensure a greater intensity of stripping of electrodes from dust.

4. Results and discussion of the improved cleaning system of electrodes of a plate-type electrostatic precipitator

In the chosen version of the improvement of the electrodes cleaning system of the plate electrostatic precipitator, the disadvantage when a shaking pulse is applied to the electrode in any one place is excluded due to the fact that the collecting and corona electrodes with a height of 14 ÷ 25 m are shaken in two levels, while the collecting parts horizontally or vertically directed blows, and from below by horizontal blows at the level from the bottom of the electrode 0.001 ÷ 0.01 of the height of the collecting electrode each; the corona electrodes are shaken from above with vertically directed shocks and from the side with horizontally directed shocks at a level from the bottom of the electrode 0.1 ÷ 0.5 of the height of the corona electrode each. This arrangement of the mechanisms for shaking the corona and collecting electrodes makes it possible to provide the required acceleration values over the entire area of the electrodes with a height of 14 ÷ 25 m. Due to this, there will be no unshakeable areas on the electrodes, which excludes a decrease in the efficiency of the electrostatic precipitator [4].

The proposed design of a multilevel system for cleaning electrodes from dust of a plate-type electrostatic precipitator is shown in Fig. 1.

The presented design of a plate electrostatic precipitator with an improved system for cleaning electrodes is shown in Fig. 1 contains a shaking hammer of the discharge electrode from above and from the side 1, anvils 2 and 3, a suspension beam of a collecting electrode 4, elements of a collecting electrode 5, a frame of a corona electrode 6, hammers for shaking the collecting electrodes from above and below 7 and 8, an element of a corona electrode 9, an anvil of shaking collecting electrodes 10, collecting electrode 11, corona electrode 12, drive for shaking the collecting electrodes from the bottom 13, drive for shaking the collecting electrodes from above 14, a drive for shaking the discharge electrodes from above 15, a mechanism for shaking the discharge electrode.

Polluted air enters from one end of the horizontal plate electrostatic precipitator, passing through the rows of plates, ionized particles settle on the 11 collecting and 12 corona electrodes, while tapping off by mechanisms 1, 7, 8, 16 occurs, while the corona electrode and two adjacent collecting electrodes are not shaken off at the same time [4].

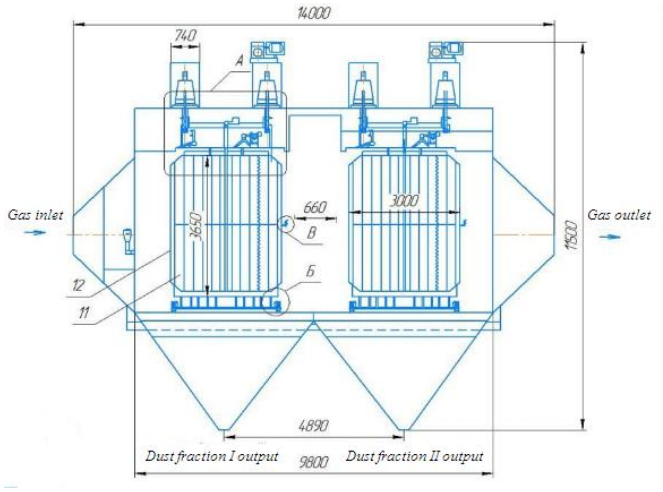

Fig. 1 *The design of a plate-type electrostatic precipitator with an improved multi-level electrode cleaning system.*

Fig. 2, 3, 4 shows the designs of a multilevel impact-hammer system for crushing a plate electrostatic precipitator in an improved system for cleaning electrodes from dust: from above (Fig. 2), from below (Fig. 3) and from the side (Fig. 4).

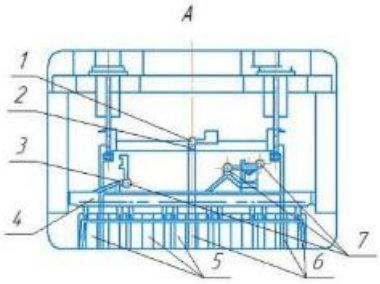

Fig. 2 *General view of the hammer-impact system for stripping electrodes from above in an improved plate electrostatic precipitator*

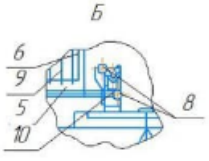

Fig. 3 General view of the hammer-impact system for stripping electrodes from below in an improved plate electrostatic precipitator



Fig. 4 *General view of the hammer-impact system for stripping electrodes from the side in an improved plate electrostatic precipitator*

The activation of the shaking mechanisms in the upper and lower parts can be carried out in two ways:

- separate inclusion;
- simultaneous inclusion.

With the simultaneous activation of the shaking mechanisms, oscillations are superimposed. The beats arising from the superposition of vibrations from two sources contribute to a more thorough shaking off of dust from the electrodes, since the amplitudes of the oscillations double, which leads to a twofold increase in the magnitude of the accelerations shaking off the dust [4].

5. Conclusions

The proposed improved multilevel system for cleaning the electrodes of the plate electrostatic precipitator (top, bottom and side) allows for more intensive dusting from the electrodes. Namely, to exclude the presence of an unbroken layer of dust, to ensure the required degree of cleanliness of the collecting and corona electrodes and, accordingly, to achieve the standard degree of gas purification, namely, to ensure the necessary dust emissions at a level of up to 50 mg / m³.

5. References

1. I. V. Kovalenko, V.V. Malinovsky. *Calculations of basic processes, machines and devices of chemical production. Tutorial.* Kyiv: Norita-plus, (2007), 289 p.
2. G.S. Ratushnyak, O.G. Lyalyuk. *Technical means of cleaning gas emissions. Tutorial.* Vinnytsia: VNTU, (2005), 158 p.
3. Glushchenko O.L. *Methodical instructions for independent work in the discipline "Dust collection and treatment of industrial emissions" for part-time students in the direction of 6.050601 - "Heat".* Kamyanske, DSTU (2018). 33 p.
4. L.V. Чекалов, Yu.I. Sanaev. Description of the invention to the author's certificate, RU 2368426, IPC B03C 3/76 (2006.01). *The method of shaking the electrodes of the electrostatic precipitator.* Publ. 27.09.2009

Ecological aspects of metallurgy and mechanical engineering at the beginning of the 21st century

Yavor Lukarski, Hristo Argirov
Institute of metal science, equipment and technology with Centre of hydro and aerodynamics,
Bulgarian Academy of Science, Sofia, Bulgaria
yasu@abv.bg; h.argirov@ims.bas.bg

Abstract: *At the beginning of the XXI century the anthropogenic uncontrollable industrial activity continuously disturbs the equilibrium of the planet formed for millions of years. A number of metals of vital importance decrease calamitously or disappear completely. The desire for high profits on behalf of a definite group of people leads to disappearing of fertile areas and whole mountains. This imposes the sensible part of humanity to undertake measures to return part of the breached balance.*
This elaboration suggests several innovative technologies for use in metallurgy and foundry as well as technologies for mechanical engineering, which ensure saving of material sources and achieve significant ecological effect on the environment.
The proposed technologies represent a complex of classical and modern methods for obtaining, processing and use of mineral and energy earth resources. Methods for utilization of some metal wastes to obtain fit for use products are also indicated.

Keywords*: METALLURGY, FOUNDRY, MECHANICAL ENGINEERING, ECOLOGY, ALTERNATIVE RAW MATERIALS, ENERGY SOURCES, RAW MATERIAL SOURCES, ALTERNATIVE SOLUTIONS*

1. Introduction

The development of human civilization is determined by the available energy and raw material resources of the Earth. The interaction between the natural and socioeconomic factors and the not always reasonable and prospective human activity in the XIX, and especially in the XX century, were the reason for the threatening reduction of the amount of continental ore resources.

Current data prove that by the year 2000 mankind has exhausted 25 to 75% of the continental metallogenic potential, including 45 to 75% of the reserves of Pb, Sn and Ag, 25% of Au and up to 45% of Cu, Ni, Co, Zn, Mn and Al [1].

Recently the conducted investigations on the environmental aspects of the extraction of mineral and energy raw materials have revealed many results concerning the residual presence of important metals in the Earth's crust. This is true especially for manganese, which is the main and strategic raw material in the production of steel and cast iron, as well as for some non-ferrous metals – Cu, Co, Ni, etc. [2].

Nature represents a self-regulating and self-controlling but fragile system. The harsh human intervention is an external factor in it and it makes its best to reject this interference or to neutralize it to a certain extent. This implies that if man does not make steps in the right direction, nature itself will do the things necessary to return in its original state. One of the ways to mitigate this situation is to find new alternative sources of raw materials as well as to use effectively the existing ones [1].

Otherwise, something that has been already described in science fiction will happen (Daniel Quinn's character – the gorilla, says in the book "Ihsmael": "It is a fact that in this moment we kill slowly and irreversibly the Earth and ourselves too").

The present work shows alternative solutions for reducing the consumption of mineral and energy resources and finding answers to a number of environmental problems. These solutions are mainly in two directions:

- Search for new raw material sources in addition to the existing ones;
- Development of new methods and technologies that guarantee economical use of the resources and protection of the environment.

2. New raw material sources

2.1. The World Ocean

According to the pessimistic forecasts of the experts, the main part of the relatively rich mineral and energy resources of the Earth will be depleted in the near future. This will impose the necessity of searching raw materials in the atmosphere and in the water. The problem of finding raw materials in the atmosphere is at a very early stage. Therefore, the bottom of the World Ocean remains. For example, the amount of the manganese raw materials in the Pacific Ocean is estimated to be $1{,}6.10^6$ Mt [2]. The increased attention to manganese is due to its wide application in the production of steel and cast iron, where it is used as an oxidizing, desulphurizing and alloying element. Industrial non-alloyed steels contain 0,4-0,8% of manganese, highly alloyed steels – 12-16% and even up to 30%, austenitic cast iron (manganese, manganese-nickel and manganese-aluminum) – 4-7% [3].

A comparison between the amounts of metal resources found on the land and in the ocean is shown in Fig. 1. It is seen that the content of some of the most commonly used metals in industry is higher on the ocean floor than their distribution in the Earth's crust.

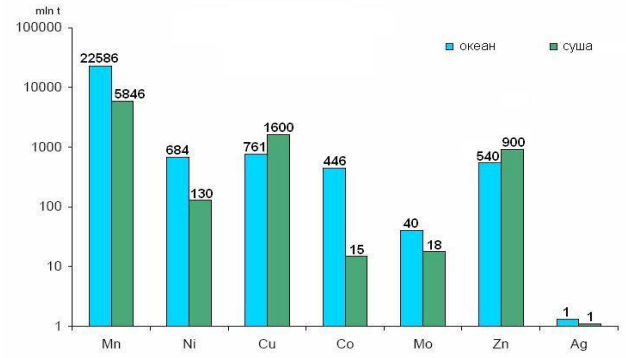

Fig. 1 *Comparison between the metal reserves on dry land and on the World Ocean floor*

The figure shows also that the raw materials on the ocean floor are with polymetallic composition. In addition to the manganese compounds, these formations contain a broad spectrum of valuable metals. The content of metals as zinc, copper, the deficient and expensive nickel, etc., on the ocean floor is very impressive.

The unique Clipperton-Clapeyron ore-bearing field arises the interest of the industrially developed countries. It is located near the territorial water of the Republic of Peru. Due to the interest in this ore-bearing field of many countries, the United Nations took control over this activity.

The participation of Bulgaria in this context has been within the framework of the Interoceanmetal Consortium (IOM) since 1987. Its headquarters are in Szczecin, Poland. The members of the consortium after 1990 are Bulgaria, Cuba, Poland, Russia, Slovakia and Czechia. IOM has the exclusive right to conduct economic activity in the designated for this region with an area of 150 000 km^2. The estimated reserves of wet bottom formations (concretions) in the explored so far 75 000 km^2 of the own area of IOM amount to 478,9 Mt and the quantities of some metals in them

are: Fe – 20,6 Mt, Mn – 98,8 Mt, Ni – 4,1 Mt, Cu – 3,8 Mt, Co – 0,6 Mt.

The problems of extraction and processing of deep-water polymetallic formations are considered in detail in the monograph [4]. The results of the numerous studies on their properties as well as some technologies for processing and manufacturing new finished products are presented in this work. The possibility of these formations to replace the ore raw materials excavated from the ground has been proved.

2.2. Utilization of secondary raw materials

The attention in this paragraph will be focused on an issue, which we claim to be strongly underestimated, moreover entirely undeservedly. The problem concerns the utilization of metal waste. Utilization by definition represents the use of waste to manufacture products or provide services, including reuse of the waste without preparation (recycling) or return to the production cycle after regeneration, as well as recovery of useful and valuable components from the waste for their next implementation [5].

Utilization in Bulgaria is restricted to the mechanical collection of wastes and their delivery for scrap. This approach does not meet the ever growing requirements for sorting and utilizing metal secondary waste.

2.2.1. Recovery of iron waste

To be convincing, several technological processes should be mentioned, where significant amounts of secondary waste are generated that have to be either returned to the production process or be treated separately:

First, this is the huge quantity of scale (iron oxides). It is formed during the thermal processing of reinforcing iron (hot drawing), rolling, heating of finished blocks and castings during thermal treatment and many other processes.

There are two possibilities of utilizing this scale. One is to return the scale directly to the furnaces as scrap. In this case reducing agents should be added to remove oxygen from the oxides [5].

The other option is also studied in the Institute of metal science, equipment and technologies – Bulgarian Academy of Sciences (IMSETCHA-BAS). According to this method the reduction takes place outside the furnace and pure secondary iron is fed inside it. These experiments are still at a laboratory level and various methodologies are still being tested to reduce the oxides.

However, it can be stated with certainty that both methods result in significant savings of metal and ferroalloys, which proves that valuable mineral and energy resources are spared. The indirect environmental effect of the reduced amount of extracted, transported and processed ore and energy resources should also be taken into account.

2.2.2. Recovery of titanium waste

The second global example, object of our attention, is the utilization of waste of titanium and titanium alloys. We can say that this is an especially important technological and environmental problem having in mind that hundreds of types of titanium alloys are used worldwide and the amount of waste increases by 8-10% annually [6]. For example, in the production of turbines for aircraft industry, the quantity of waste can reach 80% of the mass of the initial billet.

Titanium is a light and strong metal, 60% heavier than aluminum but twice as strong and with a very high strength/mass ratio. The tensile strength of titanium for commercial purposes is 454 MPa, which is comparable to that of some steels with 45% lower mass [7]. At the same time it has to be mentioned that titanium and its alloys are with a relatively high cost.

For this reason different methods are developed on a world scale to utilize this waste. They are in two directions:

- returning the obtained titanium scrap in the production of titanium alloys. Different methods are used, both pyrometallurgical and hydrometallurgical;
- processing of the titanium waste according to different methods with the aim of manufacturing various products with diverse application in the branches of technology and industry.

In the USA about 40% of the titanium scrap is processed and reused. In Europe this percentage is relatively lower – up to 30%. Large scale investigations are carried out at present in Romania on the recovery of titanium waste from the production of turbines for power generation and oil output [8].

One of the methods for utilizing the titanium waste is the treatment of scrap with hydrogen until titanium dihydride is obtained. It is a gray-black powder with molecular weight of 49,53-49,90 g/mol, relative density of 3,75 g/cm^3 and hydrogen content in the interval 3,85-4,02% (wt.). The main requirements towards the titanium dihydride powders are: titanium content at least 95% and hydrogen content at least 3,8%.

Titanium dihydride finds application in: chemical industry, metallurgy, spacecraft technology, nuclear engineering, etc. It is particularly effective as a foaming agent in the production of foamed metals (for example Al). Titanium dihydride is used as a soldering agent for ceramic and metal-ceramic products, in automotive industry, etc. [9].

In IMSET-BAS, in cooperation with researchers from the Faculty of Metal Science of the Polytechnic University – Bucharest, Romania, equipment was developed and investigations were carried out for producing titanium dihydride from waste raw materials.

The scheme of the experimental setup is shown in Fig. 2. The main feature of the equipment is the use of a hydrogen accumulator as a source of hydrogen for the process. In this way the risks of using hydrogen bottles and other mobile hydrogen sources are avoided.

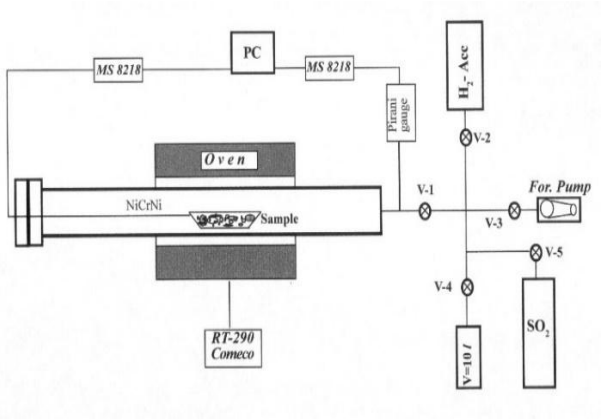

Fig. 2 *Scheme of the installation for TiH_2 production*

Two types of initial raw materials were used for hydrogenation – shavings of pure titanium and of titanium alloy, used in the Etropal plant, Etropole, Bulgaria. The main chemical elements are shown in Table 1.

Table 1: *Chemical composition of the initial raw materials for producing TiH_2.*

Sample number	Origin	Elements, % (mass)		
		Al	Mn	V
1	Pure Ti	0,0180	0,0014	0,0034
2	Etropal	0,5040	0,0065	0,0197

In addition, there is also iron, cobalt and nickel content in negligibly small amounts.

Experiments were conducted for titanium hydrogenation at temperatures from 400 to 700°C at every 50°C.

The following conclusion can be drawn based on the performed experiments and analysis of the obtained results:

A technology has been developed for the production of titanium dihydride from titanium waste and the technological parameters of the process – temperature, pressure and duration, are determined.

In this way a possibility is provided for the utilization of the increasing amounts of titanium and titanium alloy waste till a finished product is obtained, with all ensuing beneficial effects for the environment.

2.2.3. Processing of vanadium waste

Another example of solving economic and environmental problems is the utilization of vanadium from vanadium catalysts.

Vanadium is broadly applied in metallurgy, chemical industry, etc. When added to steel, vanadium removes the granularity of the matrix and the presence of carbon, transforming it in carbides. In this way vanadium steel is especially durable and resistant to impact and flexure. Almost all tool steels contain vanadium in quantities from 0,10% to 5%. It ensures the preservation of hardness and cutting ability of the tool at high temperatures. When added in the amount of several percents, vanadium makes aluminum very hard.

In the process of operation the vanadium catalyst is deactivated. Hence significant amounts of catalysts are accumulated, which contain the deficient vanadium.

An effective technology has been developed in the University of Chemical Technology and Metallurgy, Sofia, for extraction of vanadium by pyrometallurgical processing of manganese ore from the Obrochishte deposit and waste vanadium catalysts [9]. So the environmental problems related with the toxic vanadium are solved and economic problems with this deficient and expensive metal are solved.

2.2.4. Utilization of radioactive waste

At the beginning of the XXI century shutdown and decommissioning were launched of about 50 nuclear reactors all over the world, which were put into operation at the end of the XX century. Therefore the problems related to the utilization of radioactive waste according to the D&D (dismantling + decontamination) system have acquired special importance recently.

The dismantling of the WWER type reactors leads to accumulation of metal waste with different extent of contamination. It is necessary to sort this waste according to radioactive contamination, size and shape. The materials not contaminated with radionuclides (waste from the third circuit and the Machine Room) are unconditionally released from control and sold for scrap. The remaining metal waste is recycled and, depending on the degree of residual radioactivity, is used as scrap or disposed till the complete decay of radionuclides [10].

A team with the participation of the authors of this publication has developed a pyrometallurgical technology for radioactive waste processing. The main stage in it is metal melting and treatment of the melt with special fluxes oxidizing the radioactive elements and transferring them to the slag. Part of the nuclides is captured by the HEPA-filters and a very small part (about 5%) remains in the melt.

Thus, after the realization of the recycled metal on the market, the self-cost of decontamination is reduced. Moreover, the ecological problem with the possible radioactive pollution of the environment and population is solved [11].

3. Production of new materials and replacement of conventional with newly developed ones

3.1. Replacement of the initial material

One of the methods for improving the mechanical properties of the materials is to replace the conventional brands with newly developed ones. In this way saving of materials and raw materials is achieved due to the lower mass of the elements at higher strength and longer exploitation resource. The production of grinding hammers for lignite coal is based on GE 300N steel. It is subjected to abrasive wearing and should possess high impact toughness (KCV>0,27 MJ/mm^2) to guarantee safe work of the hammers without destruction at operation temperatures of up to 560° C.

The same type of hammers in a Greek power plant work for more than 800 hours. The operational resource under the conditions of the Maritsa-Iztok 1 plant is 450 hours. A photo of the worn out hammers is shown in Fig. 3.

Several steel grades were chosen to replace GE 300N. Investigations were conducted and the following steel types were offered to the consumer that met entirely the operation requirements: X120Mn12; 34NiCrMoV145; X155CrVMo121; Mn4.



Fig. 3 *A photo of worn grinding hammers*

The wear resistant X120Mn12 steel (Hadfield steel) has turned out to be most suitable for the hammer production, having the best combination of properties. It is manufactured by introducing nanomaterials into the liquid metal, which leads to more fine-grained structure and higher exploitation properties of the steel. The tests on the properties of this steel (quenched in water at T=1050-1100ºC) show increased wear resistance, as well as higher resistance against abrasive wearing. The impact toughness is 31 MJ/m^2 [12].

It is possible to subject the hammers to weld overlaying but the operation is economically unprofitable [13].

Another example of replacing the initial material with a new one with higher physical properties and longer service life is the development of a new steel brand for the automotive industry. This steel is with 10% higher strength and plastic properties compared to that used so far [14].

In this case, in addition to the saving of raw material and energy resources due to the longer operation cycle of the elements and the emission of lower amount of exhaust gases during its production, another significant environmental effect is also observed. The elements produced with the new steel are lighter because of their higher performance properties. This decreases the weight of the whole car, so reducing fuel consumption. The lower fuel consumption will lead to lower exhaust gas emissions in the atmosphere.

The technology of the new steel production includes the following stages:

A database with 92 alloys, shown in [15], is used in the investigation. The relationship between the chemical composition and the mechanical properties of the alloys is given in it.

After the analysis of patent information it has been established that the analogue of the developed steel should be the 34CrNiMo6 (DIN 17200) steel with the following chemical composition: C=0,30-038%; Si≤0,40%; Mn=0,40-0,70%; P and S≤0,035%; Cr=1,40-1,70%; Mo=0,15-0,30%; Ni=1,40-1,70%.

Based on the analysis of reference literature the limits of alteration of the individual alloying elements are determined, keeping the strength and plasticity requirements, as follows: C 0,12-0,52%; Si 0,27-1,40%; Mn 0,35-1,75, Ni 0-4,2%; S/P 0,0252-0,0350%; Cr 0,15-2,50%; Mo 0-1,5%; V 0-0,45.

Applying an innovative approach the dependence of mechanical properties of steel on the alloying element content has been modeled. Models with artificial neural networks have been elaborated, approximating the dependence of the mechanical properties of alloys on the alloying component content. The optimized parameters are: yield strength Re, tensile strength Rm, relative elongation A, relative shrinkage Z, impact strength KCU and hardness NB.

A modern method is used in [16] and an algorithm for modeling with artificial neural networks to determine an optimized composition of an iron-based alloy as well as a rational technological mode of operation. Alloyed steel compositions with high exploitation resource are proposed on the basis of the optimized composition of the iron-based alloys.

The following values of the mechanical characteristics were obtained after the performed simulation and tests – Table 2.

Table 2 *Mechanical characteristics of the steels (simulation)*

No	Rm	R_{02}	A	Z	HB
1	1111,9	943,8	10,2	50,0	240,9

The newly developed steel was produced in an induction furnace (capacity of 10 kg) of the Leybold Heraeus company – Germany [15].

The results obtained from the mechanical testing after thermal treatment and plastic deformation are shown in Table 3.

Table 3. *Results from mechanical testing*

Mechanical characteristics						
	R_{02}, MPa	Rm, MPa	A_5, %	Z, %	KC, MJ/m^2	HB
DIN 17200	900	1160-1270	10	45	0,48	-
34CrNiMo6	885	1180	10	44	0,46	230

As seen in the table, the new steel (DIN 17200) is superior to that used so far according to some strength parameters and is compatible with respect to others.

3.2. Metallurgy under pressure

During the last decades great attention has been focused on metallurgy under pressure and high nitrogen steels in particular [17, 18]. The term "high nitrogen steels" (HNS) is used for steels obtained under gas pressure, when nitrogen concentration exceeds N standard solubility. A team from IMSETCHA-BAS follows these trends and has definite success in this prospective area. High nitrogen steels possess proven potential and are applied in various fields of technology, in some cases their parameters being superior to the conventional brands by 30 to 150%. Such an example are the steels (type 355 G2+N according to DIN EN 10225 (2009) developed in IMSETCHA-BAS with manganese content of 1,2-1,6% [17]. In this situation the grain size of ferrite in the steels with 0,09% C decreases from 216 μm to 65 μm, the critical temperature of embrittlement becomes lower – from -58°C to -118°C.

Another advantage of HNS is the possibility of efficient and ecological alloying of the melt with such exotic and easily evaporating elements as Ca, Pb, Zn, Mg, etc.

The Bulgarian contribution to the progress in this area is that developing our metallurgy under pressure (technologies) the scientists and experts created the equipment and technical basis of the method of "bulk alloying". Installations for steel melting were constructed: UPL-2, UPL-2M, UPL-2M1, UPL-2A, equipment for electroslag remelting ESPH-2, ESPH -2,5 furnace and a furnace for solid-phase nitriding of ferro-alloys – VTP-2. High nitrogen tool, corrosion-resistant, heat-resistant non-magnetic, wear-resistant non-magnetic, spring and other steel types are produced in these units, which are applied in various fields of technology [17].

In the context of the Bulgarian achievements in the area of HNS, the name of the founder and engine of this technology Prof. D.Sc. Eng. Tsolo Valkov Rashev should be specially mentioned.

All these achievements would have been impossible without the serious support of the team of experts, specialized in the implementation of modern research methods [18, 19].

4. Conclusions

The current work represents a contribution to the human efforts in favour of the environmental protection. We introduce innovative technology, used in metallurgy and machine building, that ensures cost economies of the material resources and achievements with considerable ecological effect for the environment.

This technology is only a part of the efforts related to ecological friendly extraction, processing and exploitation of the mineral and energy resources on the Earth. Besides, some metal waste methods of utilization are pointed out.

5. References

1. https://www.conex.net/nc8/2021/bg/26.html *Basic Principles of National Policy and Strategy for Underground Riches and Sustainable Development of the Bulgarian Mining Industry.*
2. Kotlinski, R. Mineral Resources of the World Oceans-Their Importance for Global Economy in 21st Century.- *Proc. of the Fourth (2001) ISOPE Ocean Mining Symposium*, pp. 1-8, Szczecin, Poland.
3. Gavrilova, R., Lazarova, R., Manolov, V. Influence of the Nitrogen Content on the 6Cr3MoNiV Steel Structure. *5th International Cong. "Mechanical Engineering Technologies-06"*, Varna, Bulgaria, (2006).
4. Lukarski, Y. *Production of manganese alloys from alternative raw materials-deep-sea polymetallic particulars*. Sofia, IMSETCHA, 2012, p. 190, ISBN: 978-954-92552-4-9.
5. *Waste Processing*, http://www.ru.wikipedia.org/wiki/
6. Lukarski, Y., L. Anestiev, J. Georgiev et al. *A prospective method for production of TiH_2 and Ti powders from Titanium Wastes*.- J. Powder Metallurgy Progress, V. **11**(2011), No 3-4, ISSN 1335-8987.
7. http://www.basel.int/meetings/twg/twg17/predocs/twg17_02.pdf
8. http://www.specialmetals.chemetall.com/pdf/Titanium_hydride_P.pdf
9. Petrov, P, M. Marinov. *Preparation of agglomerate of manganese concentrate and vanadium catalyst in a laboratory agglomeration*, - In Scientific session „Development, Future, Perspectives and Innovations in Science", Sofia, VI, 2005.
10. Atanasov, I., S. Todorov. *Process flow Problems and Perspectives Upon Radioactive Metal Waste*. - Proc. VIth Int. Scientific Conf., Summer Session, Industry 4.0, June, 23 – 26, 2021, Varna, Bulgaria, Int. Scientific J. "Industry 4.0", ISSN PRINT 2534- 8582, ISSN ONLINE 2534-997X.
11. Lukarski, Y., I. Atanasov, Ch. Argirov. *Protection of the Personnel from Irradiation During Pyrometallurgical Processing of the Base of Model Calculations*. - Proc.of 27th Int. Conf. Ecological Truth and Environmental Research–EcoTER 2019, 18-21.06. 2019, Bor, Serbia, pp. 404-411.
12. Argirov, H., Y. Lukarski. *Ressearches for determination of an optimal steel brand intended for work in coal industry*. - Scientific Proc. of Scientific and Technical Union of Mechanical Engineering, Year XXII, Feb., 2015, № 2 (140).
13. Tashev, P. *Introduction of nanoparticles into the liquid phase during welding*, Sofia, Prof. Marin Drinov Publishing House of BAS, 2020 г., p. 191, ISBN 978-619-245-065-6
14. Lukarski, Y., S. Popov, N. Tonchev et al. *A Design of new Brands of Martenzite Steels by Artificial Neural Networks*. - Proc. of Int. Conf. on Advanced Technologies and Materials UgalMat '11, October 21-22, 2011, Galati, Romania, p. 54-60.
15. http://www.splav.kharkov.com/choose_type.php
16. Tontchev N., S. Popov, P. Koprinkova-Hristova et al. *Comparative Study on Intelligent and Classical Modeling and Composition Optimization of Steel Alloys*, - J. of Materials Sciences and Engineering with Advanced Technology, 4(1), (2011), p. 69-91.
17. Rashev, Ts. *High Nitrogen Steels. Metallurgy Under Pressure*. Sofia, Academic publishing house "Prof. M. Drinov", 1995, p. 255.
18. Mirchev, Y., K. Kalchevska, M. Mihovski et al. *Physical Basis, Methods, Materials and Means for Capillary Non-destructive Control*. Sofia, Academic publishing house "Prof. Marin Drinov" 2019, p. 140, ISBN 978-619-90662-2-5.
19. Kalchevska, K., Y. Mirchev, M. Mihovski. *Physical Basis, Methods, Means and Technologies for Visual-optical and Measuring Non-destructive Control*. Sofia, Academic publishing house "Prof. Marin Drinov", 2020, p. 196, ISBN 978-619-245-038-0.

Microcrystallites, granularity and agglomerates of detonation nanodiamonds

Evgeny Petrov, Vetrova Anastasia, Pribavkin Andrey Borisovich, Udalova Anastasia
Biysk Technological Institute of Altai State Technical University named after I.I. Polzunov, Biysk city, Russia[1],
E-mail: htemi@bti.secna.ru
"CLL Research and Production Enterprise "SIDAL", Kachkanar city, Russia[2]
E-mail: andreya.pribavkin@yandex.ru

Abstract: *Energy-saturated materials are considered to be a source of cheap energy, while detonation synthesis is a new promising form of the basic technology for producing nanodiamonds and other super hard and ceramic nanomaterials. Nanodiamonds is a unique product that combines both the properties of diamond and the advantages of nanostructures. The given work investigated the synthesis products, obtained under industrial conditions, while having detonation of a mixture of trinitrotoluene (TNT) with gecsogen (RDX) and RDX with graphite. The sizes of microcrystallites were, estimated by X-ray diffraction analysis and particle grain size according to the measurement of specific surface area, agglomerate in water suspension after treatment by ultrasound. There was, shown the evolution of nanodiamonds particle sizes and microstructures, both in the primary synthesis products and after enrichment from non-diamond forms of carbon and technological impurities.* Changes in the microstructure indicate a high reactivity of nanodiamonds. *The obtained results can be useful for studying the mechanism of synthesis and practical application of detonation nanodiamonds.*
Keywords*: NANODIAMOND, DETONATION SYNTHESIS, MICROCRYSTALLITES, MICROSTRUCTURE, GRANULARITY, ULTRASOUND, AGGLOMERATE.*

1. Introduction

Energy-saturated materials are considered to be a source of cheap energy, while detonation synthesis is a new promising form of the basic technology for producing nanodiamonds and other super hard and ceramic nanomaterials. Nanodiamonds (ND) is a unique product that combines both the properties of diamond and the advantages of nanostructures [1-3]. At the present, moment science and technology use detonation synthesis ND, obtained both from the carbon of an explosive molecule and from a mixture of explosive with the addition of graphite or soot. In the latter case, the diamonds are larger. 39 years have passed since the discovery of nanodiamonds, there was established certain production not only in Russia but also abroad, however the work as for the research, modification and application of ND continues to be relevant.

The physical and chemical properties of nanomaterials are mainly dependent on the microstructure and the grain size. To put it in practice, ND of detonation synthesis, are produced from both carbon explosive molecule [4,5], and from a mixture of explosives with the addition of graphite or soot [6]. The general technology for ND production in both cases is the same, however, with the use of graphite, diamonds are usually larger in size [7,8]. Experimental experience shows that the size of diamond may also depend on the mass of explosives and the cooling conditions of the detonation products in the chamber [9,10]. In the production process, diamonds go through the stages of crystal nucleation and growth, hardening in the process of expansion of detonation products and enrichment from condensed detonation products, moreover due to surface activity of nanoparticles, the sizes of microcrystallites and grains can vary. The given research paper presents the results of studies as for determination and comparison the sizes of microcrystallites, grain and agglomerates of ND obtained both from explosive molecules and from a mixture of explosives with the graphite addition. It is important to note that the studies were carried out on explosive charges of industrial synthesis and under equal experimental conditions.

2. Research objectives

The detonation synthesis of ND was carried out in an industrial explosive chamber with a volume of 4 m^3 in a buffer cooling medium from its own gaseous detonation products. There were used cast charges of TNT – RDX alloys in a ratio of 40/60 and extruded charges of RDX with graphite in a ratio of 80/20 by weight, respectively. The mass of the explosive charge in the experiments is 0.5-2.0 kg.

There were, estimated the sizes of microcrystallites by means of X-ray diffraction analysis and particle grain size according to the measurement of specific surface area. The crystal structure and crystallite sizes of the samples were determined on a Rigaku Ultima IV X-ray diffractometer. There was used Cu radiation, at a shooting speed of 1 deg./min, with the step of 0.01 deg. and scanning angles of 5-75 deg. The diffraction patterns were, processed using the PDXL software package; the phase composition was determined using the ICDDPDF2 database.

The specific surface area (*S*) was, determined by the BET adsorption method in a stream of nitrogen at the "ASAP-2000" automatic microvolume vacuum unit, Micromeritics. Granularity was calculated according to the formula for spherical particles: $D = 6/ S \bullet \rho$, where ρ is the density of ND.

The size distribution of particles was measured in water suspension (under ultrasound) was determined by the method of a laser diffraction on Horiba LA-950 laser analyzer. The frequency of ultrasound was 20 kHz.

3. Experimental results and discussion

The (Table 1) shows the results of studies of microcrystallites (d_1), granularity (D_1), and specific surface area (S_1) for enriched ND obtained in experiments with different mass and composition of explosives. The sizes of microcrystallites measured in condensed detonation products (d_2) before its enrichment are, shown.

Table 1. *Sizes of microcrystallites and ND grain size for explosives of various mass and composition*

Explosive Composition	The mass of explosives, kg	S_1, sm^2/g	D_1, *nm*	d_1, nm	d_2, nm	S_2, sm^2/g
RDX Graphite	0.5	23.4	75.4	6.55	4.72	47,4
	1.0	32.2	54.8	7.40	5.02	54,5
	1.2	21.0	84.0	6.84	5.24	61,4
RDX TNT	0.5	246.3	7.60	4.90	3.25	315,6
	1.0	232.6	8.10	4.71	3.56	302,5
	2.0	231.3	8.10	4.51	3.44	390,5

The results show that ND from explosives and graphite have similar values in sizes d_1 and d_2, but differ significantly in S_1 and D_1. The sizes D_1 for graphite diamonds are considerably larger. With an increase in the explosive mass, the sizes of microcrystallites and grain size of ND increase. It is interesting to note that for all samples, d_2 is noticeably less than d_1. In the

process of enrichment in a mixture of sulfuric and chloric acids at a temperature of 180-240^{0}C, the sizes of microcrystallites increased. This is possible, since the particle of ND microcrystallites has an amorphous phase at the periphery of the crystal [11]. In the process of enrichment, the amorphous phase recrystallizes with an increase in the size of ND microcrystallites.

It should, be noted that for primary fusion products in the region of 200-400°C, a significant thermal effect is almost always observed on the DTA curve, which is comparable to a number of samples with the heat of combustion. Moreover, no mass loss is, observed on the TGA curve (for example, Fig. 1). This behavior can, be explained by the presence of excess surface energy, the destruction and oxidation of the surface layer. Этот результат также подтверждает о возможной перекристаллизации ND при нагревании. This result also confirms the possible recrystallization of ND during heating.

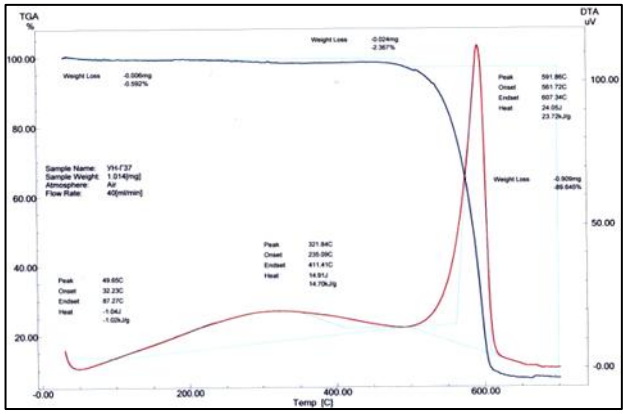

Fig. 1. *DTA and TGA (RDX/TNT, the mass of explosives – 1, 0 kg).*

The results of specially conducted experiments are, presented in (Table 2). Parts of one sample were, heated at different temperatures in the atmosphere. As a sample, primary products of ND.

As can be seen from (Table 2), with the increase in the temperature d_2 and D_2 grow. The proportion of the amorphous phase in the samples decreases. For a sample obtained at 450^{0}C or 530^{0}C, R_2 and D_2 are higher than for a similar sample of ND enriched with acids (Table 1). Thus, it is obvious that the microcrystallites and granularity of diamonds increase in the process of enrichment. Changes in the microstructure indicate a high reactivity of nanodiamonds.

Table 2. *The microcrystallites ND in the world of the temperature*

Explosive Composition	Temperature, ^{0}C	amorphous phase, %	d_2, nm	S_2, см^2/г	D_2, *nm*
RDX /TNT (The mass of explosives, 1,0kg)	25	24,0	3,56	302,5	7,93
	280	26,0	3,70	341,9	7,02
	350	35,0	3,72	287,1	8,03
	450	39,0	7,80	164,8	11,74
RDX Graphite (The mass of explosives, 1,2kg)	25	29,0	5,24	61,4	39,1
	250	31,0	6,30	63,5	39,4
	480	42,0	15,4	19,1	92,4
	530	48,0	22,7	14,8	119,2

Nanomaterials, thanks to the active surface, from a system of units. The looseness of the units grows as they enlarge, and the strength decreases.

Studies of ND units in water suspensions are given on (Fig. 2-5) and in (Table 3).

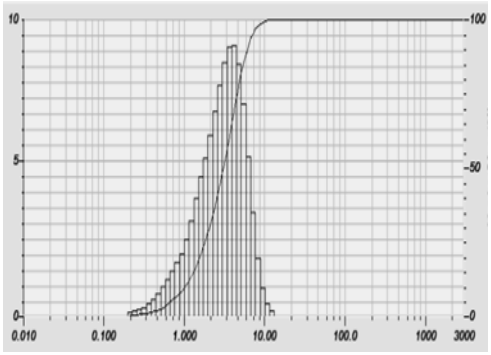

Fig. 2. *Particle Size Distribution for ND (RDX /TNT, the mass - 0.5 kg).*

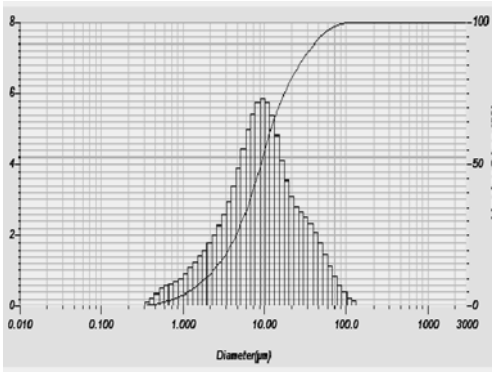

Fig. 3. *Particle Size Distribution for ND (RDX/Graphite, the mass - 1.2 kg).*

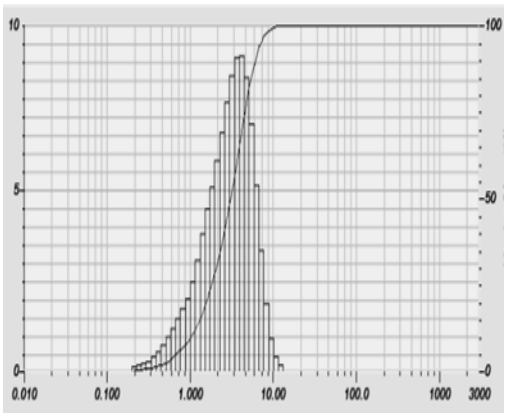

Fig. 4*. Particle Size Distribution for ND (RDX/Graphite, the mass - 1.2 kg, Ultrasound).*

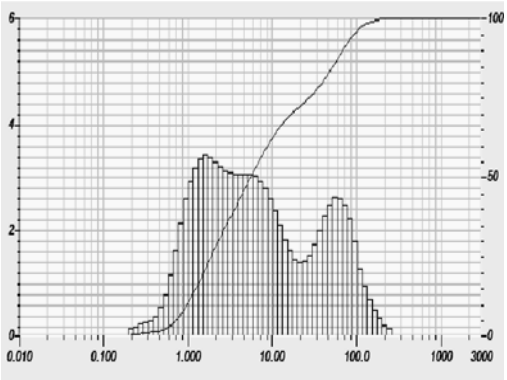

Fig. 5. *Particle Size Distribution for ND (RDX /TNT, the mass - 0.5 kg, Ultrasound).*

Table 3. *The size of the ND particles depending on the time of exposure to ultrasound*

Explosive Composition	The mass of explosives, kg	Time, sec	Mean size, μm	Median size, μm	Mode size, μm
RDX Graphite	0,5	0	14.79	9.54	10.78
		120	9.13	6.14	7.19
	1,2	0	14.71	9.03	9.44
		60	3.39	3.08	4.16
RDX TNT	0.5	0	238.91	180.45	245.20
		125	21.80	5.59	1.62
	1.0	0	63.34	48.80	82.45
		120	2.43	2.03	2.78
	2.0	0	35.09	21.67	54.90
		15	25.55	15.49	12.37

The particle distribution curves are given in size for ND samples obtained using and with, out ultrasound. The frequency of ultrasound was 20 kHz. For all samples, the average size of the units is much lower than the grain of nanodiamonds. There is the following dependence, the smaller the size of the grain, the larger the size of the units. The use of ultrasound reduces the size of stable units by about an order of magnitude. Nanodiamonds from the explosive molecule is more prone to aggregation.

Analyzing of the results, we reached the conclusion that the ND particles from the explosive molecule are a single crystal formation, since d_1 and D_1 have the same size values. Graphite ND particles are polycrystals formed from 8-10 microcrystallites. Particles of ND pass through three stages of formation. The first stage is the condensation, formation and growth of microcrystallites in the area of chemical reactions in the detonation wave and the merging or sintering of microcrystallites (formation D) in the Taylor wave in the second stage. At the third stage (chemical cleaning, drying), microcrystallites, granularity and structure of stable ND agglomerates are finally formed.

4. Conclusion

While conducting the present research there were determined the sizes of microcrystallites and the ND granularity obtained under industrial conditions both from the explosive molecule and from the explosive with the addition of graphite. The sizes of microcrystallites are approximately equal, and the granularity differs significantly. ND particles from explosives have mainly a single-crystal structure with a grain size of 7-8 nm, and ND particles from explosives with graphite are polycrystals with a grain size of 54-84 nm. As the charge, mass increases, the sizes of single crystals and grains increase too. During the chemical cleaning, the size of microcrystallites and the grain of ND increase. Changes in the microstructure indicate a high reactivity of nanodiamonds. After chemical cleaning, stable units with a size from 0.1 to 100 μm are, formed in the water suspension. NA from the explosive molecule is more prone to aggregation.

The obtained results can be useful for studying the mechanism of synthesis and practical application of detonation ND.

Acknowledgment

The study was, carried out with the financial support of the Russian Federal Property Fund in the framework of a scientific project No. 18-29-19070 MK.

References

[1] Sakovich G. V., Komarov V.F. and Petrov E.A. “Synthesis, properties and application of nanosized synthetic diamonds. Part 1. Synthesis and properties,” Superhard. Materials., No. 3, 2002, pp. 3–18.

[2] Sakovich G. V., Komarov V.F. and Petrov E.A. “Synthesis, properties and application of nanosized synthetic diamonds. Part 2. Application and manufacturing,” Superhard. Materials., No. 4, 2002, pp. 8–23.

[3] Dolmatov, V. Y. Detonation Synthesis Ultradispersed Diamonds: properties and Applications. Russ. Chem. Rev. 70, 2001, pp. 607–626.

[4] Lyamkin A. I. et al., “Production of diamond from explosives,” Dokl. Akad. Nauk SSSR, vol. 302 **(**3), 1988, pp.705–706.

[5] Griener F. E. et al.,“Diamonds in detonation soot,” Nature, vol. 333 **(**172), 1988, pp.440–442.

[6] Drobyshev V.N., “Detonation synthesis of superhard materials,“ Combustion, Explosion and Shock Waves, vol. 19(5), 1983, pp. 677-678.

[7] Petrov E.A., Kolesova A.A., Pribavkin A.B., “Properties of nanodiamonds of industrial detonation synthesis”: International scientific journal "Machines. Technologies. Materials." 13(8), 2019, pp. 373-375.

[8] Vereschagin A. L., Sakovich G. V., Komarov V. F., and Petrov E.A., “Properties of ultrafine diamond clusters from detonation synthesis,” Diamond and Related Materials, No. 3, 1993, pp.160–162.

[9] Danilenko V.V., “Explosion: physics, engineering, technology*”,* Moscow*:* Energoatomizdat, 2010, 784 p.

[10] Petrov E.A., Sakovich G. V., Brylyakov P. M., “Condition of diamonds safety under detonation synthesis,” Dokl. Akad. Nauk SSSR, vol. 313**(**4),1990, pp. 862–864.

[11] Solovyeva K.N., Kolesova A.A., Petrov E.A., Khimich, M.A. ‘The texture of the surface and substructure of industrial detonation nanodiamonds’ No. 6 (34), 2020, pp. 96-100.

Analysis of the influence of environmental factors on the properties of cellulosic electrical insulating materials

Ardeleanu Mircea-Emilian[1], Scornea Aurelia[2], Stănescu Dan-Gabriel[1], Sîrbu Ioana-Gabriela[1], Buligioiu Alexandru[1]
University of Craiova,Romania[1]
National Research, Development and Testing Institute for Electrical Engineering - ICMET Craiova, Romania[2]
mircea_emilian@yahoo.com, scornea@icmet.ro, dstanescu@elth.ucv.ro, osirbu@elth.ucv.ro, buligioiualexandru96@gmail.com

Abstract- *From the practical experience regarding maintenance and service life of power transformers, it is important to know the state of degradation (ageing) of the solid insulation and oil transformer. Therefore, it is important to study and analyse how certain factors influence the dielectric properties of insulating materials used in electrical power transformers. This work proposes the experimental study of the behaviour of cellulose type solid materials used to insulate electrical transformers. The aim was to consider the hygroscopicity of cellulose-based products, the influence of temperature, humidity on the insulation resistance, dielectric strength and proof tracking index (PTI) in humid conditions. Experimental determinations were carried out in the framework of the RENAR accredited laboratory within ICMET Craiova. Experimental results have showed that environmental factors (low temperature -40°C and damp heat steady state for 24 hours at 70°C and relative humidity of 95%) strongly negatively influenced some dielectric properties such as insulation resistance and the PTI.*
Keywords: *DIELECTRIC STRENGTH, INSULATION RESISTANCE, PRESSBOARD, TRAFOBOARD, PROOF TRACKING INDEX*

1. Introduction

It is known from the practice of operation and maintenance of electrical equipment (transformers, motors and generators, etc.) that to ensure safe operation and functionality it is necessary to know, among other things, the condition of the insulation system, because about 40% of defects which occur in operation are due to insulation failures, in some cases approaching even close to 100% [1, 2].

The electrical insulating materials, used in different insulation systems, are subjected – both in the manufacturing process and also during operation – to various, more or less accidental, long or short-term stresses, etc. such as: mechanical, electrical, thermal stresses, due to the environment, radiation, etc. The effect of these stresses leads to the appearance of physical-chemical changes that produce a worsening of the dielectric properties [3–9].

Therefore, the study on how some factors such as temperature and humidity can influence the properties of cellulose-type solid electrical insulating materials used for the insulation system of power transformers is recommended and of interest.

Cellulose-based products such as pressboard, trafoboard, NOMEX paper are commonly used as cellulose-type materials for the solid insulation of electrical power transformers.

This work proposes the experimental study of the influence of environmental factors (temperature, humidity) on important dielectric properties of cellulose type insulating materials given their hygroscopicity (insulation resistance, dielectric strength and proof tracking index - PTI in humid conditions).

The following materials were studied: pressboard, NOMEX paper, trafoboard (1-3 mm), 0.05 mm transformer paper.

They were conditioned in climate chambers manufactured by VÖTSCH Germany (cold for 24 hours at a temperature of –40°C and damp heat steady state for 24 hours at a temperature of 70°C and relative humidity of 95%).

Experimental determinations of dielectric strength were carried out with a 50 kV station, by applying a sinusoidal AC voltage with a frequency of 50 Hz between two circular electrodes with a diameter of 75 mm.

A tracking tester produced by the Italian company GALBUSERA was used to determine the PTI – the resistance to leakage currents on the surface of insulating cellulose materials in humid conditions - an important test but rarely present in the literature.

Both the climatic conditioning of the cellulosic materials and the experimental determinations were carried out in the RENAR accredited laboratory within the National Research, Development and Testing Institute for Electrical Engineering - ICMET Craiova.

2. General aspects regarding cellulose-based electrical insulating materials

Cellulose is essentially a linear, macromolecular polymer with molecules that form concentrated bundles in the form of thin tubes (known as micelles). By joining these very thin tubes, fibres with lengths of the order of mm and with a very small diameter of the order of 70μm are achieved. Pores appear between the yarns, which can reach up to 40-50% of the volume of the material, this structure explains the high porosity and hygroscopicity of cellulose-based materials (paper and cardboard) [3,10,11].

The dielectric properties of cellulose-based materials are known to vary very much with density, moisture content, temperature, frequency of the electric field, etc.

Also, cellulosic insulating materials may undergo ageing processes resulting in the degradation of dielectric properties due to climatic, electrical, radio-chemical, biochemical or mechano-chemical ageing phenomena [3].

Thus, in the case of electrical insulating materials, as mentioned above, degradation, ageing and, consequently, the loss of important dielectric properties is favoured by the presence of certain disturbing factors.

For example, the resistivity of electrical insulating materials, such as cellulose, depends on the presence of impurities, temperature, humidity, etc.

The increase in temperature is also known to intensify the movement of charge carriers (ions in the crystal grid) and decreases resistivity.

Moisture, especially in hygroscopic materials such as cellulose and cellulose-based products, leads to an increase in the number of carriers, which has the effect of reducing resistivity.

The dielectric strength, in the case of solid electrical insulating materials, is influenced by the chemical structure and composition, the environment, the temperature, the degree of humidity.

Regarding the cellulosic materials, which have a porous structure, the dielectric strength is lower than in the case of materials which have a compact structure.

Also, the increase of the humidity degree due to the hygroscopicity of the cellulose-based products, leads to the appearance of some phenomena of intensification of the conduction process and obviously to a decrease of the dielectric rigidity [11,12].

3. Materials to be studied

Solid cellulosic type electrical insulating materials were used for this study in the construction of the insulation system of electrical transformers used in the power transmission and distribution network.

3.1 NOMEX paper

NOMEX paper is made of two types of aromatic polyamide polymer, provides high electrical insulation, good mechanical strength, behaves well in the presence of solvents and is very resistant to acid and alkaline solutions. It is not sensitive to moisture, is non-toxic, flame retardant, has very strong dielectric strength and intrinsic mechanical strength (resistance to breakage and wear). It has a good dielectric strength E_{str} = 18-40 kV / mm [13].

3.2 Pressboard

The pressboard, known in the literature as electrotechnical cardboard, is made of very thin layers of paper, pressed wet. It has good dielectric and mechanical properties, it is resistant to the action of transformer oil, which is important in its use in the insulation of electrical transformers with oil. It has a density between 1.2 .. 1.3 kg / dm^3 and a dielectric strength E_{str} = 9..12 MV/m [11].

3.3 Trafoboard

Trafoboard is used as the basic insulating material in power, distribution and special transformers. It has a good electrical and mechanical resistance.

4. Experimental determinations

4.1 Thermal conditioning of materials

The climatic conditioning of the cellulosic materials as well as the experimental determinations were carried out in the RENAR accredited laboratory within the National Research, Development and Testing Institute for Electrical Engineering - ICMET Craiova.

Material samples measuring (10 x 10) cm were used.

Tested materials were thermally preconditioned to cold (at a temperature of –40°C for 24 h in a climate chamber of type VÖTSCH C180) and to damp heat steady state (temperature of 70°C, relative humidity 95% for 24 h in a climate chamber of type VÖTSCH VC4060) [14,15].

The fig.1 shows the used climatic chambers.

To determine the proof tracking index, the studied samples of cellulose type materials were conditioned for 24 hours in a climatic chamber at a constant temperature of 23°C and 50% humidity [16].



a) b)

Fig.1 *Climatic chambers that were used:* a) Climatic chamber type VÖTSCH C180; b) Climatic chamber type VÖTSCH VC 4060

4.2 Determination of insulation resistance

The measurement of the insulation resistance of the samples was carried out by placing them between two circular electrodes with a diameter of 75 mm, between which a continuous voltage of 1000 V was applied, except the insulating paper with a thickness of 0.05 mm, which was tested at 500 V.

The experimental determinations were performed with a METRISO 5000D-PI Megohmmeter.

The achieved values are presented in Table 1.

Table1*: Experimental results for determination of the insulation resistance*

Type	Thick-ness [mm]	Insulation resistance [MΩ]		
		Labora-tory test trial	Test after cold conditionning 24h, –40°	Test after conditioning in continuous humid heat 24h, temperature 70°C, relative humidity 95%
Pressboard	0.35	18.5	0.79	0.63
NOMEX	0.2	$13.8 \cdot 10^3$	$10.7 \cdot 10^3$	$9.3 \cdot 10^3$
Transformer paper	0.05	19.7	1.5	2.07
Trafoboard	1	220	12.6	9.79
Trafoboard	1.5	290	28.4	12.3
Trafoboard	2	330	36.9	10.8
Trafoboard	3	349	119	26.1

4.3 Determination of dielectric strength

The dielectric strength E_{str} represents the minimum value of the electric field intensity for which a material penetrates. It is determined as the ratio between the breakthrough voltage U_{str} and the distance d between the electrodes (thickness of the material).

The conditioned materials were afterwards subjected to an alternating voltage with a frequency of 50 Hz, generated by a 50 kV substation and applied between the same electrodes used to determine the dielectric strength.

The values achieved experimentally are presented in Table 2.

Table2*: Experimental results for determination of the dielectric strength*

Type	Thick-ness [mm]	The voltage at which the breakdown occurred [kV]		
		Labora-tory test trial	Test after cold conditionning 24h, –40°	Test after conditioning in continuous humid heat 24h, temperature 70°C, relative humidity 95%
Pressboard	0.35	2	2	2
NOMEX	0.2	12	12	12
Transformer paper	0.05	2	2	2
Trafoboard	1	6	6	6.5
Trafoboard	1.5	10	10	8
Trafoboard	2	14	12.5	8
Trafoboard	3	28	24	9.5

4.4 Experimental verification of proof tracking index (PTI)

The proof tracking index (PTI) is the numerical value of the proof voltage in volts at which test specimens withstand the test period for 50 drops without tracking failure and without a persistent flame occurring [16].

The verification of PTI was performed according to the specifications provided in [16] using a tracking tester manufactured by GALBUSERA, Italy (Fig.2).



Fig.2 *The GALBUSERA tracking tester.*

For the performed tests a voltage of 400 V and a frequency of 50 Hz were chosen, and the short-circuit current of the electrodes was set to 1 A. In principle, this test consists in wetting the surface of the sample between the electrodes with 50 drops of 0.1% ammonium chloride solution, drop by drop, at regular intervals (30 ± 5 s) and the drops must fall in the center of the surface between the electrodes from a height of 30 ± 40 mm [16].

The material samples were conditioned for 24 hours in a climatic chamber at a constant temperature of 23°C and 50% humidity.

Prior to the start of the tests, a visual examination of the surface condition of each material was carried out in order to identify any non-uniformities on the surface to be tested.

Fig.3 shows images during the PTI check.



Fig.3 *Images during the PTI tests.*

Fig. 4 shows the material samples after checking the proof tracking index (PTI).

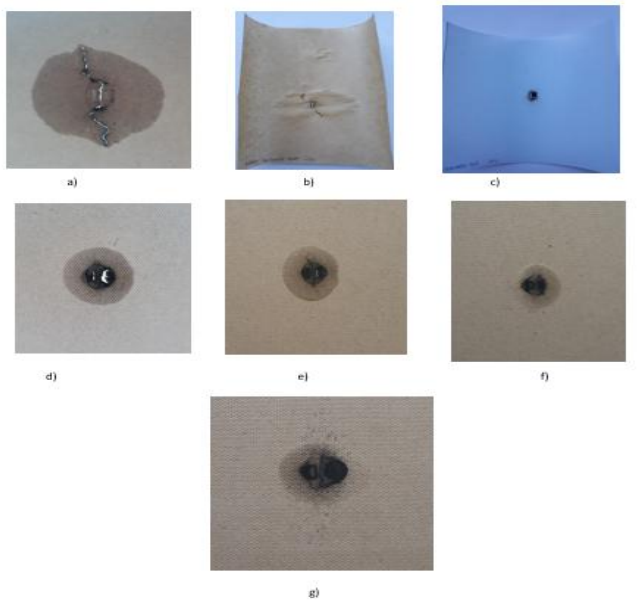

Fig.4 Samples of cellulosic material after PTI verification: a) pressboard; b) NOMEX; c) transformer paper 0.05 mm; d) trafoboard 1 mm; e) trafoboard 1.5 mm; f) trafoboard 2 mm; g) trafoboard 3 mm.

Following the tests, the subsequent behaviours of the studied materials were observed:

-In the case of the pressboard sample, at first some incandescences appeared which led to the ignition of the sample, but as it was wetted, the incandescence decreased in intensity and a sinuous path was formed between the electrodes, which is a perforation in the pressboard due to tracking between conducting parts [16].

-The NOMEX 0.2 mm paper initially ignited with flame, then incandescences appeared and the material between the electrodes burned, causing the tracking failure.

- 0.05 mm insulating paper was moistened and perforated. It did not light up, but incandescence was observed.

- In the case of the 1 mm trafoboard sample, the material around the electrodes was wetted and incandescence was maintained, which perforated the sample.

- In the case of the 1.5 mm trafoboard sample, wetting of the material around the electrodes was observed and incandescence was maintained, which perforated the sample.

- When testing the 2 mm trafoboard sample, the surface between the electrodes was moistened and blackened, and the incandescences determined an electrical erosion - wearing away insulating material by the action of electrical discharges [16] in the sample material. The sample was not penetrated. The erosion depth was 1.4 mm.

- For the 3 mm trafoboard sample an air arc (arc between the electrodes above the surface of the sample [16]) formed on the wet surface between the electrodes and the ignition of the material in the vicinity of one of the electrodes was observed. The material burned, turned black, but the sample was not penetrated during the test. The erosion depth was 0.92 mm.

5. Analysis of experimental results

Important and interesting aspects can be seen in the determinations made on insulation resistance.

By analyzing the achieved results (Table I) it can be observed that, due to the high hygroscopicity of the studied cellulose-based materials, substantial changes of insulation resistance occur, decreasing significantly from the order of hundreds of MΩ to tens of MΩ or in the case of pressboard below 1 MΩ. In the case of

NOMEX paper, there is no significant influence in the variation of the insulation resistance.

By analyzing the results achieved in the determination of the dielectric strength (Table II) it can be seen first of all that the values of the breakdown voltage for the determinations carried out in the laboratory environment and with unconditioned materials are within the values known from the literature [11, 12] and from the technical data sheet of cellulosic electrical insulating materials [17].

One can also see that there are no substantial changes in the breakdown voltage of the tested materials following the thermal conditioning.

In case of verification of the endurance index at surface runoff in humid conditions – the proof tracking index, according to the norms in force [16], the pressboard, the transformer paper with the thickness of 0.05 mm, the NOMEX paper and the trafoboard samples of 1 and 1.5 mm did not behave properly when checking the PTI because they penetrated at the 400 V applied voltage.

6. Conclusions

The aim of this paper was to study how certain environmental factors (humidity, high temperatures or low temperatures) can influence certain electrical properties, namely dielectric strength, insulation resistance and the PTI for some cellulose type materials (NOMEX paper, pressboard, trafoboard) used to insulate both dry and oil-based electrical transformers.

A strong and negative influence of high or low temperatures and humidity was observed on the values of the insulation resistance at which strong decreases were reported (from hundreds of MΩ to tens or even a few MΩ).

Regarding the proof tracking index PTI, only the samples of trafoboard with the thickness of 2 and 3 mm carried out well in terms of the requirements of the standard [16].

Future studies and analyses on the behaviour of solid cellulose insulation for power transformers will follow the effect over time of transformer oil on the properties of cellulose materials.

7. References

[1] M. Ghiorghiu, C. Ghiorghiu and D. Zlatanovici, *Checking the Insulation of Electrical Equipment* (*Verificarea izolației echipamentelor electrice*), Bucharest: Ed. Tehnica, 1984.

[2] G. Tănăsescu, P. Notingher, et al, "Online monitoring and diagnostic system (SMD) for AT 3200 MVA 220/110 kV from Turnu-Măgurele substation" ("Sistem de monitorizare și diagnosticare (SMD) on-line pentru AT 3200 MVA 220/110 kV din stația Turnu-Măgurele"), National Symposium - Optimizing Energy Services, 5th Edition,, Buzău, Romania, 2008, p.1-6.

[3] P. Notingher, *Insulation Systems* (*Sisteme de izolație*), Bucharest: Printech, 2002.

[4] K.S. Kassi, I. Fofana, F. Meghnefi, A. Betie, J. Perron and Z. Yeo, "Comparative study between conventional and hybrid solid insulation systems," IEEE Conference on Electrical Insulation and Dielectric Phenomena CEIDP 2014, p.1-4.

[5] V. Wasserberg, H. Borsi and E. Gockenbach, "Effects of different drying procedures on the composition of a liquid impregnated solid insulation," IEEE International Symposium on Electrical Insulation, Boston, USA, 2002, p.346-349.

[6] Z. Yan, M. Dong, Y. Shang and M. Muhr, "Ageing diagnosis and life estimation of paper insulation for operating power transformer," IEEE International Conference on Solid Dielectrics, Toulouse, France, 2004, Vol.2, pp. 715-718.

[7] L. Ruijin, T. Chao, Y. Lijun and C. Huanchao, "Thermal aging studies on cellulose insulation paper of power transformer using AFM," IEEE 8th International Conference on Properties & Applications of Dielectric Materials, Bali, Indonesia, 2006, pp. 722-725.

[8] V. Sivaramalakshmi, M. Ravindran, M. W. Iruthayarajan and M. Bakrutheen, "Aging performance of natural ester impregnated Nomex paper insulation," 2019 Fifth International Conference on Electrical Energy Systems (ICEES), Chennai, India, 2019, pp. 1-4.

[9] S. Y. Matharage, Q. Liu, Z. Wang and D. Walker, "Effect of paper type and water content in paper on the partitioning of 2-FAL between liquid and paper insulations," IEEE International Conference on High Voltage Engineering and Application, Beijing, China, 2020, pp. 1-4.

[10] G. Floriganță, *Materials in Techniques* (*Materiale în tehnică*), Craiova: Ed. ICMET, 2002.

[11] A. Ifrim and P. Noțingher, *Electrotechnical Materials* (*Materiale electrotehnice*), Bucharest: Ed. Didactic and Pedagogical, 1979.

[12] A. Ifrim and P. Noțingher, *Electrotechnical Materials* (*Materiale electrotehnice*), Bucharest: Ed. Didactic and Pedagogical, 1992.

[13] http://ro.hh-pap.com/insulation-paper/dupont-nomex-paper.html

[14] SR EN 60068-2-78:2013 - Environmental tests. Part 2-78: Tests. Cab test: Wet, continuous heat.

[15] SR EN 60068-2-1: 2007 - Environmental tests. Part 2-1: Tests. Test A: Cold.

[16] IEC 60112:2003 - Method for the determination of the proof and the comparative tracking indices of solid insulating materials.

[17] www.brioelectric.ro.

The impact of high voltage electric discharge treatment on the properties of Cu – Al powder mixture

Syzonenko Olha, Torpakov Andrii, Lypian Yevhen, Prystash Mykola
Institute of Pulse Processes and Technologies of the National Academy of Sciences of Ukraine – Mykolaiv, Ukraine
sizonenko43@rambler.ru

Abstract *Studies of the impact of high voltage electric discharge (HVED) treatment on the dispersion and phase composition of 87,5 % Al + 12,5 % Cu powder system were performed. It was shown that HVED treatment in kerosene with specific treatment energy of 5 MJ/kg leads to the decrease of mean diameter of treated powder from 15 to 13 μm, and the increase of specific treatment energy leads to the decrease of mean diameter of treated powder from 15 to 6 μm. X-ray diffraction analysis shows that $CuAl_2$ and Al_4C_3 are synthesized in all considered treatment regimes.*

HVED treatment with increased specific treatment energy leads to the increase of quantity of synthesized Al_4C_3 phase. The use of "three point – plane" electrode system instead of "point – plane" during HVED treatment of 87,5 % Al + 12,5 % Cu powder system leads to the increase of quantity of synthesized Al_4C_3 and $CuAl_2$ phases, while the efficiency of powders dispersion slightly decreases. Up to 40% of particles in powder mixture, treated by HVED in kerosene with the use of "three point – plane" electrode system, have diameter close to the diameter of the initial powder mixture.

Keywords*: HIGH VOLTAGE ELECTRIC DISCHARGE, POWDER, POWDER METALLURGY, SYNTHESIS, GRINDING, ALUMINUM, CUPRUM*

1. Introduction

Currently in Ukraine there is a problem of replacing morally and physically obsolete rolling stock of urban electric transport and ensuring its high level of reliability. At the present time, Morgan Carbon, PanTrac and Hoffman companies are the leading manufacturers of electrical materials for urban electric transport in Europe. Most types of electrical contact inserts, made by thee companies, contain carbon and copper components [1]. Such current collection elements are made in an aluminum frame and are fastened with special adhesives or bolted joints, and are often placed in copper clamps. Sliding electrical contacts are the most common mobile connections in urban electric transport. The analysis of technical conditions shows that the materials of current-collecting sliding elements must provide high electrical conductivity, arc resistance, hardness, strength and wear resistance [1]. In this case, ensuring the durability of both the current collector (body) and the contact wire (counter-body), which is determined by the low coefficient of friction, is an important condition.

A number of materials, based on carbon-containing powders clad with copper, have been developed in Ukraine for the manufacture of current collector inserts. However, such materials have unsatisfactory resistivity, wear resistance and strength. Given the disadvantages of existing materials for these friction pairs, there is a need to develop new materials that would have high performance properties, especially high wear resistance. However, the available materials do not fully meet the technical and operational requirements, in particular, put forward on the criterion of durability of this system. They have unsatisfactory specific resistance (from $3 \cdot 10^{-5}$ Ohm · m to $8 \cdot 10^{-5}$ Ohm · m), wear resistance (from 0,1 to 0,4 mm of loss of diameter during 20 h), and durability (from 40 to 82 MPa). Therefore, the creation of materials that would meet the stringent requirements of operation in extreme conditions is an urgent scientific task.

The need to create new metallic materials with high physical, mechanical and operational properties that will provide the necessary reliability of products in extreme conditions, is relevant for the development of modern technology. Unfortunately, the possibilities of obtaining them using conventional metallurgical methods are largely exhausted. Therefore, scientists and engineers are facing an important task of the development of physical principles for creating new materials under conditions of high-energy action and extreme high-speed effects of temperatures and pressures, which will allow the obtainment of nanostructured materials, which do not exist in conventional conditions, from elements that do not have mutual solubility. Materials, consolidated by the methods of spark plasma sintering (SPS), self-propagating high-temperature synthesis (SHS), or selective laser sintering, have significantly (1.5–2 times) higher physical and mechanical properties than those obtained by conventional metallurgical methods due to less exposure at high temperature, which ensures the preservation of the grain heterophase structure of the powder mixture in the structure of the consolidated material [2].

But the properties of consolidated materials depend not only on the method of consolidation, but also on the chosen method of preparation of powders. The use of the method of preparation of starting powders of metal-matrix materials by high-voltage electric discharge (HVED) in hydrocarbon liquid, developed in IIPT of NAS of Ukraine, allows to achieve significant dispersion of particles of processed powders as well as to provide synthesis of dispersion-strengthening phases, in particular, carbides [2–9].

During the HVED treatment, metal powder particles are exposed to a combined effect of mechanical (shock wave, hydro flows, cavitation) and thermoelectric (discharge channel plasma, microplasma formations between particles, discharge current) factors, which leads to their dispersion. The use of hydrocarbon liquid prevents the oxidation of particles of the processed metal. In addition, as it is shown in [3–9], the difference between high-voltage electric discharge (HVED) in a hydrocarbon liquid is its pyrolysis (rupture of chemical bond chains) under the influence of the temperature of the plasma discharge channel and pulse pressure with the formation of active carbon nanoparticles up to C_{70} [2, 6], which creates conditions for the synthesis of dispersion-strengthening compounds, in particular, carbides [3–9].

Unfortunately, the possibility of using high-voltage discharge treatment in a hydrocarbon liquid for the preparation of starting powders of metal-matrix composites of the Al – Cu system for the manufacture of current collector inserts has not been sufficiently studied. In particular, there is no information on the patterns of changes in the dispersion and phase composition of the initial powders of the Al – Cu system under the influence of HVED treatment.

Therefore, the **goal of the work** is to investigate the influence of high-voltage discharge treatment in kerosene on the dispersion and phase composition of 87.5% Al + 12.5% Cu powder system.

2. Methodology

Elemental Al powders PA1 GOST 6058-73 (ПА1 ГОСТ 6058-73) with d_0 = 25 μm and Cu PMS-1 GOST 4960-75 (ПМС-1 ГОСТ 4960-75) with d_0 = 15 μm were selected as initial materials for the study, on the basis of which a mixture of 87.5 % Al + 12.5% Cu mass composition with an initial diameter of 22 μm was prepared. Kerosene of the TS-1 brand (GOST 10227-86) was used as a working liquid. The ratio of solid to liquid phases in the studies was 1:15 (the weight of the processed powder was 100 g, the volume of the working liquid was 1.5 l).

The scheme and detailed description of the experimental stand for high-voltage electric discharge processing and, in particular, the working chamber, are given in [3–5]. Investigations of HVED in "liquid dielectric – metal powder" disperse system were performed at a voltage U = 50 kV, the inductance of the discharge circuit L from 0.5 to 1 μH (limit technological values) and the discharge interval l_p ~ 17 mm. In the process of research, the specific energy of processing was varied by changing the number of discharges n. The capacity of the drive C was 0.8 μF, so the value of the stored energy of a single discharge W_1 was 1 kJ.

Two structural types of electrode systems (ES) were used in the research, namely "point – plane" (P – P) and "multipoint anode – plane" (MP – P) with 3 tips. These ESs were used due to the fact that according to the results of [3–6, 8–10] the change of the electric field configuration due to the use of different types of ESs allows to create conditions for changing the distribution of plasma formations in the volume of processed powder.

In turn, if the plasma formations are distributed over the entire volume of the processed powder, it will intensify the processes of erosion and hydrodynamic dispersion and synthesis of carbide and intermetallic compounds during HVED treatment [3–6, 8, 9]. When using the point–plane system, HVED develops according to the classical mechanism of spark discharge (SD) in a dispersed system, while the use of "multipoint anode – plane" type ES allows the implementation of the mode of volume-distributed multi-spark discharge (VMD).

The use of different electrode systems allowed controlling the distribution of the intensity of the influence of the main factors of HVED impact [3–6, 8–10]. Thus, if in the case of the implementation of SD most of the accumulated energy was transformed into shock waves, the implementation of VMD using multi-point anodes allows to increase the intensity of thermal and current impact factors.

In order to evaluate the degree of influence of HVED in kerosene on the morphology and particle size of powders, the following hardware and software was used –BIOLAM-I (БІОЛАМ-І) optical microscope with a maximum magnification of × 1350, REMMA-102 (РЕММА-102) raster electron microscope with a magnification range from 10 to × 250000 (IPM NASU), Canon digital camera. Powder samples for optical microscopy were taken in accordance with GOST 23402-78 (ГОСТ 23402-78). After obtaining a sharp image, magnification was recorded and photographs were taken, which were processed for further analysis.

Since the average diameter of particles and their shape factor are the most informative in materials science in terms of describing the morphology of the powder, the diagnosis of morphological characteristics was performed before and after HVED treatment by average diameter (d_m) and shape factor (F) in accordance with GOST 25849-83 (ГОСТ 25849-83). The number of particles that came into the field of view of the microscope eyepiece was not less than 2000 pieces, and at least five samples were considered for each studied mode. As a result of processing, the values of the above characteristics were obtained for each particle that came into view. This allowed to present data in the form of graphs and histograms with a confidence interval of 0.96.

The study of the phase composition of the powders was performed by X-ray phase analysis. The diffraction patterns were recorded using a DRON-4-07 (ДРОН-4-07) diffractometer under CuKα radiation. A Ni β-filter was used to reduce the background on the diffractograms as well as to reduce the probability of β-lines. Phase identification on diffraction patterns was performed using POW_COD databases [11]. A standard made of quartz was used to determine the instrumental function.

3. Results and discussion

The study of the effect of HVED treatment on the change in the properties of 87.5% Al + 12.5% Cu powder system was performed in the modes shown in table 1. After processing, the features of the high-voltage electric discharge process in the modes with different types of used ES were compared. The initial mixture of 87.5% Al + 12.5% Cu powders had an average diameter of 22 μm and was characterized by a monomodal size distribution, the main peak of which was at the point of 20 μm (~ 55%) (see Fig. 1, curve 1).

HVED treatment of this powder mixture in kerosene with single-point EC at W_s = 5 MJ / kg leads to a change in dispersion (see Fig. 1, curve 2) – the particle size distribution retains a monomodal appearance and shifts to the area of smaller diameters, and the average diameter decreases to ~ 12 μm. Increasing the specific processing energy to 10 MJ / kg leads to an increase in the dispersion efficiency (see Fig. 1, curve 2) – the particle size distribution undergoes a significant shift to the area of smaller diameters, and the average particle diameter of the mixture decreases to 7 μm. Increasing specific processing energy to 20 MJ / kg leads to the further decrease of the average particle diameter of the mixture to 6 μm.

Table 1: *Modes of HVED treatment of 87.5% Al + 12.5% Cu powder system in kerosene.*

No. of mode	Number of points of the electrode system	W_s, MJ/kg
1	1	20
2	1	10
3	1	5
4	3	20
5	3	10
6	3	5

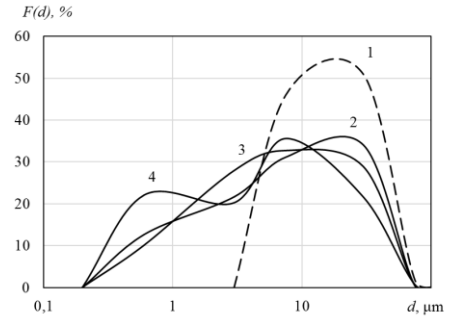

Fig. 1 *Particles size distribution of initial 87.5% Al + 12.5% Cu powder (1) and after HVED treatment in kerosene in SD mode with different values W_s = 5 MJ/kg (2), W_s = 10 MJ/kg (3) and W_s = 20 MJ/kg (4)*

Changing the type of used ES from one-point to three-point did not affect the dispersion efficiency (see Fig. 2). Treatment with W_s = 5 MJ / kg allowed reducing the average particle diameter to 13 μm (see Fig. 3). Treatment with W_s = 10 MJ / kg reduced the average diameter of the mixture after treatment to ~ 9 μm, and with W_s = 20 MJ / kg to 7 μm.

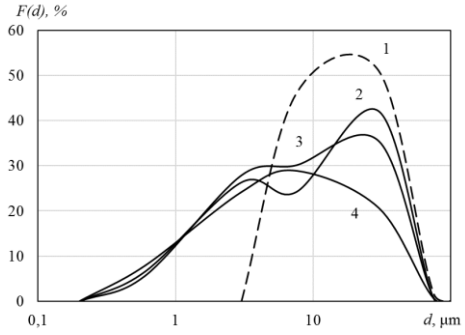

Fig. 2 *Particles size distribution of initial 87.5% Al + 12.5% Cu powder (1) and after HVED treatment in kerosene in VMD mode with different values W_s = 5 MJ/kg (2), W_s = 10 MJ/kg (3) and W_s = 20 MJ/kg (4)*

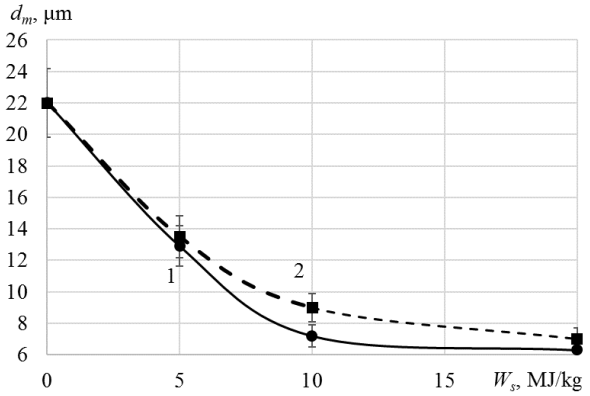

Fig. 3 *Dependence of the average particle diameter of 87.5% Al + 12.5% Cu powder on the specific processing energy when using SD mode (1) and VMD mode (2) in kerosene*

X-ray phase analysis of the initial mixture of 87.5% Al + 12.5% Cu powders confirmed that only aluminum and copper are present in the composition of the initial mixture (see Fig. 4), no significant impurity content was detected.

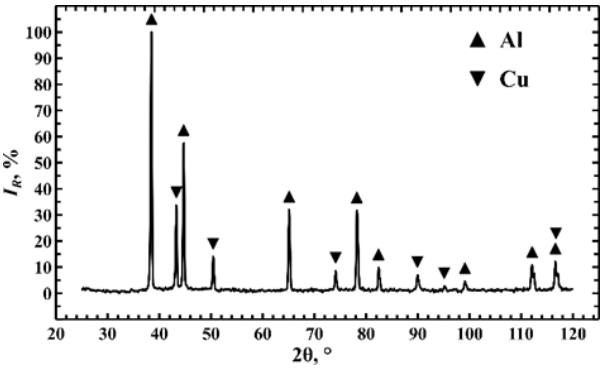

Fig. 4 *X-ray diffraction patterns of 87.5% Al + 12.5% Cu initial powder mixture*

HVED treatment of 87.5% Al + 12.5% Cu powder mixture in kerosene with SD leads to a change in its phase composition (see Fig. 5, a, c, e). In the composition of the powder, in addition to the initial Al and Cu, as a result of HVED treatment with a specific energy of 5 MJ/kg, reflexes appear, corresponding primarily to $CuAl_2$ intermetallic phase and aluminum carbide Al_4C_3 (see Fig. 5, a). Increasing the specific energy to values of 10 and 20 MJ/kg increases the quantity of synthesized phases, as evidenced by some increase in the corresponding peaks on X-ray diffraction patterns (see Fig. 5, c, e).

The use of VMD for HVED treatment of 87.5% Al + 12.5% Cu powder mixture in kerosene does not fundamentally change the dynamics of the synthesis of new phases in comparison with SD (see Fig. 5, b, d, f). First of all, we can point to the appearance of $CuAl_2$ intermetallic compound, as well as Al_4C_3 carbide when exposed to a specific energy of 5 MJ/kg (see Fig. 5, b), the number of which increases with increasing specific energy to 10 and 20 MJ/kg (see Fig. 5, d, f).

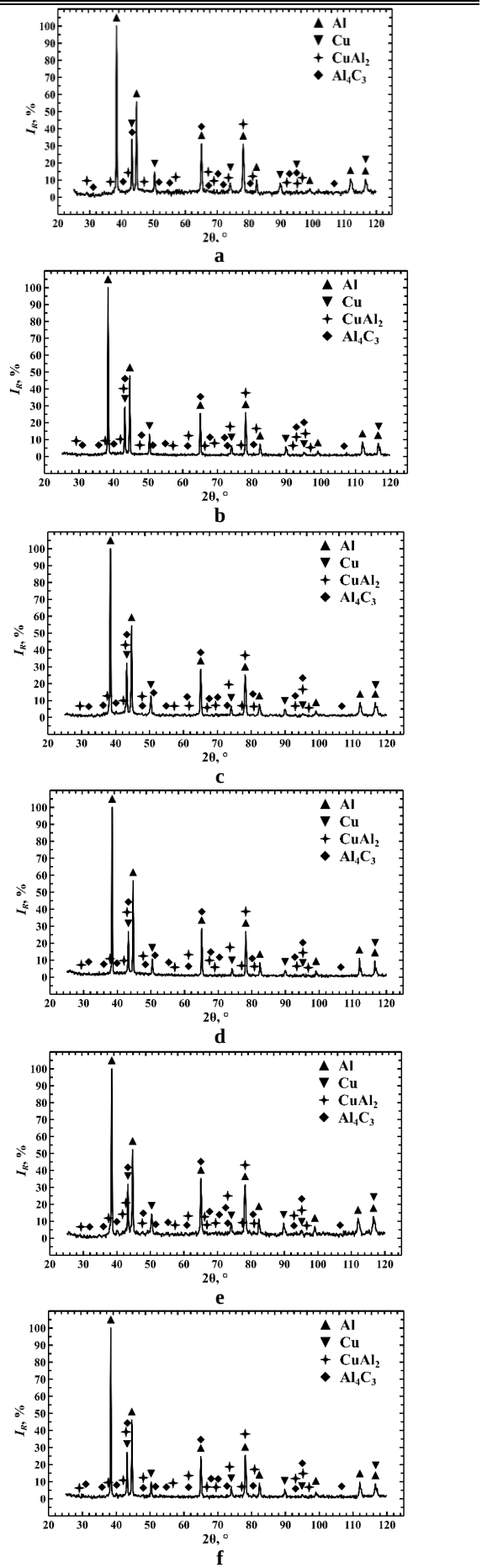

Fig. 5 *X-ray diffraction patterns of 87.5% Al + 12.5% Cu powder mixture after HVED treatment in kerosene in the modes of SD (a, c, e) and VMD (b, d, f) with a specific energy of 5 MJ/kg (a, b), 10 MJ/kg (c, d) and 20 MJ/kg (e, f)*

4. Conclusions

1. The possibility of using HVED treatment in a hydrocarbon liquid for the preparation of the initial mixture of powders for metal-matrix composites of Al – Cu – C system is shown.

2. The regularities of high-voltage electric discharge treatment of 87.5% Al + 12.5% Cu powder mixture in kerosene were studied and it was shown that HVED treatment with W_s = 5 MJ/kg leads to a decrease in the average particle diameter of the treated mixture from 15 μm to 13 μm, and increasing the specific processing energy to W_s = 20 MJ / kg allows to reduce the average particle diameter of the treated mixture to 6 μm.

3. It is found out that regardless of HVED mode, treatment of 87.5% Al + 12.5% Cu powder mixture leads to the synthesis of $CuAl_2$ intermetallic compound and Al_4C_3 carbide, the amount of which increases with increasing specific processing energy.

5. References

1. I. S. Yefremov, V.M. Kobozev, V. V. Shevchenko, *Tehnicheskie sredstva elektricheskogo transporta* (Vyshaya Shkola, Moscow, 1985) (In Russian)
2. O. M. Syzonenko, M. S. Prystash, A. S. Torpakov, Machines. Technologies. Materials. **12**, № 1. 41–44 (2018).
3. O. Sizonenko, S. Prokhorenko, A. Torpakov, D. Żak, Y. Lypian, R. Wojnarowska-Nowak, J. Polit, E. M. Sheregii,AIP Adv. **8**, № 8. 085317 (2018).
4. O. N. Sizonenko, E. G. Grigoryev, N. S. Pristash, A. D. Zaichenko, A. S. Torpakov, Ye. V. Lypian, V. A. Tregub, A. G. Zholnin, A. V. Yudin, A. A. Kovalenko, High Temp. Mat. Proc. **36**, № 9. 891–896 (2017).
5. O. N. Sizonenko, N. A. Oleinik, G. A. Petasyuk, G. D. Il'nitskaya, G. A. Bazalii, V. S. Shamraeva, É. I. Taftai, A. S. Torpakov, A. D. Zaichenko, E. V. Lipyan, Powder Metall. Met. Ceram. **52**, № 7–8. 365–369 (2013).
6. O. M. Syzonenko, P. I. Loboda, A. D. Zaichenko, Ye. V. Solodkiy, A. S. Torpkov, M. S. Prystash, V. O. Trehub // J. Superhard Mater. **39**, № 4. 243–250 (2017).
7. N. I. Kuskova , O. M. Syzonenko, A. S Torpakov, High Temp. Mat. Proc. **39**, № 1. 357–367 (2020).
8. O.M. Syzonenko, S.V. Prokhorenko, E.V. Lypyan, A. D. Zaichenko, M.S. Prystash, A.S. Torpakov, M.O. Pashchyn, R. Voinarovska-Novak, E. Sherehii, Materials Science. **56**, № 2. – 232–239 (2020).
9. O. M. Syzonenko, P. Tashev, M. S. Prystash, A. S. Torpakov, Ye. V. Lypian, V. Dyakova, M. Kandeva, E. I. Taftai, Y. G. Kostova, Engineering Sciences. **58**, № 2. 79–94 (2021).
10. A. V. Ivanov, V. N. Tsurkin, Surf. Eng. Appl. Electrochem. **55**, № 1. 53–64 (2019).
11. S. Grazulis, D. Chateigner, R. T. Downs, A. T. Yokochi, M. Quiros, L. Lutterotti, E. Manakova, J. Butkus, P. Moeck, A. Le Bail, Journal of Applied Crystallography. **42**. 726–729 (2009).